ORIGINAL PAPER

# Constitutive and Geometric Nonlinear Models for the Seismic Analysis of RC Structures with Energy Dissipators

**P. Mata · A.H. Barbat · S. Oller · R. Boroschek**

**Abstract** Nowadays, the use of energy dissipating devices to improve the seismic response of RC structures constitutes a mature branch of the innovative procedures in earthquake engineering. However, even though the benefits derived from this technique are well known and widely accepted, the numerical methods for the simulation of the nonlinear seismic response of RC structures with passive control devices is a field in which new developments are continuously preformed both in computational mechanics and earthquake engineering. In this work, a state of the art of the advanced models for the numerical simulation of the nonlinear dynamic response of RC structures with passive energy dissipating devices subjected to seismic loading is made. The most commonly used passive energy dissipating devices are described, together with their dissipative mechanisms as well as with the numerical procedures used in modeling RC structures provided with such devices. The most important approaches for the formulation of beam models for RC structures are reviewed, with emphasis on the theory and numerics of formulations that consider both geometric and constitutive sources on nonlinearity. In the same manner, a more complete treatment is given to the constitutive nonlinearity in the context of fiber-like approaches including the corresponding cross sectional analysis. Special attention is paid to the use of damage indices able of estimating the remaining load carrying capacity of structures after a seismic action. Finally, nonlinear constitutive and geometric formulations for RC beam elements are examined, together with energy dissipating devices formulated as simpler beams with adequate constitutive laws. Numerical examples allow to illustrate the capacities of the presented formulations.

P. Mata (✉) · A.H. Barbat · S. Oller
Department of Structures and Strength of Materials,
Technical University of Catalonia, UPC, 08034 Barcelona, Spain
e-mail: pmata@cimne.upc.edu

A.H. Barbat
e-mail: alex.barbat@upc.edu

S. Oller
e-mail: sergio.oller@upc.edu

R. Boroschek
Department of Civil Engineering, University of Chile,
837-0449 Santiago, Chile
e-mail: rborosch@cec.uchile.cl

## 1 Introduction

Conventional seismic design practice permits designing reinforced concrete (RC) structures for forces lower than those expected from the elastic response on the premise that the structural design assures significant energy dissipation potential and, therefore, the survival of the building when subjected to severe earthquakes [96]. Normally, energy dissipation during seismic actions occurs in critical zones of the structure specially designed to admit large ductility demands [23]. Frequently, the dissipative zones are located near the beam-column joints and, due to cyclic inelastic incursions during earthquakes, several structural members can suffer a great amount of damage with irreversible degradation of the mechanical properties of the materials, cracking and yielding of the steel reinforcements etc. For a complete survey about reinforced concrete structures subjected to seismic actions, see Fardis [78].

Even if a limited level of structural damage dissipates part of the energy induced by the earthquake and uncouples the dynamic response from resonance offering a certain level of protection against seismic actions [164], the large displacements required for developing hysteretic cycles in dissipative zones can cause severe damage to non structural

components. Moreover, these deformations can produce irreparable damage in those members; this situation is generally considered economically acceptable if life safety and collapse prevention are achieved.

In the last decades, new concepts for the design of buildings, based on the manipulation of the energy dissipation, have improved the seismic behavior of the structures providing higher levels of safety for the occupants, the buildings and the nonstructural components. The new techniques consist of adding devices to the buildings with the main objective of dissipating the energy demand imposed by the earthquake alleviating the ductility demand on primary structural elements, such as beams, columns or walls and decreasing the acceleration response [96, 223]. The devices can be installed in new or in existing structures and can be used in seismic design or rehabilitation. The purpose is to *control* the seismic response of the buildings by means of a set of dissipating devices which constitutes the *control system*, adequately located in the structure.

In general, control systems can be classified in four major groups:

(i) *Active control systems*. These systems work measuring, by means of sensors, the external excitation and/or the structural response. Based on these data and using algorithms, the control forces needed to improve the seismic response of the building are calculated. Control forces are applied to the structure by means of actuators, which take the energy from an external supply (see [9, 27, 28, 135, 226] among others). The simulation of the linear and nonlinear response of the controlled structures is usually performed by discretizing the equations of motion starting from their state space formulation [140].

(ii) *Passive control systems*. The passive control systems mostly used in reducing the seismic response of buildings are *base isolation* and *energy dissipating devices* (EDD). In this case, the EDDs localize and concentrate the nonlinear phenomena of the structure and thus the damage in the devices without the need of an external energy supply [97, 223, 232].

(iii) *Semi active systems*. In this case the control algorithm changes some of the properties of the control devices in order to obtain a better seismic performance of the structure. In this category of control systems control actuators do not add energy directly to the structure and the devices can be seen as *controllable* passive devices [153, 224, 228, 244].

(iv) *Hybrid systems*. This systems are typically defined as a combination of different active and/or passive systems. A comparative study of the response of structures for different control systems can be reviewed in [30, 190]. A rather brief state of the art review about theory and practice using control techniques in civil engineering structures can be found in Ref. [224].

Today, the passive control of structures is a well understood technique and its use is widely accepted by the engineering community even in the case when passive systems are not able to adapt their behavior to the seismic response of the building [226].

Base isolation uncouples the structure from the soil introducing flexible supports between foundations and the rest of the structure [204]. The isolation system transforms the building into a rigid body moving over flexible supports, shifting thus the fundamental period of the structure and enhancing the energy dissipating characteristics of the isolation-superstructure system [2, 203]. A detailed presentation of theory, numerical analysis and of the practical applications of base isolation systems can be reviewed in [121]. More specific aspects of this technique, such as analytical models for bearings, linear equivalent models for practical design of structures, etc. can be consulted in [3, 46, 122, 123].

EDDs, also called *supplemental dampers*, are devices located throughout the structure to absorb and dissipate an important part of the energy input induced in the structure by earthquakes. They are applicable to a wider range of structures than base isolation but the benefits obtained in reducing the seismic response of the structure are usually less significant. Many practical application of EDDs to real structures are summarized by Aiken in Ref. [2].

The effectiveness of the implementation of EDDs in RC structures can be analyzed starting from the energy balance equation as [6]:

$$E_I = E_K + E_S + E_D + E_\pi, \tag{1}$$

where $E_I$ is the absolute earthquake energy input, $E_K$ is the absolute kinetic energy, $E_S$ is the elastic strain energy, $E_D$ is the energy dissipation due to inelastic behavior in the structure (including viscous effects) and $E_\pi$ is the contribution of energy dissipation due to the addition of EDDs. Using the assumption that the term $E_\pi$ has no influence on $E_I$, it is possible to see from (1) that increments of the contribution of $E_D + E_\pi$ implies reductions of $E_K + E_S$ and, therefore, lower displacements and velocities are obtained when extra energy dissipation is provided [2, 223]. The main objective of designers when applying passive control in improving the seismic behavior of RC structures is defining appropriately the properties of the EDDs in such a way that the inelastic demand on primary structural members $E_D$ be transferred to the term $E_\pi$. After a sever earthquake, EDDs can be replaced by new ones if necessary.

EDDs can be classified according to the nature of their dissipative mechanism into *displacement dependent*, *e.g.* friction, metallic and extrusion devices, *velocity dependent* *e.g.* viscous, *mixed e.g.* viscoelastic and others such as tuned liquid and tuned mass dampers; each of these types is described in Sect. 2 of this article. A great amount of works

comparing the ability of different passive EDDs in controlling the seismic response of structures is available in the literature; for example, the responses of frame structures equipped with viscoelastic and viscous devices are compared in [85]; in Ref. [120] an approximated method is used to carry out a comparative study considering metallic and viscous devices. Guidelines and methods for testing and characterizing different types of EDDs can be consulted in [97, 98, 195].

Other points of view are admissible for considering the incorporation of passive control in RC structures; for example, Aiken presents in Ref. [2] the contribution of the extra energy dissipation due to EDDs as an *equivalent damping* added to the linear bare structure and *displacement reduction factors* are given as a function of the damping ratio added to buildings by means of the EDDs. A critical review of the reduction factors and design force levels can be consulted in [136]. Connor *et al.* [60] propose a method for a preliminary design of passively controlled buildings under the hypothesis that the structure is composed of two systems, the bare frame and the dissipative one, that work together to satisfy a design criterium. In Ref. [87] the optimal control theory is used to design supplemental viscous and viscoelastic passive damping systems in seismic control. In Refs. [137, 138] Lin and Copra study the accuracy in estimating the dynamic response of asymmetric one-story buildings equipped with EDDs, when the dissipating devices are replaced by their energetic equivalent linear viscous dampers; a correction factor is provided estimating the maximum forces in the EDDs. Other procedures for the analysis and design of structures with EDDs can be consulted in [57].

Today, only a few countries have codes to design RC buildings with EDDs; one of them is United States, where there are several codes that provide procedures and requirements for design of passive energy dissipating devices. Particularly, the US *Federal Emergency Management Agency* (FEMA) proposes code provisions and standards along with other references pertaining to the design of EDDs devices for use in buildings. The document includes *Prestandard and Commentary for the Seismic Rehabilitation of Buildings* (FEMA 356) [80] and NEHRP *Recommended Provisions for Seismic Regulations for New Buildings and Other Structures* (FEMA 368) [79], which covers the detailed design of EDDs in an Appendix to Chap. 13.

As mentioned in Ref. [167], in the case of Europe efforts have been focused in developing codes for base isolation in some countries such as Italy or the Russian Federation. In the case of EDDs, the developments have been limited to guidelines rather than codes or official standards. The (draft) version of Eurocode 8 of the year 2003 (Ref. No: prEN 1998-1:2003 E) [75] contains the Chapter 10 devoted to Base isolation systems, but no guidelines or recommendations are made for other kind of passive control.

In the case of Japan a fully review of the state of the art in passive control of structures is given in [239], however, no mentions are made in this work to available codes, standards or guidelines for practitioners.

As it can be concluded from the existing codes, guidelines and technical literature, a great part of the design methods proposed for RC (or steel) structures are based on supposing that the behavior of the bare structure remains in the elastic range, concentrating the energy dissipation demands on the control system. However, even though this assumption can be useful for a preliminary design, experimental and theoretical evidence show that inelastic behavior will occur in the main structural elements during severe strong motion as noted by Shen and Soong in Ref. [209]. Therefore, these authors recommend to eliminate the assumption of a linear structural response and propose a design method based on the damage control. However, it is widely recognized that nowadays it is possible to carry out nonlinear time-history analysis, which can provide a most precise and complete evaluation of the responde of structural systems incorporating EDDs (see [26, 165, 235]), but it also requires relatively large amounts of analysis expertise and computational time. It is also recognized that equivalent linear static or dynamic procedures require the least amount of time and computational effort, but they are not able to represent the complexity of the nonlinear dynamic behavior of RC structures. Regarding the most adequate kind of analysis for simulating the response of RC building with dissipators, the FEMA code recommends the use of a combination of rationality and admissible computational cost. The code describes four different types of analysis procedures: (1) linear static; (2) linear dynamic; (3) nonlinear static; and (4) nonlinear dynamic analysis. Linear methods are based on force reduction factors and can be applied subjected to limitations specified in the code [232]; in other cases, nonlinear analysis have to be carried out.

Independently of the type of analysis chosen, it is clear that the nonlinear time history analysis has gained space in the passive control of RC structures subjected to earthquakes; therefore, sophisticated numerical tools became more necessary for both academics and practitioners. For example, Lu presents in Ref. [142] a comparative study between numerical simulations and experimental tests carried out on scaled RC structures. During the last decades, great efforts have been done in developing numerical formulations and their implementation in computer codes for simulating the nonlinear dynamic response of RC structures; a recent state of the art review for the case of concrete structures can be found in Ref. [225]. The engineering community agrees with the fact that the use of general fully three-dimensional numerical technics, such as finite elements (FE) with suitable constitutive laws, constitute the most precise tools for the simulation of the behavior of RC buildings subjected to

earthquakes [110, 223, 227] or to other kind of loads [126]. However, usually the computing time required when using full models of real structures make their application unpractical. Several approaches have been developed to overcome this difficulty; some authors propose the use of the so called *macro–elements*, which provide simplified solutions for the analysis of large scale problems [68, 70, 76]. Considering that most of the elements in RC buildings are columns or beams, one dimensional formulations for structural elements, obtained throughout the reduction of spatial dimensions by means of kinematic assumptions [7], appear as a solution combining both numerical precision and reasonable computational costs [163]. Experimental evidence [38] shows that nonlinearity in beam elements can be formulated in terms of cross sectional forces and/or moments and displacements and/or curvatures, which is frequently quoted in literature as *plastic hinges* models [59, 77]. Some formulations of this type have been extended to take into account geometric nonlinearities [222, 236, 237] allowing to simulate the P–$\Delta$ effect, which occurs due to the changes of configuration of the structure during the earthquake [49, 93, 242]. Several limitations have been reported to this kind of models, specially for the modeling of RC structures with softening behavior in the dynamic range [230]. A discussion about topics such as step by step methods, path bifurcation, overall stability, limit and deformation analysis in the context of the plastic-hinges formulation for beam structures can be consulted in Ref. [58]. An additional refinement is obtained considering inhomogeneous distributions of materials on arbitrarily shaped beam cross sections [235]. Specific numerical models based on a secondary discretization of the beam cross sections have been developed allowing to include multiple materials. In this case, the constitutive force-displacement and/or moment–curvature relationship at cross sectional level is deduced by integrating the stress field over selected points on the cross section. Therefore, using this approach, the mechanical behavior of beams constituted by complex combinations of materials, such as RC beams, can be simulated [33, 94]. In general, the engineering community agrees with the fact that, although this models are more expensive in terms of computational cost than the plastic-hinges ones, they allow to estimate more precisely the response nonlinear response of RC and other kind of structures [69, 230]. Formulations of this kind considering both constitutive and geometric nonlinearity are rather scarce [72]; moreover, most of the geometrically nonlinear models for beams are limited to the elastic range of materials, as it can be consulted, for example, in Refs. [104, 159, 212] and the treatment of constitutive nonlinear behavior has been mainly restricted to plasticity [43, 92]. A theory for the stress analysis of composite beams is presented in Ref. [83], however, the formulation is only valid for moderated rotations and the behavior of the materials remain in the elastic range. Recently, Mata *et al.* [163, 164] have extended the geometrically exact formulation for beams due to Reissner and Simo [192, 193, 212, 219, 220] but considering an arbitrary distribution of composite materials on the cross sections for the static and dynamic cases.

From the numerical point of view, the nonlinear behavior of EDDs has been usually described in a global sense by means of force–displacement or moment-curvature relationships [223] which intend to capture appropriately the force/moment level and the energy dissipating capacity existing in the devices. That is, a rather simplified description appears to be enough for the mechanical characterization of EDDs, independently on the micro-mechanisms involved in the energy dissipation or in the stress distribution of each of their components [162].

The inclusion of EDDs in a software package for the seismic analysis of RC structures is frequently done by means of link elements equipped with the mentioned nonlinear relationships [223]. In this way, the link elements connect the different points of the structural model which represent the anchorage points of the EDDs in the real buildings. During the seismic event, the relative displacement and/or rotation between the anchorage points activates the dissipative mechanisms of the devices [239].

Nowadays, there are several numerical codes available for the study of the nonlinear seismic response of RC structures with EDDs. For example, a detailed presentation of a computer program able to simulate the static and dynamic (seismic) behavior of different types of buildings with EDDs is presented in Ref. [235]. Other softwares such as those described in Refs. [66, 67, 82] have incorporated different kinds of inelastic analysis including beam element with plastic–hinges and specific link elements for EDDs. A comparative study of the performance of different commercial software packages for simulation the P–$\Delta$ effect in structures can be consulted in Ref. [205].

In this work, a state of the art review of the current nonlinear methods for the determination of the seismic response of RC buildings equipped with EDDs is performed. The layout of the article is as follows:

In Sect. 2 the most commonly used types of EDDs are described, explaining their work mechanism, advantages, limitations and the numerical models available for their incorporation in computational simulations. Section 3 is devoted to the revision of the different approaches followed for simulating the dynamic inelastic response of structures composed by beam elements. Special attention is paid to the most advanced formulations, which can take into account both geometric and constitutive sources of nonlinearity. A special element for EDDs is described considering as beam element without rotational degrees of freedom. Aspects such as kinematics, strain and stress measures and consistent linearization are also covered. Section 4 regards to the treatment of constitutive laws for composite materials. A detailed

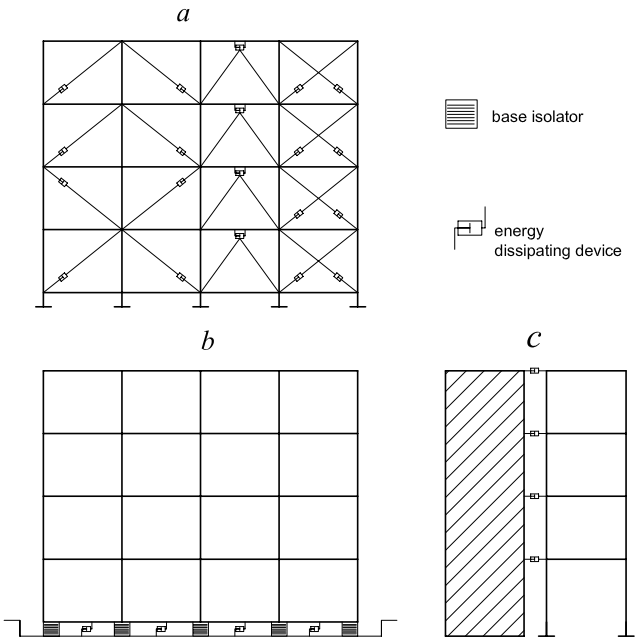


**Fig. 1** EDD's location in buildings. (**a**): Diagonal elements. (**b**): Base level elements. (**c**): Connecting elements

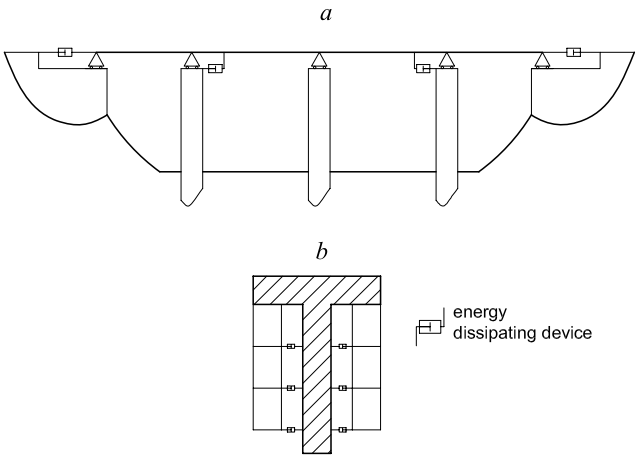


**Fig. 2** EDD's location in a bridge. (**a**): Longitudinal direction. (**b**): Transversal direction

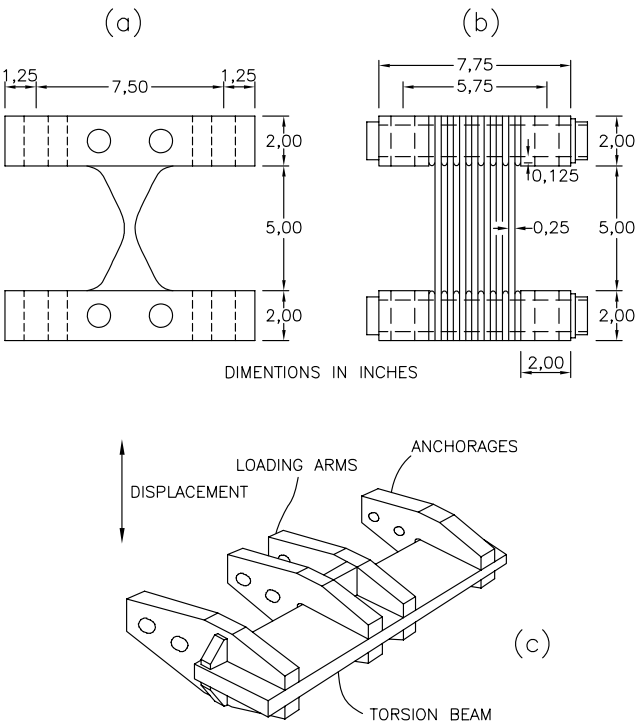


**Fig. 3** Plastic devices. (**a**, **b**): ADAS devices, front and lateral views. (**c**): Torsional beam

description of cross sectional analysis is presented. A brief presentation of damage indices capable of estimate the remaining load carrying capacity of buildings is also given. Section 6 is devoted to time stepping schemes including the updating procedures for the kinematic variables. The discretization by means of the FE method and the numerical implementation is explained in 7. Finally, in Sect. 8 some numerical examples showing the ability of the described formulations in simulating the dynamic inelastic response of RC buildings with and without EDDs are provided.

## 2 EDD's in RC Building Structures

EDDs are located in the structure to absorb and dissipate an important part of the energy input induced in the structure by earthquakes or other dynamic actions (*e.g.* hurricanes or machinery induced vibrations). Figures 1a–c, 2a–b show the location of several types of energy dissipating devices. There are a great number of available EDDs, a tentative classification can be seen in Soong and Dargush [223]. In following, five types are identified according to their working mechanism:

### 2.1 Metallic Devices

In the case of metallic devices, energy dissipation depends upon plastic deformation of metallic materials, such as mild steel or aluminium [223]. A large set of possible geometries have been used, which includes torsional beams, U-strips, braced systems etc. As an example, Figs. 3a–b show the geometric characteristics of X-shaped (ADAS) devices and 3c a torsional beam.

A large set of mathematical models have been developed for describing the force-displacement relationship of metallic devices [241]. In any case, classical plasticity models can provide good results [145, 215]. Specific design methods for incorporating metallic dissipators in structures can be consulted in [169]. An example of the effects of several types of devices, including metallic ones, is presented in [154].

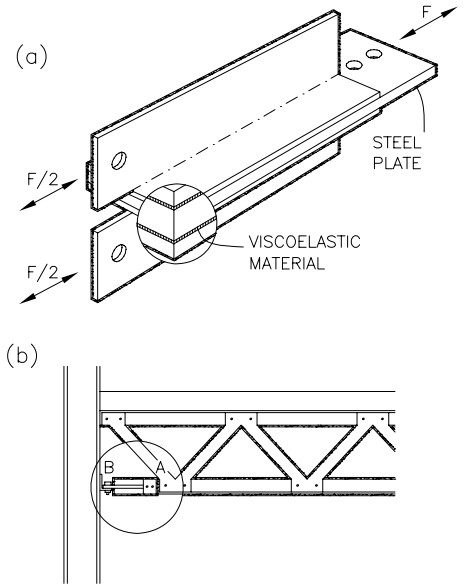


**Fig. 4** VED. (**a**): Device. (**b**): Location in a building

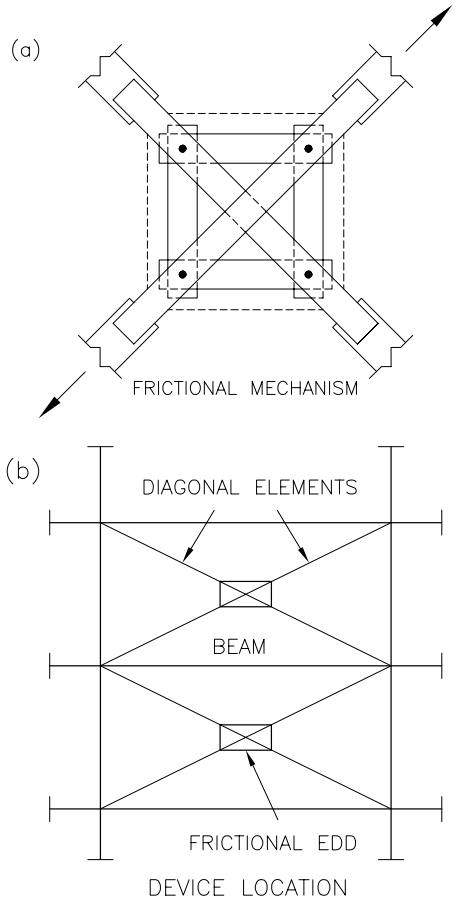


**Fig. 5** FD. (**a**): Device. (**b**): Location on a typical building

### 2.2 Visco Elastic Devices

Visco elastic dampers (VED) use polymeric materials which dissipate energy when subjected to shear deformations. Originally, applications for controlling vibration were focused on the aircraft and aerospace industry and more recently on earthquake engineering. The main effects and benefits are due to the fact that VDEs increases the global damping of the structures [122].

A typical VED is depicted in Fig. 4a; it consists of visco elastic layers bounded with steel plates and its typical location in a building is shown in 4b. Dissipation in the VED layers reduces the relative motion between elements of the structure.

In general, the shear stress-strain relationship is frequency and temperature dependent as it can be consulted in [162, 223]. A detailed study about the modeling of the dynamic properties of filled rubber is presented in [1]. Asano *et al.* [18] carry out the experimental study of visco elastic dampers and formulate an analytical model. Kojima and Yoshihide [125] study the performance and durability of high damping rubber bearings for earthquake protection. Other analytical models for visco elastic materials can be consulted in [102, 161]. Design recommendations for buildings incorporating VED can be consulted in [121, 223].

### 2.3 Friction Devices

Friction dampers (FD) dissipate energy throughout the friction that develops between two solid bodies sliding relative each to the another. The force developed in the devices depends on the friction coefficient between the materials and on the normal force, according to the well known Coulomb's law [223]. Several geometric choices have been proposed; for example, in Fig. 5a a FD based on the relative motion of two diagonal element enclosed by two steel plates is shown; Fig. 5b shows the location of the devices in a typical frame.

The numerical modeling of their behavior is commonly based on the use of bilinear hysteretic rules; however, more complications can appear in the numerical study of the seismic response of buildings with FDs. Aiken *et al.* [5] study the seismic response of a nine-story steel frame with FDs located in the cross-bracing system. Ryan and Chopra [202] estimate the seismic displacement of friction pendulum isolators based on time history responses obtained from nonlinear analysis. Additional references can be consulted in the same works.

### 2.4 Fluid Based Devices

Fluids can also be used as basic material in order to control the seismic response of flexible structures. The original efforts have been oriented toward converting the applications developed for the military and heavy industry to the civil engineering field. Several application of this kind of devices have been focused on the control of vibrations derived

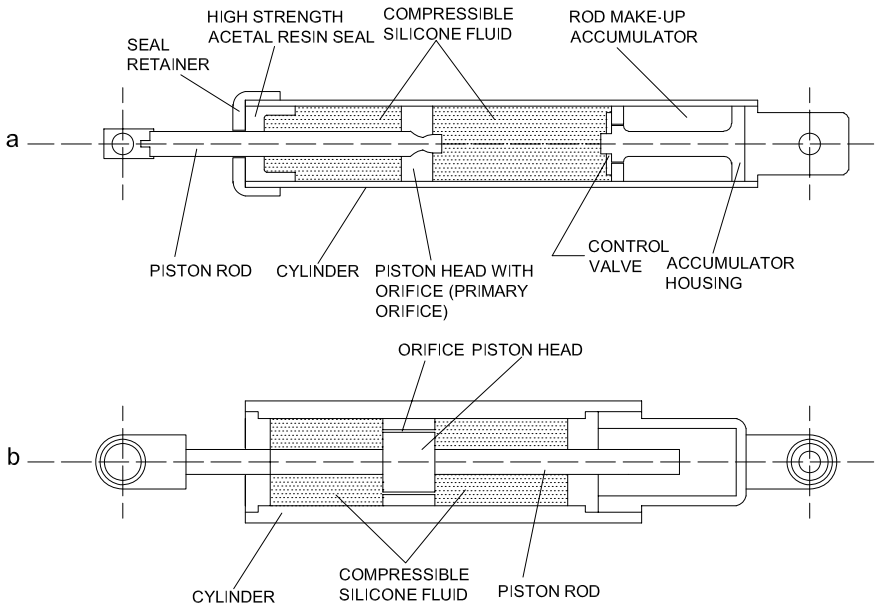


**Fig. 6** Typical VFD. (**a**): Device based on a highly compressible fluid. (**b**): Device based on the flow of fluid throughout orifices

from shock and ambient excitations. For example, the fluid damper technology is described in a wide context in [130].

Viscous fluid dampers (VFD) dissipate energy when subjected to a velocity input. Usually, dissipation occurs due to the conversion of the mechanical work of a piston moving in a highly viscous fluid, such as silicon gel, into heat. In general, VFDs act forcing the fluid to pass throughout small orifices by mean of a piston [223]. Larger viscosity values imply a greater energy dissipation. Materials which exhibits both frequency and temperature dependency are currently used.

Several kinds of devices have been proposed as VFD; for example, the behavior and effectiveness of viscous–damping walls [169] in controlling wind-induced vibrations in multistory buildings is investigated in [245]. Other applications combine base isolation systems with VFD for controlling the lateral displacement of base isolated building. In this case, the VFDs increase the damping of the isolation system. Figure 1b shows several VFDs working in parallel with the base isolation system.

Figure 6 show two typical longitudinal sections of VFDs. Both consist of a stainless steel piston with an orifice head and are filled with viscous liquid, such as silicon oil. One of them has an accumulator while the other has a run-through rod instead. The difference of pressure between each side of the piston head results in the damping force, and the damping constant of the damper can be determined by adjusting the configuration of the orifice of the piston head. The device of Fig. 6a contains compressible silicone oil.

Practical applications of this kind of EDD can be reviewed in [234, 246]. Analytical and experimental studies to evaluate a strategy for structural health monitoring of nonlinear viscous dampers are presented in [243]. An extensive overview of the testing program for the viscous dampers used in the retrofit of the Golden Gate Bridge is provided in [4].

### 2.5 Extrusion Dissipators

A particular case of metallic devices are the extrusion dissipators. The energy dissipation is produced by the rearrangement of the crystalline red of special metals (such as lead) due to the imposition of a deformation (extrusion) but maintaining confined the dissipative nucleus of the device.

Figure 8a shows a typical extrusion device while in 8b the experimental force-displacement hysteretic curve is given [186, 197].

Additional types of devices can be added to the present list. For example, *Tuned Mass* dampers are devices are added to the structures with the objective of receive and dissipate a part of the vibrational energy. In the simplest case they can be modeled as a spring–dashpot system attached to the main structure. Usually, tuned mass dampers contribute to reduce the structural response in the fundamental mode of vibration and, therefore, for environmental actions with a wide frequency content, they are used in combination with other types of devices [223, 224].

## 3 Nonlinear Models

The numerical simulation of the seismic nonlinear response of RC beam structures has constituted a very active field in structural analysis, computational mechanics and earthquake engineering. The sophistication of the numerical models has been increased as the capacity of the computers has grown and, today, it is possible to find beam models

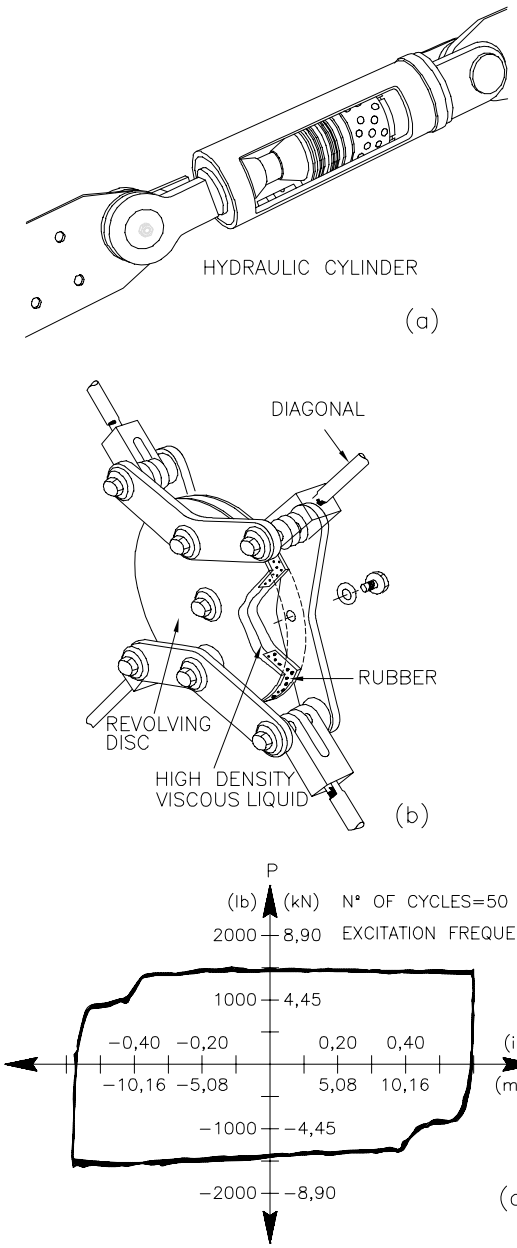


**Fig. 7** Hydraulic dampers. (**a**): Cylinder. (**b**): Revolving disc device. (**c**): Force-displacement characteristic curve

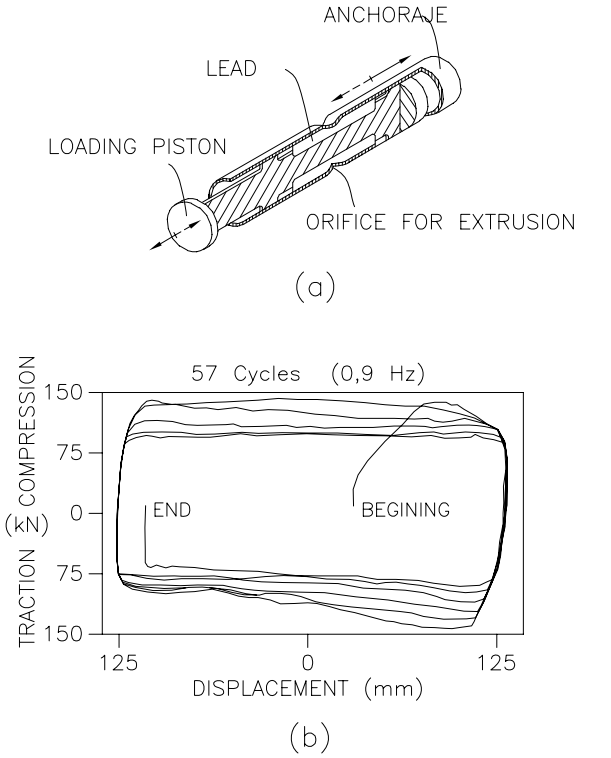


**Fig. 8** Lead extrusion dampers. (**a**): Device. (**b**): Force-displacement characteristic curve

able to consider both geometric and constitutive nonlinearity with a solid thermodynamical basis [163, 164]. Therefore, it is a hard, if not an impossible, task to make an exhaustive presentation of all possible alternatives for the numerical simulation of the dynamic behavior of RC structures with EDDs. For example, a brief summary of the different methodologies used for the seismic analysis of RC structures is given in Ref. [78]. In this section the main approaches are described highlighting their advantages and limitations.

### 3.1 RC Beam Structures

The inclusion of constitutive nonlinearity in beam models has been carried out based on two different approaches: the *lumped* and *distributed* models [184]. Experimental evidence shows that inelasticity in beam elements can be formulated in terms of cross sectional quantities and, therefore, their behavior can be described by means of *concentrated* (lumped) models, some times called *plastic hinges*, which focalize all the inelastic behavior at the ends of linear elastic structural elements by means of *ad-hoc* force-displacement or moment-curvature relationships (see *e.g.* Bayrak and Sheikh [38] or Lubliner [145], among many others). It is important to note that, in this case, the constitutive laws are valid only for specific geometries of the cross section and, in many cases, the mechanical behavior of the cross sections in their two perpendicular directions is completely uncoupled. For example in the work of Kwank and Kim [127] a moment-curvature relationship is defined for the study of reinforced concrete (RC) beams subjected to cyclic loading. This method is recommended by certain authors due to its numerical efficiency when compared with the full three-dimensional formulation of the nonlinear problem. It is important to stand out that the computational efficiency becomes a determining factor when the numerical models are used in the study of a great number of real structures subjected to several seismic actions.

On the other hand, in the distributed models, a set of cross sections along the beam axis is selected and the nonlinear constitutive behavior has to be calculated in a number of control points located on them. Each control point corresponds to a fiber directed along the beam axis and due to this reason, this approach is frequently quoted in the literature as *fiber approach* [208]. In this way, as the loading level is increased (and then the strain level on points of the selected cross sections) the inelasticity can be *distributed* along the structural element. It is widely accepted that the employment of fibers allows to obtain more realistic estimations of the evolution of the strain-stress state at cross sectional level, but it requires the definition of constitutive laws for each fiber, increasing significatively the computational cost during calculations. A common limitation of the distributed formulations is given by the fact that, the constitutive nonlinearity is limited to the component of the stress vector in direction normal to the cross section and the shearing components of the stress are treated elastically. This assumption does not considers the nonlinear coupling existing with the other stress components, resulting in models where cross sectional shear forces and torsion moments are transmitted elastically across the elements [69, 171]. An example is given by Mazars *et al.* [166] where a refined fiber model is used for the analysis of concrete elements including torsion. Monti and Spacone [170] use a fiber beam element for considering the *bond-slip* effect in reinforced concrete structural elements. In most of the cases, both types of models, the concentrated and the distributed ones, have been formulated under the hypothesis of infinitesimal deformation.

As consequence of the uncoupling between normal and tangential components of the cross sectional stress field, the mode of failure of the elements is predefined[1], limiting the participation of shear forces only to the obtention of the equilibrium [69]. Some examples of numerical works using this type of models for the study of the seismic behavior and the (static) collapse loads of RC buildings can be found in Refs. [71, 124], respectively.

Two versions of the distributed plasticity models can be found in literature: the *stiffness* (displacement based) [148] and *flexibility* (force based) methods [29, 172, 184]. The first one is based on the interpolation of the strain field along the elements. A precise representation of forces and moments requires a refined FE mesh for each structural element in which inelastic behavior is expected to appear. In the second method, the sectional forces and moments are obtained interpolating the nodal values and satisfying the equilibrium equations even in the nonlinear range [207].

As it will be explained in more detail in Sect. 4, realistic simulations of the dynamic behavior of RC structures require taking into account constitutive laws for materials which exhibits softening behavior [164, 175]. This situation inevitably leads to the localization of the strains in the volume associated to a specific cross section undergoing softening behavior. An extensive review of the strain localization in force-based frame elements is presented by Coleman and Spacone in [59]. Then, the structural response becomes mesh dependent if no appropriate corrections are considered for ensuring the *objectivity*[2] of the response. Different approaches has been developed for obtaining a *mesh-independent* response, for example in Ref. [207] a new integration method for force based elements is proposed; in Ref. [25] the energy dissipated at material point level is regularized according to the specific fracture energy of the material [175] ensuring that the global structural response remains objective, but the length of the softening zone keeps being mesh dependent. Other recent approaches applies strong discontinuities in the study of beam structures with softening behavior but in this case the fractured length is reduced to zero [14]. Theoretical works about this topic are given in [13, 73] for a plastic hinge model incorporated into a infinitesimal formulation for Euler-Bernoulli beams.

As it has been detailed in Refs. [163, 164] in the most of the cases, both concentrated and distributed models, are formulated under the small strain and small displacement kinematic hypothesis, neglecting geometric nonlinearity. These assumptions does not allows to consider the fact that normally, second order effects are coupled with constitutive nonlinearity in RC structures subjected to earthquake loading. On the other hand, geometrically nonlinear beam models have been mainly focused on the elastic case with simplified linear constitutive relations in terms of cross sectional quanties [173].

Geometric nonlinearity in rod elements has been developed by two different approaches: (i) The so called *inexact* or *co-rotational* formulations which consider arbitrarily large displacements and rotations but infinitesimal strains and (ii) the *geometrically exact* formulations obtained from the full three dimensional problem by means of a reduction of the dimensions obtained imposing adequate restrictions on the kinematics of the displacement field.[3]

A complete survey about the co-rotational techniques for rod elements is carried out in the textbooks of Crisfield [62] in Chaps. 7 and 17 for static problems and Chap. 24 for the dynamic case; which also includes in Chap. 16 a complete review of the mathematical treatment for large rotations from an engineering point of view. The classical text-

[1] Classically, it corresponds to the formation of a plastic hinge.

[2] Note that in this case, the term *objectivity* is used for referring to a mesh independent response of the structure in stead of the usual sense in continuous mechanics where it refers to an invariant response under rigid body motions.

[3] Other approaches such as the core-congruential formulation for beam finite elements can also be consulted *e.g.* in [81].

books of Bathe [31] and Hughes [101] consider the formulation of beam elements with different degrees of detail. Specific research papers are also available *e.g.* in Ref. [63] where the dynamics of the co-rotated beam models is investigated. Hsiao *et al.* [100] develop a consistent co-rotational finite element formulation for geometrically nonlinear dynamic analysis of 3D beams. Battini and Pacoste [34] develop co-rotational beam elements with warping effects for the study of instabilities problems.

Considering the many works devoted to the topic and the wide range of applications, probably the more successful formulations are the geometrically exact ones [159]. The theoretical basis for the process that makes the dimensional reduction for obtaining rod models can be consulted in the book of Antman [7]. An additional work of the same author covering invariant dissipative mechanism for the motion of artificially damped rods can be reviewed in Ref. [8]. A theoretical discussion about the dimensional reduction using nonconvex energy is given in [51]. A complete work about the exact theory of stress and strain in rods and shells can be consulted in the text of Ericksen and Truesdell [74].

Zupan and Saje [250] develop a FE formulation of geometrically exact rods based on interpolation of strain measures; in Ref. [253] the linearized theory is considered and in [251] a rod formulation based on curvature is presented. In Ref. [206] a rod element based on the interpolation of the curvature is developed. Hjelmstad and Taciroglu [99] develop a mixed variational methods for finite element analysis of geometrically nonlinear Bernoulli-Euler beams. Complementarily, theoretical works are also available (see *e.g.* Refs. [111, 128, 139] among others). The nonlinear equations for thin and slender rods are developed in [188, 191], respectively. Rosen *et al.* [200] develop a general nonlinear structural model of a multirod systems. A theoretical work about constitutive relations for elastic rods is developed by O'Reilly in Ref. [182]. Simmonds [211] discusses the possibility of developing a nonlinear thermodynamic theory of arbitrary elastic beams.

The most invoked geometrically exact formulation is that originally proposed by Simo [212] which generalize to the three dimensional dynamic case the formulation originally developed by Reissner [192, 193] for the plane static problem. This formulation should be regarded as a specific parametrization of a three-dimensional extension of the classical Kirchhoff–Love [141] model employing a *director type* approach for describing the time varying configuration of the beam cross sections (see also Antman [7]). Posteriorly, Simo and Vu-Quoc [219, 220] implemented the corresponding numerical integration of the equations of motion, using the FE, for the static and dynamic cases. They have considered a straight and unstressed rod as reference configuration and the hypothesis of planar sections.

Posteriorly, Ibrahimbegović extends the formulation given in Ref. [212] to the case of an initially curved and twisted reference configuration of the beam [104] and proposes an alternative parametrization of rotations [105]. Li [134] and Kapania and Li [117, 118] develop a careful presentation of the initially curved and twisted rod theory based on the principles of the continuum mechanics. Jelenić and Saje [112, 114] develop a formulation eliminating the rotational variables of the model and avoiding thus the shear locking phenomenon. The usual FE procedures violate the objectivity condition of the strain measures; In Refs. [64, 113] several solutions are proposed for this problem. Additional numerical work to obtain frame indifference of the strain measurements are presented by Betsch and Steinmann [41].

A formulation equivalent to that proposed by Simo has been employed by Cardona and Gerardin [53]. In Ref. [54] this formulation is used for evaluating the bifurcation points of flexible mechanisms. Ibrahimbegović *et al.* [106] employ their own formulation for studying the buckling and post buckling behavior of framed structures. Vu-Quoc and Li in [238] use the Reissner–Simo formulation for studying the some complex dynamic problems observed in the behavior of sliding beams.

Simo *et al.* extend [221] the formulation of rod elements with warping of arbitrary cross sections considering a small strain formulation for elastic visco plastic constitutive materials. An outstanding work studying the warping of cross sections made of elastic plastic materials is due to Gruttmann *et al.* [90, 92]. The FE analysis of the Saint Venant torsion problem considering the exact integration of the elastic plastic constitutive equations is developed in Ref. [240]. Nukala and White [173] develop a mixed finite element for studying the stability behavior of structures. Isotropic hardening is included in the model presented by Park and Lee [185]. Shi and Atluri [210] employ a plastic hinge formulation for the elastic plastic analysis of space–frames considering large deformations. Recently, Mata *et al.* [163, 164] have extended the geometrically exact formulation for rods due to Reissner and Simo to include an arbitrary distribution of composite materials with inelastic constitutive laws on the cross sections for the static and dynamic cases; thermodynamically consistent constitutive laws of visco damage and plasticity are developed in terms of the material form of the *first Piola Kirchhoff* stress vector in the framework of the *mixing theory* for composites. Other kind of beam theories can be formulated starting from the variational asymptotic method (VAM) (see *e.g.* [56, 189, 247]). Some of these techniques has been successfully adapted for the analysis of the deformation field in beam cross sections [248].

In following, the geometrically exact Reissner-Simo formulation for beams is described for the case when plane cross sections remain plane during the motion and considering an intermediate initially curved and twisted reference configuration. This formulation has been selected for due to

its versatility for simulating very large changes of configuration and its relative simplicity. The formulation is extended, considering constitutive nonlinearity at material point level according to the results given in [163, 164].

### 3.1.1 Kinematics

One of the main conceptual difficulties arising in the Reissner–Simo formulation is due to the fact that the resulting configuration space for the rod in no longer a linear space but a infinite-dimensional nonlinear differentiable manifold. Concretely, the mentioned manifold is obtained by the pairing $\mathbb{R}^3 \times SO(3)$, where $SO(3)$ is the rotation group [11]. Therefore, the application of the standard techniques of continuum mechanics and numerical methods has to be carried out taking into account the intrinsic nonadditive nature of a part of the kinematics of the rods. Other earlier works on finite deformation of rod elements can be found in the works of Atluri and Vasudevan [20], Bathe and Bolourchi [32], Iaura and Atluri [103] and Meek and Loganathan [168] among others.

As it will be explained in next sections, the configuration manifold of the rod model involves large rotations and literature about the parametrization of the rotational motion can be found in the papers of Bauchau and Trainelli [37], Trainelli [233], Bauchau and Choi [35], Argyris [10], Argyris and Poterasu [11] and Grassia [89], among many others; about the coupling between large displacements and rotations of displacement fields in solid mechanics in [19]; and on the Lie group methods for rigid body dynamics in [55].[4]

Let $\{\hat{E}_i\}$ and $\{\hat{e}_i\}$ $(i = 1 \ldots 3)$ be the *material* and *spatial* frames respectively, corresponding to spatially fixed coordinate systems. Lets introduce the following three configurations:

(1) The *straight reference beam* is defined by the curve $\hat{\varphi}_{00} = S\hat{E}_1$, with $S \in [0, L]$ being the arch-length coordinate on the curve. Cross sections are described by means of the coordinates $\xi_\beta$ directed along the axis $\{\hat{E}_{\beta=2,3}\}$ and the position vector of any material point on the cross section is $\hat{X} = \xi_i \hat{E}_i$ $(\xi_1 \equiv S)$.

(2) The *initially curved reference beam* is defined by a fixed curve with its position vector given by $\hat{\varphi}_0(S) = \varphi_{0i}(S)\hat{e}_i$, where $S$ is defined as before and the total length of the curve coincide with $L$. Each point on this curve has rigidly attached an orthogonal triad $\hat{t}_{0i}(S) = \mathbf{\Lambda}_0 \hat{E}_i$, where $\mathbf{\Lambda}_0 \in SO(3)$ is the orientation of the plane of the cross section.[5] The beam cross section is described by $\xi_\beta$ but directed along $\{\hat{t}_{0\beta}\}$ and initially, one has the condition[6]: $\hat{\varphi}_{0,S} = \hat{t}_{01}$. Then, the position vector of any material point on the curved reference beam is

$$\hat{x}_0 = \hat{\varphi}_0 + \hat{\mathcal{T}}_0 = \hat{\varphi}_0 + \mathbf{\Lambda}_0 \hat{\mathcal{E}}, \tag{2}$$

where $\hat{\mathcal{E}} \equiv \xi_\beta \hat{E}_\beta$ is the position vector of a material point referred to $\hat{\varphi}$.

(3) *Current beam*. Due to the motion, the curved reference beam is moved from $\hat{\varphi}_0(S)$ to $\hat{\varphi}(S,t) = \hat{\varphi}_0(S) + \hat{u}(S,t)$ at time $t$; where $\hat{u}(S)$ is the translational displacement. At the same time $\mathbf{\Lambda}_0(S)$ is rotated together with the cross-section to $\mathbf{\Lambda}(S,t) = \mathbf{\Lambda}_n \mathbf{\Lambda}_0$ by means of the *incremental rotation tensor* $\mathbf{\Lambda}_n \equiv \hat{t}_i \otimes \hat{E}_i$ which determines the new orientation of the cross section at time $t$. In general, the normal vector $\hat{t}_1$ does no coincides with $\hat{\varphi}_{,S}$ because of the shearing [103]. The current position vector of any material point is

$$\hat{x}(S, \xi_\beta, t) = \hat{\varphi}(S,t) + \hat{\mathcal{T}}(S, \xi_\beta, t) = \hat{\varphi} + \mathbf{\Lambda}\hat{\mathcal{E}}. \tag{3}$$

Figure 9 shows a description of the beam configurations involved in the formulation. Therefore, the current beam configuration is completely determined by pairs with the following form: $\hat{\Phi} \equiv (\hat{\varphi}, \mathbf{\Lambda})$ [152, 219]. The *spatial placement*

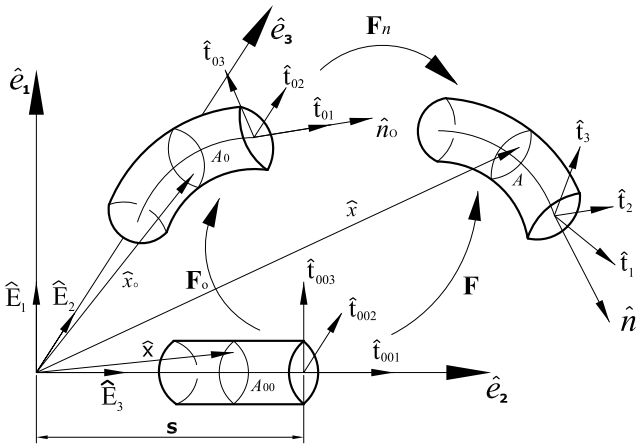


**Fig. 9** Configurational description of the beam

[4] Additionally, a survey about integration of differential equations on manifolds can be reviewed in [50]. About the parametrization of finite rotations in computational mechanics in [40, 152]. Ibrahimbegović in [105] presents a discussion about the choice of finite rotation parameters. Gerardin and Cardona [86] employ a Quaternion algebra for parameterizing the kinematics and dynamics of rigid and flexible mechanisms. Ritto-Corrëa and Camotin in [196] develop a complete survey about the differentiation of the Rodrigues's formula and its significance for the vector-like parametrization of Reissner–Simo theory. An analysis about the interpolation of rotations in rod theories is given in [198]. A classical work about the parametrization of the rotation group is provided by Stuelpnagel in Ref. [229].

[5] It is worth to note that $\mathbf{\Lambda}_0$ is an element of $SO(3)$ and therefore, the configuration of the curved reference beam is described in $\mathbb{R}^3 \times SO(3)$; [212, 219].

[6] $(\bullet)_{,x}$ denotes partial differentiation with respect to $x$.

*of the beam*, $\mathcal{B}_t$, is the set composed by all the spatial points $\hat{x}$ defined according to (2), such that $(S, \xi_\beta) \in [0, L] \times \mathcal{A}$. The *tangent space* to $\mathcal{B}_t$ at $\hat{x}$ is given by $T_x\mathcal{B}_t := \{\hat{\zeta} \in \mathbb{R}^3 \mid \hat{x} \in \mathcal{B}_t\}$, *i.e.* the set formed by three-dimensional vectors emanating from $\hat{x}$.

### 3.1.2 Strain and Strain Rate Measures

Starting from the determination of the deformation gradient of the current beam configuration relative to the curved reference beam, $\mathbf{F}_n$, it is possible to calculate the spatial form of strain vector acting on the plane of the beam cross section as [117, 118, 163, 219]

$$\hat{\varepsilon}_n = f_0(\hat{\gamma}_n + \widetilde{\boldsymbol{\omega}}_n \hat{\mathcal{T}}), \tag{4a}$$

$$\hat{\gamma}_n = \hat{\varphi}_{,S} - \hat{t}_1, \tag{4b}$$

$$\widetilde{\boldsymbol{\omega}}_n = \boldsymbol{\Lambda}_{n,S}\, \boldsymbol{\Lambda}_n^T, \qquad \hat{\omega}_n = \text{axial}[\widetilde{\boldsymbol{\omega}}_n], \tag{4c}$$

where $f_0 = |\mathbf{F}_0|^{-1}$ is the inverse of the determinant of $\mathbf{F}_0$ (relative to the curved reference configuration), $\hat{\gamma}_n$ is the spatial form of the reduced translational strains and $\widetilde{\boldsymbol{\omega}}_n$ is the spatial form of the curvature (skew-symmetric) tensor of the current beam configuration relative to the curved reference beam with its associated axial vector given by $\hat{\omega}_n$. The corresponding material forms are calculated employing the pullback by $\boldsymbol{\Lambda}$, and they are given by

$$\hat{\mathcal{E}}_n = \boldsymbol{\Lambda}^T \hat{\varepsilon}_n = f_0(\hat{\Gamma}_n + \widetilde{\boldsymbol{\Omega}}_n \hat{\mathcal{E}}), \tag{4d}$$

$$\hat{\Gamma}_n = \boldsymbol{\Lambda}^T \hat{\gamma}_n = \boldsymbol{\Lambda}^T \hat{\varphi}_{,S} - \hat{E}_1, \tag{4e}$$

$$\widetilde{\boldsymbol{\Omega}}_n = \boldsymbol{\Lambda}^T \widetilde{\boldsymbol{\omega}}_n \boldsymbol{\Lambda} = \boldsymbol{\Lambda}_n^T \boldsymbol{\Lambda}_{n,S}, \qquad \hat{\Omega}_n = \boldsymbol{\Lambda}^T \hat{\omega}_n. \tag{4f}$$

The rotation tensor $\boldsymbol{\Lambda}$ is the responsible for the rigid body motion. A schematic representation of the strain vectors acting on the face of the current beam configuration is shown in Fig. 10a. Taking the time derivative of $\boldsymbol{\Lambda} = \boldsymbol{\Lambda}_n \boldsymbol{\Lambda}_0$, it is possible to obtain the spatial and material forms of the angular velocity as

$$\widetilde{\boldsymbol{v}}_n = \dot{\boldsymbol{\Lambda}}_n \boldsymbol{\Lambda}_n^T = \dot{\boldsymbol{\Lambda}} \boldsymbol{\Lambda}^T = \widetilde{\boldsymbol{v}}, \tag{5a}$$

$$\widetilde{\boldsymbol{V}}_n = \boldsymbol{\Lambda}_n^T \dot{\boldsymbol{\Lambda}}_n, \tag{5b}$$

$$\widetilde{\boldsymbol{V}} = \boldsymbol{\Lambda}^T \dot{\boldsymbol{\Lambda}} = \boldsymbol{\Lambda}_0^T \widetilde{\boldsymbol{V}}_n \boldsymbol{\Lambda}_0 = \boldsymbol{\Lambda}^T [\widetilde{\boldsymbol{v}}_n] \boldsymbol{\Lambda}, \tag{5c}$$

where $\widetilde{\boldsymbol{v}}_n = \widetilde{\boldsymbol{v}}$ is the *spin*, relative to the curved reference configuration. In the same manner, $\widetilde{V}$ and $\widetilde{V}_n$ are the material forms of the spin tensor relative to the straight and curved reference configurations, respectively. Taking the time derivative of (5a) to (5c), it is possible to calculate the acceleration tensors as [150, 163, 219]

$$\widetilde{\boldsymbol{\alpha}}_n = \dot{\widetilde{\boldsymbol{v}}}_n = \ddot{\boldsymbol{\Lambda}}_n \boldsymbol{\Lambda}_n^T - \widetilde{\boldsymbol{v}}_n^2 = \dot{\widetilde{\boldsymbol{v}}} = \widetilde{\boldsymbol{\alpha}}, \tag{6a}$$

$$\widetilde{\boldsymbol{A}}_n = \dot{\widetilde{\boldsymbol{V}}}_n = \boldsymbol{\Lambda}_n^T \ddot{\boldsymbol{\Lambda}}_n - \widetilde{\boldsymbol{V}}_n^2, \tag{6b}$$

$$\widetilde{\boldsymbol{A}} = \dot{\widetilde{\boldsymbol{V}}} = \boldsymbol{\Lambda}^T \ddot{\boldsymbol{\Lambda}} + \dot{\boldsymbol{\Lambda}}^T \dot{\boldsymbol{\Lambda}} = \boldsymbol{\Lambda}^T \widetilde{\boldsymbol{\alpha}} \boldsymbol{\Lambda}, \tag{6c}$$

where $\widetilde{\boldsymbol{\alpha}}_n = \widetilde{\boldsymbol{\alpha}}$ is the spatial acceleration tensor of the current beam cross section relative to the curved reference beam and $\widetilde{\boldsymbol{A}}_n$ and $\widetilde{\boldsymbol{A}}$ are the corresponding material forms. Their corresponding axial vectors are denoted by $\hat{v}_n = \hat{v} = \boldsymbol{\Lambda} \hat{V}$ and $\hat{\alpha}_n = \hat{\alpha} = \boldsymbol{\Lambda} \hat{A}$, respectively [104, 219]. Using (4a) to (6c) and the Lie's derivative operator [212], it is possible to calculate the time and derivatives of the translational and rotational parts of the strain vectors as [164]

$$\dot{\hat{\gamma}}_n = \dot{\hat{\varphi}}_{,S} - \widetilde{\boldsymbol{v}}_n \hat{t}_1, \qquad \dot{\hat{\Gamma}}_n = \boldsymbol{\Lambda}^T \left[\dot{\hat{\varphi}}_{,S} - \widetilde{\boldsymbol{v}}_n \hat{\varphi}_{,S}\right], \tag{7a}$$

$$\dot{\widetilde{\boldsymbol{\omega}}}_n = \widetilde{\boldsymbol{v}}_{n,S} + \widetilde{\boldsymbol{v}}_n \widetilde{\boldsymbol{\omega}}_n - \widetilde{\boldsymbol{\omega}}_n \widetilde{\boldsymbol{v}}_n, \qquad \dot{\widetilde{\boldsymbol{\Omega}}}_n = \boldsymbol{\Lambda}^T \widetilde{\boldsymbol{v}}_{n,S}\, \boldsymbol{\Lambda}, \tag{7b}$$

which can be identified as *translational* and *rotational strain rate* vectors. In the same way, the co-rotated strain rate measures are

$$[\overset{\triangledown}{\hat{\gamma}}_n] = \boldsymbol{\Lambda} \dot{\hat{\Gamma}}_n = \dot{\hat{\varphi}}_{,S} - \widetilde{\boldsymbol{v}}_n \hat{\varphi}_{,S}, \tag{8a}$$

$$[\overset{\triangledown}{\widetilde{\boldsymbol{\omega}}}_n] = \boldsymbol{\Lambda} \dot{\widetilde{\boldsymbol{\Omega}}}_n \boldsymbol{\Lambda}^T = \widetilde{\boldsymbol{v}}_{n,S}. \tag{8b}$$

The corresponding associated *rotational strain rate* vectors are

$$\dot{\hat{\omega}}_n = \hat{v}_{n,S} - \widetilde{\boldsymbol{\omega}}_n \hat{v}_n = \hat{v}_{n,S} + \widetilde{\boldsymbol{v}}_n \hat{\omega}_n, \tag{9a}$$

$$\dot{\hat{\Omega}}_n = \boldsymbol{\Lambda}^T \hat{v}_{n,S}, \tag{9b}$$

$$[\overset{\triangledown}{\hat{\omega}}_n] = \boldsymbol{\Lambda} \dot{\hat{\Omega}}_n = \hat{v}_{n,S} = \dot{\hat{\omega}}_n + \widetilde{\boldsymbol{\omega}}_n \hat{v}_n. \tag{9c}$$

Using (7a) to (9c), it is possible to construct an *objective* measure of the *strain rate* vector $\hat{s}_n$ acting on the current cross section [164] as

$$\hat{s}_n = [\overset{\triangledown}{\hat{\varepsilon}}] = [\overset{\triangledown}{\hat{\gamma}}_n] + [\overset{\triangledown}{\widetilde{\boldsymbol{\omega}}}_n]\, \hat{\mathcal{T}} = \dot{\hat{\varphi}}_{,S} - \widetilde{\boldsymbol{v}}_n \hat{\varphi}_{,S} + \widetilde{\boldsymbol{v}}_{n,S}\, \hat{\mathcal{T}}, \tag{10a}$$

$$\hat{\mathcal{S}}_n = \dot{\hat{\mathcal{E}}}_n = \boldsymbol{\Lambda}^T \hat{s}_n = \boldsymbol{\Lambda}^T \dot{\hat{\varphi}}_{,S} - \widetilde{\boldsymbol{V}}_n \boldsymbol{\Lambda}^T \hat{\varphi}_{,S} + \dot{\widetilde{\boldsymbol{\Omega}}}_n \hat{\mathcal{E}}. \tag{10b}$$

Equation (10a) corresponds to the objective strain rate measured by an observer located on $\{\hat{t}_i\}$ and (10b) is the corresponding material form obtained by using the pull-back relation between spatial and material descriptions [152].

### 3.1.3 Stresses, Stress Resultants and Stress Couples

The Cauchy stress tensor $\boldsymbol{\sigma}$ at any material point $(S, \xi_\beta)$ referred to a differential volume of the current rod cross section is given by $\boldsymbol{\sigma} \equiv \hat{\sigma}_j \otimes \hat{t}_j$ with material form given by $\boldsymbol{\Sigma} = \boldsymbol{\Lambda}^T \boldsymbol{\sigma} \boldsymbol{\Lambda}$. The term $\hat{\sigma}_j$ is the stress vector acting on the current face and referred to the *real* area of the same face of the current rod with $\hat{t}_j$ as unit normal vector.

The *first Piola Kirchhoff* (FPK) stress tensor can be written as a linear combination of stress vectors $\mathbf{P} = \hat{P}_i \otimes \hat{E}_i$, where $\hat{P}_1$ is the FPK stress vector acting on a material point

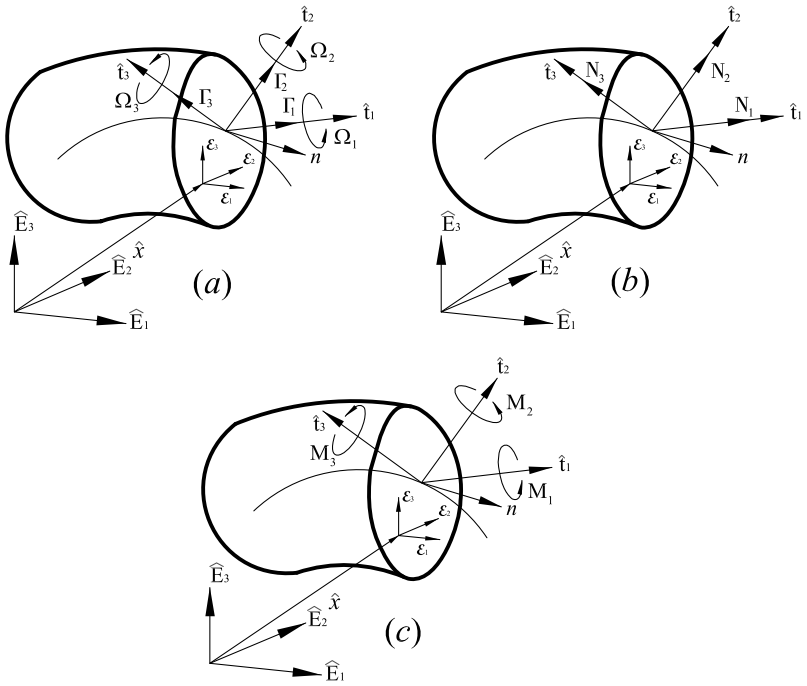


**Fig. 10** Geometric representation of (**a**): Strain vectors on the current configuration. (**b**): Stress resultants. (**c**): Stress couples

on the current cross section referred to a differential element in the undeformed cross section. In general, one has

$$\hat{P}_k = P^{\mathrm{m}}_{ki}\hat{t}_i = g_n\hat{\sigma}_k - \frac{\hat{\mathcal{E}}_{nk1}}{g_0}\hat{\sigma}_1, \qquad \hat{P}_1 = \hat{\sigma}_1,$$

where the material form of $\hat{P}_1$ is given by $\hat{P}^{\mathrm{m}}_1 = \mathbf{\Lambda}^T\hat{P}_1$.

For the purpose of presenting a reduced one-dimensional rod model, it is convenient to define the *stress resultant* which is the internal force vector acting on the current cross section and the *stress couple i.e.* the internal moment vector acting on the same cross section. The material form of the stress resultant $\hat{n}^{\mathrm{m}}(S,t)$ and stress couple $\hat{m}^{\mathrm{m}}(S,t)$ are defined as [150]:

$$\hat{n}^{\mathrm{m}} \triangleq \int_{\mathcal{A}} \mathbf{\Lambda}^T\hat{P}_1 \mathrm{d}\mathcal{A} = \int_{\mathcal{A}} \hat{P}^{\mathrm{m}}_1 \mathrm{d}\mathcal{A}, \tag{11a}$$

$$\hat{m}^{\mathrm{m}} \triangleq \mathbf{\Lambda}^T\int_{\mathcal{A}} \widetilde{\boldsymbol{\mathcal{T}}}\hat{P}_1 \mathrm{d}\mathcal{A} = \int_{\mathcal{A}} \widetilde{\boldsymbol{\varepsilon}}\hat{P}^{\mathrm{m}}_1 \mathrm{d}\mathcal{A}, \tag{11b}$$

where $\widetilde{\boldsymbol{\varepsilon}}$ is the skew-symmetric tensor obtained from $\hat{\varepsilon}$ and $\hat{P}^{\mathrm{m}}_1$ is the FPK stress vector acting in the face of the cross sectional area with normal $\hat{E}_1$. The corresponding spatial forms are given by

$$\hat{n} = \mathbf{\Lambda}\hat{n}^{\mathrm{m}} = \int_{\mathcal{A}} \hat{\sigma}_1 \mathrm{d}\mathcal{A} = \int_{\mathcal{A}} \hat{P}_1 \mathrm{d}\mathcal{A}, \tag{12a}$$

$$\hat{m} = \mathbf{\Lambda}\hat{m}^{\mathrm{m}} = \int_{\mathcal{A}} (\hat{x}-\hat{\varphi})\times\hat{\sigma}_1 \mathrm{d}\mathcal{A} = \int_{\mathcal{A}} \widetilde{\boldsymbol{\mathcal{T}}}\hat{\sigma}_1 \mathrm{d}\mathcal{A}, \tag{12b}$$

where $\widetilde{\boldsymbol{\mathcal{T}}}$ is the skew-symmetric tensor from $\hat{\mathcal{T}}$.

In (12a) and (12b) $n_1$ is the *normal* force component in the cross section with normal direction $\hat{t}_1$ while $n_2$ and $n_3$ are the *shear force* components in the directions $\hat{t}_2$ and $\hat{t}_3$, respectively; $m_1$ is the *torque* component around the normal $\hat{t}_1$ while $m_2$ and $m_3$ are the *bending moment* components around $\hat{t}_2$ and $\hat{t}_3$, respectively (see Fig. 10b–c).

### *3.1.4 Elastic Constitutive Relations*

In most of the cases, in the finite deformation theories for rods, hyper-elastic, isotropic and homogeneous materials have been assumed (see *e.g.* [81, 107, 219]) and, therefore, the reduced constitutive equations become very simple. In this section only a brief overview of elastic constitutive relations for stress resultant and stress couples is discussed.

An elastic material is said to be a *hyperelastic* or a *Green–elastic* material if a *strain energy function* per unit volume $W$ exist and the FPK stress tensor $\mathbf{P}$ can also be defined as $\mathbf{P} := \partial_{\mathbf{F}} W$, where a strain energy function invariant under rigid–body rotations has been assumed. Employing the Lie variation, pullback and push–forward operators, it is possible to write [152]

$$\delta\,[\overset{\triangledown}{W}] = (\mathbf{\Lambda}^T\mathbf{P}) : \delta(\mathbf{\Lambda}^T\mathbf{F} - \mathbf{I}).$$

Therefore, the material strain and stress tensors are defined by

$$\mathbf{\Sigma} := \mathbf{\Lambda}^T\mathbf{P}, \qquad \mathbf{H} = \mathbf{\Lambda}^T\mathbf{F} - \mathbf{I}.$$

The material stress tensor $\mathbf{\Sigma}$ can be identified with the material form FPK stress tensor and its work conjugated $\mathbf{H}$

with the material form of the strain measure $\boldsymbol{\mathcal{E}}$. Let us to consider the constitutive relation between the components of the stress tensor $\boldsymbol{\Sigma}$ and the components of $\mathbf{H}$ given by $\boldsymbol{\Sigma} = \mathcal{C}^{\mathrm{me}} : \mathbf{H}$, where the *elasticity tensor* $\mathcal{C}^{\mathrm{me}}$ is a fourth order tensor. Then, for the case of the present rod theory, we introduce the following simple linear constitutive relations in component form:

$$\Sigma_{11} = \mathrm{E} H_{11}, \qquad \Sigma_{21} = \mathrm{G} H_{21}, \qquad \Sigma_{31} = \mathrm{G} H_{31},$$

where E denotes the elastic modulus and G the shear modulus. We note that the vector $\hat{H}_{i1}\hat{E}_i$ corresponds to $\hat{\mathcal{E}}_n$ and $\hat{\Sigma}_{i1}\hat{E}_i$ to $\hat{P}_1^{\mathrm{m}} = \boldsymbol{\Lambda}^T \hat{P}_1$.

Substituting the above formulas into (11a), after integrating over the cross section, yields to the following result:

$$\hat{n}^{\mathrm{m}} = \int_{\mathcal{A}} \boldsymbol{\Sigma}_{i1}\hat{E}_i \mathrm{d}\mathcal{A} = (\mathrm{E}\mathcal{A}\hat{E}_1 \otimes \hat{E}_1 + \mathrm{G}\mathcal{A}\hat{E}_\beta \otimes \hat{E}_\beta)\hat{\mathcal{E}}. \quad (13)$$

Similarly, the material stress couple vector $\hat{m}^{\mathrm{m}}$ is obtained as

$$\begin{aligned}\hat{m}^{\mathrm{m}} &= \int_{\mathcal{A}} \widetilde{\boldsymbol{\varepsilon}}[\mathrm{E}\hat{E}_1 \otimes \hat{E}_1 + \mathrm{G}\hat{E}_\beta \otimes \hat{E}_\beta](\hat{\Gamma}_n + \widetilde{\boldsymbol{\Omega}}_n \hat{\varepsilon})\mathrm{d}\mathcal{A} \\ &= \Bigg[\left(\mathrm{G}(-1)^\beta \int_{\mathcal{A}} \xi_\beta \mathrm{d}\mathcal{A}\right)\hat{E}_1 \otimes \hat{E}_\alpha \\ &\quad + \left(\mathrm{E}(-1)^\alpha \int_{\mathcal{A}} \xi_\alpha \mathrm{d}\mathcal{A}\right)\hat{E}_\beta \otimes \hat{E}_1\Bigg]\hat{\Gamma}_n \\ &\quad + \Big[\mathrm{GI}_{\rho 0 11}\hat{E}_1 \otimes \hat{E}_1 + \mathrm{EI}_{0\alpha\beta}\hat{E}_\alpha \otimes \hat{E}_\beta\Big]\hat{\Omega}_n. \end{aligned} \quad (14)$$

In (14) the formula for the material form second (elastic) moment of inertia $\mathbf{I}_0$ has been used (see [212]).

A more general expression for the linear elastic (hyperelastic but not necessarily isotropic nor homogeneous) relation between $\hat{P}_1^{\mathrm{m}}$ and $\hat{\mathcal{E}}_n$, at any material point on the current rod cross section, is given by

$$\hat{P}_1^{\mathrm{m}} = \mathcal{C}^{\mathrm{me}}\hat{\mathcal{E}}_n, \qquad \hat{P}_1 = \mathcal{C}^{\mathrm{se}}\hat{\epsilon}_n, \quad (15)$$

where $\mathcal{C}^{\mathrm{me}} = \mathcal{C}^{\mathrm{me}}_{ij}\hat{E}_i \otimes \hat{E}_j$ and $\mathcal{C}^{\mathrm{se}} = \mathcal{C}^{\mathrm{se}}_{ij}\hat{t}_i \otimes \hat{t}_j$ are the material and spatial forms of the elastic constitutive tensors, respectively.

Substituting (15) into the formulae for the stress resultant $\hat{n}$ and stress couple $\hat{m}$ vectors in (12a) and (12b) and using the formulae for the components $\hat{\epsilon}_n$, it is possible to obtain, following analogous procedures as those given in (13) and (14), the *reduced linear constitutive relations* as

$$\hat{n} = \mathbf{C}^{\mathrm{se}}_{nn}\hat{\gamma}_n + \mathbf{C}^{\mathrm{se}}_{nm}\hat{\omega}_n, \qquad \hat{m} = \mathbf{C}^{\mathrm{se}}_{mn}\hat{\gamma}_n + \mathbf{C}^{\mathrm{se}}_{mm}\hat{\omega}_n, \quad (16a)$$

for the spatial description, and

$$\hat{n}^{\mathrm{m}} = \mathbf{C}^{\mathrm{me}}_{nn}\hat{\Gamma}_n + \mathbf{C}^{\mathrm{me}}_{nm}\hat{\Omega}_n, \qquad \hat{m}^{\mathrm{m}} = \mathbf{C}^{\mathrm{me}}_{mn}\hat{\Gamma}_n + \mathbf{C}^{\mathrm{me}}_{mm}\hat{\Omega}_n \quad (16b)$$

for the material description, where $\mathbf{C}^{\mathrm{se}}_{pq} = [\mathrm{C}^{\mathrm{me}}_{pq}]_{ij}\hat{t}_i \otimes \hat{t}_j$, $\mathbf{C}^{\mathrm{me}}_{pq} = [\mathrm{C}^{\mathrm{me}}_{pq}]_{ij}\hat{E}_i \otimes \hat{E}_j$, $\mathbf{C}^{\mathrm{se}}_{pq} = \boldsymbol{\Lambda}\mathbf{C}^{\mathrm{me}}_{pq}\boldsymbol{\Lambda}^T$ and the subscripts $p, q \in \{m, n\}$. Explicit expressions for that tensors can be found in [117, 118, 134].

If the rods are further assumed to be built of isotropic, homogeneous and linear elastic material, we may take the rod cross section geometry centroid line as the rod reference curve and align $\hat{t}_2$ and $\hat{t}_3$ to coincide with the cross section principal axes. Then, $\mathbf{C}_{nn}$ and $\mathbf{C}_{mm}$ become diagonal, and $\mathbf{C}_{nm}$ and $\mathbf{C}_{mn}$ vanish. This last simple constitutive form has been used in most of the reviewed works (see *e.g.* [103, 134, 212]) postulating the existence of a strain energy function of the form $W_{\mathrm{str}} \equiv W_{\mathrm{str}}(\hat{\Gamma}_n, \hat{\Omega}_n)$ and, therefore,

$$\hat{n}^{\mathrm{m}} \equiv \partial_{\hat{\Gamma}_n} W_{\mathrm{str}}\hat{\Gamma}_n, \qquad \hat{m}^{\mathrm{m}} \equiv \partial_{\hat{\Omega}_n} W_{\mathrm{str}}\hat{\Omega}_n, \quad (17)$$

where $\partial_{\hat{\Gamma}_n} W_{\mathrm{str}} = \mathbf{C}^{\mathrm{me}}_{nn}$ and $\partial_{\hat{\Omega}_n} W_{\mathrm{str}} = \mathbf{C}^{\mathrm{me}}_{mm}$.

## 3.2 Consistent Linearization

In this section the calculus of some admissible variations needed in the development of numerical methods for the simulation of the mechanical behavior of rod structures is presented.

### *3.2.1 Admissible Variations*

The *current configuration* manifolds at time $t$ is specified by $\mathcal{C}_t := \{(\hat{\varphi}, \boldsymbol{\Lambda}) : [0, L] \to \mathbb{R}^3 \times SO(3)\}$ which is a nonlinear differentiable manifold. It is possible to construct a *perturbed configuration* onto $\mathcal{C}_t$ as $\mathcal{C}_{t\beta} \triangleq \{(\hat{\varphi}_\beta, \boldsymbol{\Lambda}_\beta) : [0, L] \to \mathbb{R}^3 \times SO(3)\}$ obtained by setting

$$\hat{\varphi}_\beta = \hat{\varphi} + \beta\delta\hat{\varphi}, \qquad \boldsymbol{\Lambda}_\beta = \exp\big[\beta\delta\widetilde{\boldsymbol{\theta}}\big]\boldsymbol{\Lambda},$$

where $\delta\hat{\varphi} \in \mathbb{R}^3$, $\beta \in \mathbb{R}$ and $\delta\widetilde{\boldsymbol{\theta}} \in T_{\mathbf{I}}SO(3) \approx so(3)$ with the corresponding axial vectors $\delta\hat{\theta}$. It should be noted that the perturbed configuration also constitutes a possible current configuration of the rod. Alternatively, it is possible to work with the field $\hat{\eta} \triangleq (\delta\hat{\varphi}, \delta\hat{\theta}) \in T\mathcal{C}_t$ which defined the field of *kinematically admissible variations* as [150]

$$\eta^{\mathrm{s}} = \{\hat{\eta}^{\mathrm{s}} = \hat{\eta} \in \mathbb{R}^3 \times \mathbb{R}^3 \mid \hat{\eta}^{\mathrm{s}}|_{\partial_\Phi\hat{\varphi}} = 0\} \subset T\mathcal{C}_t,$$

where $\partial_\Phi\hat{\varphi}$ is the part of the boundary where displacements and/or rotations are prescribed. Employing a slight abuse in the notation: $\hat{\eta}^{\mathrm{s}}(S) \in T_\Phi\mathcal{C}_t$ *i.e.* a kinematically admissible variation belongs to the tangent space to $\mathcal{C}_t$ at $\hat{\boldsymbol{\Phi}} \in \mathcal{C}_t$.

Then, given $\mathcal{C}_t$, $\mathcal{C}_{t\beta}$ and $\hat{\eta}^{\mathrm{s}} \in T_\Phi\mathcal{C}_t$ the systematic linearization process [104, 156, 215, 219] is performed using of the notion of Gâteaux derivative as

$$\delta\hat{\varphi} \triangleq \frac{\mathrm{d}}{\mathrm{d}\beta}\hat{\varphi}_\beta\Big|_{\beta=0}, \qquad \delta\boldsymbol{\Lambda} \triangleq \frac{\mathrm{d}}{\mathrm{d}\beta}\boldsymbol{\Lambda}_\beta\Big|_{\beta=0} = \delta\widetilde{\boldsymbol{\theta}}\boldsymbol{\Lambda}. \quad (18)$$

Therefore, the position vector and its linearized increment belong to the same vector space and the additive rule for vectors applies. Repeating the procedures followed in (18) for the case of the rotation tensor from the curved reference rod to the current rod configuration, we obtain $\delta\mathbf{\Lambda}_n = \delta\widetilde{\boldsymbol{\theta}}\mathbf{\Lambda}_n$.

### 3.2.2 Linearization of the Strain Measures

In this section the admissible variations of strain measures are calculated using the chain rule for partial derivatives.

Considering the fact that $\hat{t}_1 = \mathbf{\Lambda}_n\hat{t}_{01}$, one has the following derivation for the linearized form of $\hat{\gamma}_n$:

$$\delta\hat{\gamma}_n \equiv \delta(\hat{\varphi}_{,S} - \hat{t}_1) = \delta\hat{\varphi}_{,S} + \widetilde{\boldsymbol{t}}_1\delta\hat{\theta}, \tag{19a}$$

where $\widetilde{\boldsymbol{t}}_1$ is the skew-symmetric tensor obtained from $\hat{t}_1$. In the case of the material form, $\hat{\Gamma}_n = \mathbf{\Lambda}^T\hat{\gamma}_n$, and noticing the fact that $\delta\mathbf{\Lambda}^T = -\mathbf{\Lambda}^T\delta\widetilde{\boldsymbol{\theta}}$, one obtains that

$$\delta\hat{\Gamma}_n \equiv \delta(\mathbf{\Lambda}^T\hat{\gamma}_n) = \mathbf{\Lambda}^T(\delta\hat{\varphi}_{,S} + \widetilde{\boldsymbol{\varphi}}_{,S}\,\delta\hat{\theta}), \tag{19b}$$

where[7] $\widetilde{\boldsymbol{\varphi}}_{,S} = \boldsymbol{\Pi}[\hat{\varphi}_{,S}] \in so(3)$. Employing (19a) and (19b), it is possible to show that the co-rotated variation of the translational strain vector is given by

$$\delta\overset{\triangledown}{[\hat{\gamma}_n]} = \mathbf{\Lambda}\delta\hat{\Gamma}_n = \delta\hat{\varphi}_{,S} + \widetilde{\boldsymbol{\varphi}}_{,S}\,\delta\hat{\theta}.$$

Similarly, considering the spatial form of the incremental curvature strain tensor one obtains that

$$\delta\widetilde{\boldsymbol{\omega}}_n = \delta(\mathbf{\Lambda}_{n,S}\,\mathbf{\Lambda}_n^T) = \delta\widetilde{\boldsymbol{\theta}}_{,S} + \delta\widetilde{\boldsymbol{\theta}}\widetilde{\boldsymbol{\omega}}_n - \widetilde{\boldsymbol{\omega}}_n\delta\widetilde{\boldsymbol{\theta}}. \tag{20a}$$

For the case of the material form of the incremental curvature tensor, one obtains

$$\delta\widetilde{\mathbf{\Omega}}_n \equiv \mathbf{\Lambda}_0^T\delta(\mathbf{\Lambda}_n^T\mathbf{\Lambda}_{n,S})\mathbf{\Lambda}_0 = \mathbf{\Lambda}^T\delta\widetilde{\boldsymbol{\theta}}_{,S}\,\mathbf{\Lambda}.$$

Then, the co-rotated variation is given by

$$\delta\overset{\triangledown}{[\widetilde{\boldsymbol{\omega}}_n]} = \mathbf{\Lambda}\delta\widetilde{\mathbf{\Omega}}_n\mathbf{\Lambda}^T = \delta\widetilde{\boldsymbol{\theta}}_{,S}\,. \tag{20b}$$

Equations (20a) to (20b) can be rewritten in terms of axial vectors as [219]:

$$\begin{aligned}
&\delta\hat{\omega}_n \equiv \delta\hat{\theta}_{,S} + \delta\widetilde{\boldsymbol{\theta}}\hat{\omega}_n = \delta\hat{\theta}_{,S} - \widetilde{\boldsymbol{\omega}}_n\delta\hat{\theta},\\
&\delta\hat{\Omega}_n \equiv \delta(\mathbf{\Lambda}^T\hat{\omega}_n) = \mathbf{\Lambda}^T\delta\hat{\theta}_{,S} = \mathbf{\Lambda}^T(\delta\hat{\omega}_n + \widetilde{\boldsymbol{\omega}}_n\delta\hat{\theta}),\\
&\delta\overset{\triangledown}{[\hat{\omega}_n]} = \mathbf{\Lambda}\delta\hat{\Omega}_n = \delta\hat{\theta}_{,S} = \delta\hat{\omega}_n + \widetilde{\boldsymbol{\omega}}_n\delta\hat{\theta}.
\end{aligned} \tag{21}$$

[7] In following the notation $\widetilde{\bullet} \equiv \boldsymbol{\Pi}[\bullet]$ will be used for the skew-symmetric tensor obtained from certain 'large' arguments.

Summarizing the above results in matrix form, we can rewrite (19a) to (22) as

$$\begin{bmatrix}\delta\hat{\gamma}_n\\ \delta\hat{\omega}_n\end{bmatrix} = \begin{bmatrix}\frac{\mathrm{d}}{\mathrm{d}S}\mathbf{I} & \widetilde{\boldsymbol{t}}_1\\ 0 & \left(\frac{\mathrm{d}}{\mathrm{d}S}\mathbf{I} - \widetilde{\boldsymbol{\omega}}_n\right)\end{bmatrix}\begin{bmatrix}\delta\hat{\varphi}\\ \delta\hat{\theta}\end{bmatrix} = \boldsymbol{B}^{\mathrm{s}}\hat{\eta}^{\mathrm{s}}, \tag{22a}$$

$$\begin{bmatrix}\delta\hat{\Gamma}_n\\ \delta\hat{\Omega}_n\end{bmatrix} = \begin{bmatrix}\mathbf{\Lambda}^T\frac{\mathrm{d}}{\mathrm{d}S}\mathbf{I} & \mathbf{\Lambda}^T\widetilde{\boldsymbol{\varphi}}_{,S}\\ 0 & \mathbf{\Lambda}^T\frac{\mathrm{d}}{\mathrm{d}S}\mathbf{I}\end{bmatrix}\begin{bmatrix}\delta\hat{\varphi}\\ \delta\hat{\theta}\end{bmatrix} = \bar{\boldsymbol{B}}^{\mathrm{s}}\hat{\eta}^{\mathrm{s}}, \tag{22b}$$

$$\begin{bmatrix}\delta\overset{\triangledown}{[\hat{\gamma}_n]}\\ \delta\overset{\triangledown}{[\hat{\omega}_n]}\end{bmatrix} = \begin{bmatrix}\frac{\mathrm{d}}{\mathrm{d}S}\mathbf{I} & \widetilde{\boldsymbol{\varphi}}_{,S}\\ 0 & \frac{\mathrm{d}}{\mathrm{d}S}\mathbf{I}\end{bmatrix}\begin{bmatrix}\delta\hat{\varphi}\\ \delta\hat{\theta}\end{bmatrix} = \boldsymbol{B}\hat{\eta}^{\mathrm{s}}, \tag{22c}$$

where the operator $\frac{\mathrm{d}}{\mathrm{d}S}\mathbf{I}(\bullet) = \mathbf{I}(\bullet)_{,S}$.

### 3.2.3 Linearization of the Spin Variables

Considering the spatial form of the angular velocity tensor $\widetilde{\boldsymbol{v}}_n \in T^{\mathrm{spa}}_{\mathbf{\Lambda}}SO(3)$ of the current rod relative to the curved reference rod, one obtains the following linearized form

$$\delta\widetilde{\boldsymbol{v}}_n \equiv \delta\left(\dot{\mathbf{\Lambda}}_n\mathbf{\Lambda}_n^T\right) = \delta\dot{\widetilde{\boldsymbol{\theta}}} + \delta\widetilde{\boldsymbol{\theta}}\widetilde{\boldsymbol{v}}_n - \widetilde{\boldsymbol{v}}_n\delta\widetilde{\boldsymbol{\theta}}. \tag{23a}$$

Analogously, considering the spatial form of the angular acceleration tensor referred to the curved reference rod $\dot{\widetilde{\boldsymbol{v}}}_n = \dot{\mathbf{\Lambda}}_n\dot{\mathbf{\Lambda}}_n^T + \ddot{\mathbf{\Lambda}}_n\mathbf{\Lambda}_n^T$, after several algebraic manipulations, we obtain that

$$\delta\widetilde{\boldsymbol{\alpha}}_n = \delta\ddot{\widetilde{\boldsymbol{\theta}}} + \delta\dot{\widetilde{\boldsymbol{\theta}}}\widetilde{\boldsymbol{v}}_n - \widetilde{\boldsymbol{v}}_n\delta\dot{\widetilde{\boldsymbol{\theta}}} + \delta\widetilde{\boldsymbol{\theta}}\widetilde{\boldsymbol{\alpha}}_n - \widetilde{\boldsymbol{\alpha}}_n\delta\widetilde{\boldsymbol{\theta}}. \tag{23b}$$

The corresponding axial vectors are given by

$$\delta\hat{v}_n = \delta\dot{\hat{\theta}} - \widetilde{\boldsymbol{v}}_n\delta\hat{\theta}, \qquad \delta\hat{\alpha}_n = \delta\ddot{\hat{\theta}} - \widetilde{\boldsymbol{v}}_n\delta\dot{\hat{\theta}} - \widetilde{\boldsymbol{\alpha}}_n\delta\hat{\theta}, \tag{24}$$

respectively. Employing analogous procedures as those followed in (23a) to (24), the admissible variations of the material forms of the angular velocity and acceleration tensors are

$$\begin{aligned}
&\delta\widetilde{\boldsymbol{V}} = \mathbf{\Lambda}_0^T\delta\widetilde{\boldsymbol{V}}_n\mathbf{\Lambda}_0 = \mathbf{\Lambda}^T\delta\dot{\widetilde{\boldsymbol{\theta}}}\mathbf{\Lambda},\\
&\delta\widetilde{\boldsymbol{A}} = \mathbf{\Lambda}^T[\delta\ddot{\widetilde{\boldsymbol{\theta}}} + \delta\dot{\widetilde{\boldsymbol{\theta}}}\widetilde{\boldsymbol{v}} - \widetilde{\boldsymbol{v}}\delta\dot{\widetilde{\boldsymbol{\theta}}}]\mathbf{\Lambda},
\end{aligned}$$

respectively. with axial vectors given by

$$\delta\hat{V}_n = \mathbf{\Lambda}^T\delta\dot{\hat{\theta}}, \qquad \delta\hat{A}_n = \mathbf{\Lambda}^T(\delta\ddot{\hat{\theta}} - \widetilde{\boldsymbol{v}}_n\delta\dot{\hat{\theta}}). \tag{26}$$

### 3.2.4 Linearization of the Strain Rates

On one hand, we have that the linearized form of the spatial description of the translational strain rate vector can be obtained in the following way:

$$\delta\dot{\hat{\gamma}}_n = \delta\left[\dot{\hat{\varphi}}_{,S} - \widetilde{\boldsymbol{v}}_n\hat{t}_1\right] = \delta\dot{\hat{\varphi}}_{,S} - \widetilde{\boldsymbol{t}}_1\delta\dot{\hat{\theta}} - \widetilde{\boldsymbol{v}}_n\widetilde{\boldsymbol{t}}_1\delta\hat{\theta},$$

and the linearized form of the material translational strain rate vector can be obtained as

$$\begin{aligned}\delta\dot{\hat{\Gamma}}_n &= \delta\big[\boldsymbol{\Lambda}^T(\dot{\hat{\varphi}}_{,S} - \widetilde{\mathbf{v}}_n\hat{\varphi}_{,S})\big]\\ &= \boldsymbol{\Lambda}^T\big((\tilde{\boldsymbol{\varphi}}_{,S} - \widetilde{\mathbf{v}}_n\widetilde{\boldsymbol{\varphi}}_{,S})\delta\hat{\theta} + \widetilde{\boldsymbol{\varphi}}_{,S}\,\delta\dot{\hat{\theta}} + \delta\dot{\hat{\varphi}}_{,S}\\ &\quad - \widetilde{\mathbf{v}}_n\Delta\hat{\varphi}_{,S}\big).\end{aligned} \tag{27}$$

On the other hand, the linearized form of the spatial and material descriptions of the rotational strain rate vectors can be obtained as

$$\delta\dot{\hat{\omega}}_n = \delta\big[\hat{v}_{n,S} + \widetilde{\mathbf{v}}_n\hat{\omega}_n\big] = \delta\dot{\hat{\theta}}_{,S} - \widetilde{\boldsymbol{\omega}}_n\delta\dot{\hat{\theta}} - \dot{\tilde{\omega}}_n\delta\hat{\theta}, \tag{28a}$$

$$\delta\dot{\hat{\Omega}}_n = \delta\big[\boldsymbol{\Lambda}^T\hat{v}_{n,S}\big] = \boldsymbol{\Lambda}^T\big[\delta\dot{\hat{\theta}}_{,S} - \widetilde{\mathbf{v}}_n\delta\hat{\theta}_{,S}\big]. \tag{28b}$$

Then, the co-rotated variation of the translational and rotational strain rates are given by

$$\delta\,[\overset{\triangledown}{\dot{\hat{\gamma}}}_n] = (\tilde{\boldsymbol{\varphi}}_{,S} - \widetilde{\mathbf{v}}_n\widetilde{\boldsymbol{\varphi}}_{,S})\delta\hat{\theta} + \widetilde{\boldsymbol{\varphi}}_{,S}\,\delta\dot{\hat{\theta}} + \delta\dot{\hat{\varphi}}_{,S} - \widetilde{\mathbf{v}}_n\delta\hat{\varphi}_{,S}, \tag{28c}$$

$$\delta\,[\overset{\triangledown}{\dot{\hat{\omega}}}_n] = \delta\dot{\hat{\theta}}_{,S} - \widetilde{\mathbf{v}}_n\delta\hat{\theta}_{,S}. \tag{28d}$$

It is possible to show that the linearized forms of the co-rotated rotational strain rate tensors can be expressed as

$$\begin{aligned}\delta\dot{\tilde{\omega}}_n &= \delta\dot{\tilde{\boldsymbol{\theta}}}_{,S} + \delta\dot{\tilde{\boldsymbol{\theta}}}\widetilde{\omega}_n - \widetilde{\omega}_n\delta\dot{\tilde{\boldsymbol{\theta}}} + \delta\widetilde{\boldsymbol{\theta}}\dot{\tilde{\omega}}_n - \dot{\tilde{\omega}}_n\delta\widetilde{\boldsymbol{\theta}},\\ \delta\dot{\tilde{\Omega}}_n &= \boldsymbol{\Lambda}^T(\delta\dot{\tilde{\boldsymbol{\theta}}}_{,S} + \delta\widetilde{\boldsymbol{\theta}}_{,S}\,\widetilde{\mathbf{v}}_n - \widetilde{\mathbf{v}}_n\delta\widetilde{\boldsymbol{\theta}}_{,S})\boldsymbol{\Lambda},\\ \delta\,[\overset{\triangledown}{\dot{\tilde{\omega}}}_n] &= \boldsymbol{\Lambda}(\delta\dot{\tilde{\Omega}}_n)\boldsymbol{\Lambda}^T = \delta\dot{\tilde{\boldsymbol{\theta}}}_{,S} + \delta\widetilde{\boldsymbol{\theta}}_{,S}\,\widetilde{\mathbf{v}}_n - \widetilde{\mathbf{v}}_n\delta\widetilde{\boldsymbol{\theta}}_{,S}.\end{aligned}$$

Finally, the material and co-rotated descriptions of the linearized increment of the strain rate at material point level are

$$\delta\hat{\mathcal{S}}_n = \delta\dot{\hat{\Gamma}}_n + \delta\dot{\hat{\Omega}}_n \times \hat{\mathcal{E}}, \tag{29a}$$

$$\delta\hat{s}_n = \boldsymbol{\Lambda}\delta\hat{\mathcal{S}}_n = \delta\,[\overset{\triangledown}{\dot{\hat{\gamma}}}_n] + \delta\,[\overset{\triangledown}{\dot{\hat{\omega}}}_n] \times \hat{\mathcal{T}}. \tag{29b}$$

The terms $\delta\dot{\hat{\varphi}}$, $\delta\dot{\hat{\varphi}}_{,S}$, $\delta\dot{\hat{\theta}}$ and $\delta\dot{\hat{\theta}}_{,S}$ of (28c) and (28d) do not allow to express directly the co-rotated variations of the strain rate vectors in terms of $\hat{\eta}^{\mathrm{s}}$. To this end, the specific time-stepping scheme are used providing the needed relations [220] as it will be explained in next sections.

For the present developments, lets suppose that there exist two linear operators $\boldsymbol{\mathcal{H}}_a \in \mathcal{L}(\mathbb{R}^3, \mathbb{R}^{3*})$ and $\boldsymbol{\mathcal{H}}_b(\hat{\theta}) \in \mathcal{L}(T^{\mathrm{spa}}_{\boldsymbol{\Lambda}}, T^{\mathrm{spa}*}_{\boldsymbol{\Lambda}})$ such that

$$\delta\dot{\hat{\varphi}} = \boldsymbol{\mathcal{H}}_a\delta\hat{\varphi}, \qquad \delta\dot{\hat{\varphi}}_{,S} = \boldsymbol{\mathcal{H}}_a\delta\hat{\varphi}_{,S} + \boldsymbol{\mathcal{H}}_{a,S}\,\delta\hat{\varphi}, \tag{30a}$$

$$\delta\dot{\hat{\theta}} = \boldsymbol{\mathcal{H}}_b\delta\hat{\theta}, \qquad \delta\dot{\hat{\theta}}_{,S} = \boldsymbol{\mathcal{H}}_b\delta\hat{\theta}_{,S} + \boldsymbol{\mathcal{H}}_{b,S}\,\delta\hat{\theta}. \tag{30b}$$

Therefore, (28c) and (28d) can be rearranged as

$$\begin{bmatrix}\delta\,[\overset{\triangledown}{\dot{\hat{\gamma}}}_n]\\ \delta\,[\overset{\triangledown}{\dot{\hat{\omega}}}_n]\end{bmatrix} = \left[\begin{array}{c|c}\boldsymbol{\mathcal{H}}_a[\frac{\mathrm{d}}{\mathrm{d}S}\mathbf{I}] + \boldsymbol{\mathcal{H}}_{a,S} - \widetilde{\mathbf{v}}_n[\frac{\mathrm{d}}{\mathrm{d}S}\mathbf{I}] & \tilde{\boldsymbol{\varphi}}_{,S} + \widetilde{\boldsymbol{\varphi}}_{,S}\,\boldsymbol{\mathcal{H}}_b - \widetilde{\mathbf{v}}_n\widetilde{\boldsymbol{\varphi}}_{,S}\\ \hline 0 & (\boldsymbol{\mathcal{H}}_b - \widetilde{\mathbf{v}}_n)[\frac{\mathrm{d}}{\mathrm{d}S}\mathbf{I}] + \boldsymbol{\mathcal{H}}_{b,S}\end{array}\right]\hat{\eta}^{\mathrm{s}} = \boldsymbol{\mathcal{V}}\hat{\eta}^{\mathrm{s}}. \tag{31}$$

It is worth to note that the tensor $\boldsymbol{\mathcal{V}}$ is configuration dependent and couples the rotational and translational parts of the motion.

### 3.2.5 *Linearization of the Stress Resultants and Stress Couples: Inviscid and Elastic Case*

Considering the variation of strains (22a) to (22c) one obtains that

$$\delta\hat{n}^{\mathrm{m}} = \mathbf{C}^{\mathrm{me}}_{nn}\boldsymbol{\Lambda}^T(\delta\hat{\varphi}_{,S} + \widetilde{\boldsymbol{\varphi}}_{,S}\,\delta\hat{\theta}) + \mathbf{C}^{\mathrm{me}}_{nm}\boldsymbol{\Lambda}^T\delta\hat{\theta}_{,S}, \tag{32a}$$

where $\mathbf{C}^{\mathrm{me}}_{ij}$, $(i, j \in \{n, m\})$ are the material forms of the cross sectional elastic constitutive tensors. Hence, the co-rotated variations are

$$\delta\,[\overset{\triangledown}{\hat{n}}] = \boldsymbol{\Lambda}\delta\hat{n}^{\mathrm{m}} = \mathbf{C}^{\mathrm{se}}_{nn}(\delta\hat{\varphi}_{,S} + \widetilde{\boldsymbol{\varphi}}_{,S}\,\delta\hat{\theta}) + \mathbf{C}^{\mathrm{se}}_{nm}\delta\hat{\theta}_{,S}, \tag{32b}$$

where $\mathbf{C}^{\mathrm{se}}_{ij} = \Lambda\mathbf{C}^{\mathrm{me}}_{ij}\Lambda^T$, $(i, j \in \{n, m\})$ are the spatial forms of the cross sectional elastic constitutive tensors.
Similarly, one obtains for the case of the stress couples

$$\delta\hat{m}^{\mathrm{m}} = \mathbf{C}^{\mathrm{me}}_{mn}\Lambda^T(\delta\hat{\varphi}_{,S} + \widetilde{\boldsymbol{\varphi}}_{,S}\,\delta\hat{\theta}) + \mathbf{C}^{\mathrm{me}}_{mm}\Lambda^T\delta\hat{\theta}_{,S}, \tag{33a}$$

$$\delta\,[\overset{\triangledown}{\hat{m}}] = \mathbf{C}^{\mathrm{se}}_{mn}(\delta\hat{\varphi}_{,S} + \widetilde{\boldsymbol{\varphi}}_{,S}\,\delta\hat{\theta}) + \mathbf{C}^{\mathrm{se}}_{mm}\delta\hat{\theta}_{,S}. \tag{33b}$$

The linear form of the spatial stress resultant is calculated noticing the following relation for the co-rotated variation: $\delta\,[\overset{\triangledown}{\hat{n}}] = \delta\hat{n} - \delta\widetilde{\boldsymbol{\theta}}\hat{n} = \delta\hat{n} + \widetilde{\hat{\boldsymbol{n}}}\delta\hat{\theta}$ as

$$\delta\hat{n} = \mathbf{C}^{\mathrm{se}}_{nn}\delta\hat{\varphi}_{,S} + (\mathbf{C}^{\mathrm{se}}_{n}\widetilde{\boldsymbol{\varphi}}_{,S} - \widetilde{\hat{\boldsymbol{n}}})\delta\hat{\theta} + \mathbf{C}^{\mathrm{se}}_{nm}\delta\hat{\theta}_{,S}, \tag{34a}$$

and analogously for the variation of the spatial form of the stress couple

$$\delta\hat{m} = \mathbf{C}^{\mathrm{se}}_{mn}\delta\hat{\varphi}_{,S} + (\mathbf{C}^{\mathrm{se}}_{mn}\widetilde{\boldsymbol{\varphi}}_{,S} - \widetilde{\hat{\boldsymbol{m}}})\delta\hat{\theta} + \mathbf{C}^{\mathrm{se}}_{m}\delta\hat{\theta}_{,S}. \tag{34b}$$

The results obtained for the admissible variation of the stress resultant and couples given in (32a) to (34b) can be summarized and written in matrix form as

$$\delta\hat{\Psi}^{\mathrm{m}}_{\star} = \begin{bmatrix}\mathbf{C}^{\mathrm{me}}_{nn} & \mathbf{C}^{\mathrm{me}}_{nm}\\ \mathbf{C}^{\mathrm{me}}_{mn} & \mathbf{C}^{\mathrm{me}}_{mm}\end{bmatrix}\bar{\boldsymbol{B}}^{\mathrm{s}}\hat{\eta}^{\mathrm{s}} = \mathbf{C}^{\mathrm{me}}\bar{\boldsymbol{B}}^{\mathrm{s}}\hat{\eta}^{\mathrm{s}}, \tag{35}$$

where $\delta\hat{\Psi}^{\mathrm{m}}_{\star} = [\delta\hat{n}^{\mathrm{m}}, \delta\hat{m}^{\mathrm{m}}]$ and the material form of the constitutive tensor $\mathbf{C}^{\mathrm{me}}$ has been given in (16a) to (16b).

The co-rotated admissible variation of the stress resultant and couples as

$$\delta\,[\overset{\triangledown}{\hat{\Psi}}]_\star = \begin{bmatrix} \mathbf{C}^{\mathrm{se}}_{nn} & \mathbf{C}^{\mathrm{se}}_{nm} \\ \mathbf{C}^{\mathrm{se}}_{mn} & \mathbf{C}^{\mathrm{se}}_{mm} \end{bmatrix} \boldsymbol{B}\hat{\eta}^{\mathrm{s}} = \mathbf{C}^{\mathrm{se}}\boldsymbol{B}\hat{\eta}^{\mathrm{s}}, \tag{36}$$

where $\delta\,[\overset{\triangledown}{\hat{\Psi}}]_\star = [\delta\,[\overset{\triangledown}{\hat{n}}], \delta\,[\overset{\triangledown}{\hat{m}}]]$.

Finally, the spatial form of the admissible variation of the stress resultant and couples can be expressed in matrix form as

$$\delta\hat{\Psi}_\star = \left(\bar{\mathbf{C}}^{\mathrm{se}}\boldsymbol{B} + \begin{bmatrix} 0 & -\widetilde{\boldsymbol{n}} \\ 0 & -\widetilde{\boldsymbol{m}} \end{bmatrix}\right)\hat{\eta}^{\mathrm{s}} = (\mathbf{C}^{\mathrm{se}}\boldsymbol{B} + \boldsymbol{\mathcal{N}})\hat{\eta}^{\mathrm{s}}, \tag{37}$$

where $\delta\hat{\Psi}^{\mathrm{m}}_\star = [\delta\hat{n}^{\mathrm{m}}, \delta\hat{m}^{\mathrm{m}}]$ and the tensor $\boldsymbol{\mathcal{N}}$ takes into account for the stress state existing in the current rod configuration.

The (nonlinear) operators $\bar{\boldsymbol{B}}^{\mathrm{s}}$ and $\boldsymbol{B}$ are easily constructed from (32a), (32b), (33a) and (33b).

### 3.3 External Loads

This section describes the types of loads more relevant to earthquake engineering. It is worth to note that other types (more complex) are also available, as described in Ref. [134].

*Concentrated Loads* A point load applied in a globally fixed direction is given $\hat{P}_f = P_{fi}\hat{e}_i$ and a applied point moment (about fixed axes) by $\hat{\mathrm{M}}_f = \mathrm{M}_{fi}\hat{e}_i$. In both cases, conventional procedures apply [62].[8]

*Distributed Loads* An applied load density is given per unit of unstressed arch–length of the curved configuration referred to the spatially fixed frame $\{\hat{e}_i\}$. One manner to define the *self–weight* of the structure is by employing this kind of loads, but it is difficult to define it for cross sections composed with different materials.

In general can be assumed that the differential force $\mathrm{d}\hat{f}_g$ and moment $\mathrm{d}\hat{m}_g$ applied on the differential element $\mathrm{d}S$ are calculated as:

$$\mathrm{d}\hat{f}_g = \hat{\mathcal{N}}_g(S)\mathrm{d}S, \tag{38a}$$

$$\mathrm{d}\hat{m}_g = \hat{\mathcal{M}}_g(S)\mathrm{d}S, \tag{38b}$$

respectively; where $\hat{\mathcal{N}}_g(S)$ and $\hat{\mathcal{M}}_g(S)$ are the corresponding densities. This type of loading is deformation invariant and usually conservative [62, 134].

[8] It is worth noting that point moments are in general *non-conservative i.e.* the work done by a mechanical system due to the application of a concentrated moment is *path–dependent*.

*Body Loads* Lets consider the external loading due to body forces per unit of volume denoted by the vector (density) $\hat{b}(S, \xi_\beta)$ which contributes to the terms $\hat{\mathcal{N}}$ and $\hat{\mathcal{M}}$. The evaluation of these contributions (at element level) requires the numerical integration of the following integrals

$$\hat{\mathcal{N}}_{\mathrm{b}} = \int_0^L \int_{\mathcal{A}_0} g_0\rho_0\hat{b}\mathrm{d}V_0, \tag{39a}$$

$$\hat{\mathcal{M}}_{\mathrm{b}} = \int_0^L \int_{\mathcal{A}_0} g_0\rho_0\widetilde{\mathcal{T}}\hat{b}\mathrm{d}V_0. \tag{39b}$$

If the mass centroid of the cross section is chosen as the reference curve for the rod, $\hat{\mathcal{M}}_{\mathrm{b}}$ in (39b) vanish.

### 3.4 Equilibrium Equations

In this section the equilibrium equations of motion for rods are deduced working on the *Lagrangian* side of the mechanics[9] which can be based on the variational principles behind *Newton*'s fundamental laws of force balance. The development presented consist into obtaining the necessary conditions for the minimization of the action integral of the mechanical system. The development presented are base on considering that both the forces and internal forces are conservative; however, the equations of motions can be easily extended to the nonconservative case.

Firstly, one chooses a configuration space manifold $\mathcal{C}_t$ where generic coordinates denoted by $\hat{q}_\Phi = (\hat{\varphi}, \boldsymbol{\Lambda})$. The velocity phase space $\overline{T}\mathcal{C}_t$ corresponds to the tangent bundle of $\mathcal{C}_t$. Coordinates on $\overline{T}\mathcal{C}_t$ are denoted by $(\hat{q}_\Phi, \dot{\hat{q}}_\Phi) \equiv (\hat{\varphi}, \boldsymbol{\Lambda}, \dot{\hat{\varphi}}, \dot{\boldsymbol{\Lambda}})$. The *Lagrangian* is regarded as a function $\mathfrak{L}_g : T\mathcal{C}_t \to \mathbb{R}$, $(\hat{q}_\Phi, \dot{\hat{q}}_\Phi) \mapsto \mathfrak{L}_g(\hat{\varphi}, \boldsymbol{\Lambda}, \dot{\hat{\varphi}}, \dot{\boldsymbol{\Lambda}}, t)$. Usually, $\mathfrak{L}_g$ is the kinetic minus the potential energy of the system and the following relations hold $\dot{\hat{q}}_\Phi = \mathrm{d}\hat{q}_\Phi/\mathrm{d}t$. The *Hamilton*'s principle states that the variation of the action is stationary at a solution:

$$\delta\mathfrak{S} = \delta\int_a^b \mathfrak{L}_g(\hat{q}_\Phi, \dot{\hat{q}}_\Phi, t)\mathrm{d}t = 0. \tag{40}$$

Accordingly, the action has a critical point at a solution in the space of curves, which is equivalent to the *Euler-Lagrange* equations (the equilibrium equations). If external forces are applied on the system, they have to be added to the right side of (40).

On one hand, the kinetic energy of the rod model is calculated as

$$K = \frac{1}{2}\int_{\mathcal{B}_0} \rho_0\langle\dot{\hat{x}}, \dot{\hat{x}}\rangle\mathrm{d}V = \frac{1}{2}\int_0^L (\mathcal{A}_{\rho_0}|\dot{\hat{\varphi}}|^2 + \hat{v}_n \cdot \boldsymbol{\mathcal{I}}_{\rho_0}\hat{v}_n)\mathrm{d}S$$
$$= \frac{1}{2}\int_0^L (\mathcal{A}_{\rho_0}|\dot{\hat{\varphi}}|^2 + \hat{V}_n \cdot \mathbf{I}_{\rho_0}\hat{V}_n)\mathrm{d}S. \tag{41}$$

[9] For a theoretical treatment see Refs. [156–158].

The remaining term is the potential energy $V$. The following developments consider conservative external loading which implies the existence of a potential function $W_{\mathrm{e}} : \mathcal{C}_t \to \mathbb{R}$ such that the potential energy of the system is obtained as

$$\begin{aligned} V(\hat{\varphi}, \boldsymbol{\Lambda}) &= V_{\mathrm{int}}(\hat{\varphi}, \boldsymbol{\Lambda}) + V_{\mathrm{ext}}(\hat{\varphi}, \boldsymbol{\Lambda}) \\ &= \int_0^L W_{\mathrm{str}}(\hat{\Gamma}_n, \hat{\Omega}_n)\mathrm{d}S + \int_0^L W_{\mathrm{e}}(\hat{\varphi}, \boldsymbol{\Lambda})\mathrm{d}S, \end{aligned} \tag{42}$$

where $W_{\mathrm{str}}$ is the strain energy function per unit of volume, which can be consulted in [212] for linear elastic materials and in the case of inelastic materials its explicit form is given in [163, 164]. For conservative loads then, $V_{\mathrm{ext}} = V_{\mathrm{ext}}(\boldsymbol{\Lambda}^T \hat{\varphi})$ (see [217]).

In this manner, the Lagrangian for a rod subjected to a conservative system of loads is $\mathfrak{L}_g = K - V_{\mathrm{int}} - V_{\mathrm{ext}}$ and Hamilton's principle reads

$$\delta\mathfrak{S} = \delta \int_a^b \mathfrak{L}_g \mathrm{d}t = \int_a^b (\delta K - \delta V_{\mathrm{int}} - \delta V_{\mathrm{ext}})\mathrm{d}t = 0. \tag{43}$$

The linearization of the kinetic energy is obtained as

$$\begin{aligned} \delta K &= \int_0^L (\mathcal{A}_{\rho_0} \dot{\hat{\varphi}} \cdot \delta\dot{\hat{\varphi}} + \delta\hat{V}_n \cdot \mathbf{I}_{\rho_0} \hat{V}_n)\mathrm{d}S \\ &= \int_0^L (\mathcal{A}_{\rho_0} \dot{\hat{\varphi}} \cdot \delta\dot{\hat{\varphi}} + \boldsymbol{\mathcal{I}}_{\rho_0} \hat{v}_n \cdot \delta\dot{\hat{\theta}})\mathrm{d}S \\ &= G_{\mathrm{ine}}(\hat{q}_\Phi, \dot{\hat{q}}_\Phi, \hat{\eta}^{\mathrm{s}}), \end{aligned} \tag{44}$$

where it has been used $\delta\hat{V}_n = \boldsymbol{\Lambda}^T \dot{\hat{\theta}}$, $\mathcal{A}_{\rho_0} = \int_{\mathcal{A}} \rho_0 \mathrm{d}\mathcal{A}$ and $\boldsymbol{\mathcal{I}}_{\rho_0} = \boldsymbol{\Lambda}\mathbf{I}_{\rho_0}\boldsymbol{\Lambda} = -\int_{\mathcal{A}} \rho_0 \widetilde{\boldsymbol{\mathcal{T}}}\widetilde{\boldsymbol{\mathcal{T}}}\,\mathrm{d}\mathcal{A}$.

The linearization of the internal part of the potential energy is obtained as

$$\begin{aligned} \delta V_{\mathrm{int}} &= \int_0^L (\partial_{\hat{\Gamma}_n} W_{\mathrm{str}} \cdot \delta\hat{\Gamma}_n + \partial_{\hat{\Omega}_n} W_{\mathrm{str}} \cdot \delta\hat{\Omega}_n)\mathrm{d}S \\ &= \int_0^L (\hat{n}^{\mathrm{m}} \cdot \delta\hat{\Gamma}_n + \hat{m}^{\mathrm{m}} \cdot \delta\hat{\Omega}_n)\mathrm{d}S \\ &= \int_0^L (\hat{\Psi} \cdot \boldsymbol{B}\hat{\eta}^{\mathrm{s}})\mathrm{d}S = G_{\mathrm{int}}(\hat{q}_\Phi, \hat{\eta}^{\mathrm{s}}), \end{aligned} \tag{45}$$

where $\partial_{\hat{\Gamma}_n} W_{\mathrm{str}} = \hat{n}^{\mathrm{m}}$ and $\partial_{\hat{\Omega}_n} W_{\mathrm{str}} = \hat{m}^{\mathrm{m}}$, $\hat{\Psi} = [\hat{n}, \hat{m}]$, $\hat{\eta}^{\mathrm{s}} = (\delta\hat{\varphi}, \delta\hat{\theta})$ and $\boldsymbol{B}$ is

$$\boldsymbol{B} = \begin{bmatrix} \frac{\mathrm{d}}{\mathrm{d}S}\mathbf{I} & \widetilde{\boldsymbol{\varphi}}_{,S} \\ 0 & \frac{\mathrm{d}}{\mathrm{d}S}\mathbf{I} \end{bmatrix}. \tag{46}$$

A detailed deduction of (46) can be found in [104, 219]. Denoting $\boldsymbol{\Lambda}^T\hat{\varphi} \equiv \hat{\varphi}^{\mathrm{m}}$, considering $\delta\hat{\varphi}^{\mathrm{m}} = \boldsymbol{\Lambda}^T(\delta\hat{\varphi} + \widetilde{\boldsymbol{\varphi}}\delta\hat{\theta})$ one obtains that $\delta V_{\mathrm{ext}}$ is given by

$$\begin{aligned} \delta V_{\mathrm{ext}} &= \int_0^L \delta W_{\mathrm{e}}(\hat{\varphi}^{\mathrm{m}})\mathrm{d}S = \int_0^L (\partial_{\hat{\varphi}^{\mathrm{m}}} W_{\mathrm{e}} \cdot [\boldsymbol{\Lambda}^T(\delta\hat{\varphi} + \widetilde{\boldsymbol{\varphi}}\delta\hat{\theta})]\mathrm{d}S \\ &= \int_0^L (\boldsymbol{\Lambda}\partial_{\hat{\varphi}^{\mathrm{m}}} W_{\mathrm{e}} \cdot \delta\hat{\varphi} - \widetilde{\boldsymbol{\varphi}}\boldsymbol{\Lambda}\partial_{\hat{\varphi}^{\mathrm{m}}} W_{\mathrm{e}} \cdot \delta\hat{\theta})\mathrm{d}S \\ &= \int_0^L (\hat{\mathcal{N}} \cdot \delta\hat{\varphi} + \hat{\mathcal{M}} \cdot \delta\hat{\theta})\mathrm{d}S = G_{\mathrm{ext}}, \end{aligned} \tag{47}$$

where $\hat{\mathcal{N}}$ and $\hat{\mathcal{M}}$ are the applied (conservative) load densities for unit of arch-length [217].

Then, considering (44), (45) and (47) Hamilton's principle (43) can be rewritten as

$$\delta\mathfrak{S} = \int_a^b (G_{\mathrm{ine}} - G_{\mathrm{int}} - G_{\mathrm{ext}})\mathrm{d}t = \int_a^b G\mathrm{d}t = 0. \tag{48}$$

Moreover,

$$\begin{aligned} &\int_a^b \int_0^L \mathcal{A}_{\rho_0} \dot{\hat{\varphi}} \cdot \delta\dot{\hat{\varphi}}\mathrm{d}S\mathrm{d}t \\ &= \int_0^L [\mathcal{A}_{\rho_0} \dot{\hat{\varphi}} \cdot \delta\hat{\varphi}]\Big|_a^b \mathrm{d}S - \int_a^b \int_0^L \mathcal{A}_{\rho_0} \ddot{\hat{\varphi}} \cdot \delta\hat{\varphi}\mathrm{d}S\mathrm{d}t, \end{aligned} \tag{49a}$$

$$\begin{aligned} &\int_a^b \int_0^L \boldsymbol{\mathcal{I}}_{\rho_0} \hat{v}_n \cdot \delta\dot{\hat{\theta}}\mathrm{d}S\mathrm{d}t \\ &= \int_0^L [\boldsymbol{\mathcal{I}}_{\rho_0} \hat{v}_n \cdot \delta\hat{\theta}]\Big|_a^b \mathrm{d}S - \int_a^b \int_0^L (\dot{\boldsymbol{\mathcal{I}}}_{\rho_0} \hat{v}_n) \cdot \delta\hat{\theta}\mathrm{d}S\mathrm{d}t, \end{aligned} \tag{49b}$$

and, therefore, $\delta K$ becomes

$$\delta K = \int_a^b \int_0^L \left[\mathcal{A}_{\rho_0} \ddot{\hat{\varphi}} \cdot \delta\hat{\varphi} + (\dot{\boldsymbol{\mathcal{I}}}_{\rho_0} \hat{v}_n) \cdot \delta\hat{\theta}\right]\mathrm{d}S\mathrm{d}t, \tag{50}$$

where it has been used the fact that the admissible variations of the configuration variables are zero at the initial and final times *i.e.* $\hat{\eta}^{\mathrm{s}}|_{a,b} = 0$.

Additionally,

$$\begin{aligned} \delta V_{\mathrm{int}} &= \int_a^b \int_0^L (\hat{n} \cdot \delta\hat{\varphi}_{,S} - \widetilde{\boldsymbol{\varphi}}_{,S}\hat{n} \cdot \delta\hat{\theta} + \hat{m} \cdot \delta\hat{\theta}_{,S})\mathrm{d}S\mathrm{d}t \\ &= \int_a^b (\hat{n} \cdot \delta\hat{\varphi} + \hat{m} \cdot \delta\hat{\theta})\Big|_0^L \mathrm{d}t \\ &\quad - \int_a^b \int_0^L (\hat{n}_{,S} \cdot \delta\hat{\varphi} + \hat{\varphi}_{,S} \times \hat{n} \cdot \delta\hat{\theta} + \hat{m}_{,S} \cdot \delta\hat{\theta})\mathrm{d}S\mathrm{d}t, \\ &= \int_a^b (\hat{\Phi} \cdot \delta\hat{q}_\Phi)\Big|_{\partial_\Phi\hat{\varphi}} \mathrm{d}t \\ &\quad - \int_a^b \int_0^L (\hat{n}_{,S} \cdot \delta\hat{\varphi} + (\hat{m}_{,S} + \hat{\varphi}_{,S} \times \hat{n}) \cdot \delta\hat{\theta})\mathrm{d}S\mathrm{d}t. \end{aligned} \tag{51}$$

Considering *Neumann* conditions on the subset of the boundary $\partial_\Phi\hat{\varphi} = \emptyset$; $\forall t$, and defining $\hat{\mathsf{P}} = \mathcal{A}_{\rho_0}\dot{\hat{\varphi}}$ and $\hat{\mathsf{J}} = \boldsymbol{\mathcal{I}}_{\rho_0}\hat{v}_n$, one obtains

$$\delta\mathfrak{S} = \int_a^b \int_0^L \left[\dot{\hat{\mathsf{P}}} - (\hat{n}_{,S} + \hat{\mathcal{N}})\right] \cdot \delta\hat{\varphi}\mathrm{d}S\mathrm{d}t$$

$$+\int_a^b \int_0^L \left[\dot{\hat{\mathsf{J}}} - (\hat{m}_{,S} + \hat{\varphi}_{,S} \times \hat{n} + \hat{\mathcal{M}})\right] \cdot \delta\hat{\theta}\, \mathrm{d}S\mathrm{d}t = 0. \tag{52}$$

Taking into account that $\hat{\eta}^s$ is arbitrary, the reduced equilibrium equations (the Euler-Lagrange ones) are obtained as

$$\dot{\hat{\mathsf{P}}} = \hat{n}_{,S} + \hat{\mathcal{N}}, \tag{53a}$$

$$\dot{\hat{\mathsf{J}}} = \hat{m}_{,S} + \hat{\varphi}_{,S} \times \hat{n} + \hat{\mathcal{M}}. \tag{53b}$$

The system of nonlinear differential equations (53a) and (53b) have to be supplemented with the following boundary conditions:

$$(\hat{\varphi}_{\Phi}, \mathbf{\Lambda}_{\Phi}) \in \partial_{\Phi}\hat{\varphi} \times [0, T], \tag{54a}$$

$$(\hat{n}_{\Sigma}, \hat{m}_{\Sigma}) \in \partial_{\Sigma}\hat{\varphi} \times [0, T], \tag{54b}$$

with the standard conditions $\partial_{\Phi}\hat{\varphi}_0 \cup \partial_{\Sigma}\hat{\varphi}_0 = \partial\hat{\varphi}_0$ and $\partial_{\Phi}\hat{\varphi}_0 \cap \partial_{\Sigma}\hat{\varphi}_0 = \emptyset$ assumed to hold. The additional initial data are

$$\hat{\varphi}(S, 0) = \hat{\varphi}_0(S) \quad \text{and} \quad \mathbf{\Lambda}(S, 0) = \mathbf{\Lambda}_0(S), \tag{54c}$$

$$\dot{\hat{\varphi}}(S, 0) = \dot{\hat{\varphi}}_0(S) \quad \text{and} \quad \dot{\mathbf{\Lambda}}(S, 0) = \mathbf{\Lambda}_0(S)\widetilde{\boldsymbol{V}}_{0n}(S), \tag{54d}$$

where $(\dot{\hat{\varphi}}_0, \hat{V}_{0n}) : [0, L] \to \mathbb{R}^3 \times \mathbb{R}^3$ is a prescribed velocity field. The static version can be obtained ignoring the terms of (54d) and the corresponding inertial terms in the equilibrium equations.

It is worth to note that the term $G$ in (48) corresponds to the *weak form* of the momentum balance equations (53a) and (53b) and is frequently quoted as the *principle of virtual work*.

If the structure is subjected to the base acceleration corresponding to a seismic input, the acceleration of each material point can be written as the sum of the acceleration referred to the inertial frame and the acceleration of the frame itself. The resulting expression for the acceleration of the material point is given by $\ddot{\hat{x}} = \ddot{\hat{\varphi}} + \ddot{\hat{a}} + (\widetilde{\alpha} + \widetilde{\boldsymbol{v}}\widetilde{\boldsymbol{v}})\hat{\mathcal{T}}$, where $\ddot{\hat{a}}$ corresponds to the translational acceleration of the inertial frame. Then, the translational part of the equilibrium equations has to be rewritten as

$$\hat{n}_{,S} + \hat{\mathcal{N}} = \mathcal{A}_{\rho_0}(\ddot{\hat{\varphi}} + \ddot{\hat{a}}). \tag{55}$$

The seismic acceleration vector $\ddot{\hat{a}}$ is independent of the material point and can be treated as an additional body force adding it to $\hat{b}$ in (39a).

## 4 Constitutive Nonlinearity

Normally, in engineering problems we are interested in knowing the behavior of the structures beyond the linear elastic case. Therefore, this section is focused on the treatment of constitutive nonlinearity.

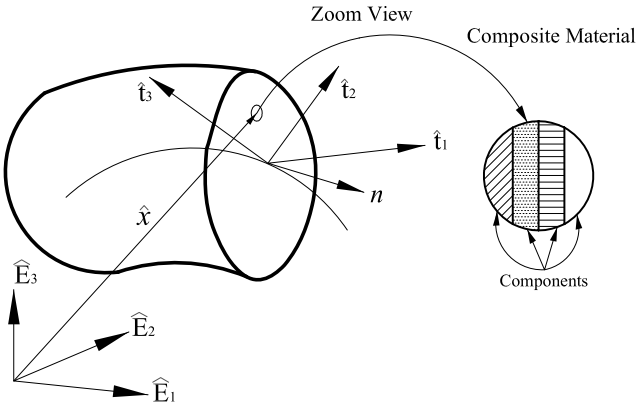


**Fig. 11** Each material point on the rod has associated a composite composed by a finite amount of simple materials

To this end, material points on the cross sections are considered as formed by a *composite material* corresponding to a homogeneous mixture of different *components*, each of them with its own constitutive law. The composite behavior is obtained by means of the *mixing theory* for composite materials (see Fig. 11). Two types of nonlinear constitutive models for simple materials are used: the *damage* and the *plasticity* models, both of then formulated in a manner that is consistent with the laws of the thermodynamics for adiabatic processes [143, 144].

The constitutive models are formulated in terms of the material form of the FPK stress vector, $\hat{P}_1^{\mathrm{m}}$, and the strain and strain rate measures $\hat{\mathcal{E}}_n$ and $\hat{S}_n$, respectively.

### 4.1 Softening Materials and Strain Localization

Failure of framed structures is frequently determined by the localization of the degradation of the mechanical properties of the materials in critical cross sections. This process usually occurs when materials presenting softening are associated to points on the cross section. Therefore, softening behavior of points on the cross section implies the induction of a softer response at cross sectional level leading to the classical concept of the formation of *plastic hinges* [58, 65, 71, 124, 176]. The inelastic analysis of rod structures in softening regime has been developed considering concentrated and distributed models.

Cross sectional degradation with softening can be modeled considering that a specific length of the rod concentrates the large localized strains and the force-displacement and/or moment-curvature relations are estimated throughout cross sectional integration of the stress field. A similar approach has been followed by several authors *e.g.* Bratina *et al.* [47] or Coleman and Spacone [59]. Among the main advantages of this approach, it is possible to mention:

(i) The definition of a finite length associated to the softening zone allows to simulate the distributed damage observed in some composite structures such as reinforced concrete [59].
(ii) The cross sectional force-displacement and/or moment-curvature relations are deduced *a posteriori* depending on the material distribution and their corresponding constitutive laws.

The *mesh independent response* of the structure can be obtained regularizating the constitutive equations according to the energy dissipated in the corresponding softening volume, limiting this value to the specific fracture energy of the material [163, 177, 181].

Some criticisms can be made to this approach in what regards to the treatment given to the softening response of rod structures, *e.g.* the fact that even in the case that the characteristic length of the materials exists (intrinsically, as a material property), this length should be largely smaller that the scales considered in the meshes [14]. Other alternative procedures based on considering the *strong discontinuity approach*[10] on the generalized displacement field of the beam can be also consulted in Refs. [13–15].

## 4.2 Degrading Materials: Damage Model

The behavior of the degrading materials is presented attending to the fact that micro-fissuration occurs due to the lack of cohesion between particles, among other processes. Different micro-fissures connect each to other generating a distributed damage zone in the material. After a certain loading level is reached a *fractured zone* is clearly defined [24, 95].

A damage model consistent with the kinematic assumption of the rod theory and based on the 3D formulation has been developed by Mata *et al.* [163]. The model has only one internal variable (isotropic) employed for simulating the mechanical degradation of the material. It shows a good equilibrium between complexity and versatility allowing it use in large numerical simulations.

### *4.2.1 Secant Constitutive Equation and Dissipation*

In the case of thermally stable problems, the free energy density $\Psi$ in terms of the material form of the elastic free energy density $\Psi_0$ and the damage internal variable $d$ [155] is given by

$$\Psi(\hat{\mathcal{E}}_n, d) = (1-d)\Psi_0 = (1-d)\left(\frac{1}{2\rho_0}\hat{\mathcal{E}}_n \cdot (\mathcal{C}^{\text{me}}\hat{\mathcal{E}}_n)\right), \quad (56)$$

where $\hat{\mathcal{E}}_n$ is the material form of the strain vector, $\rho_0$ is the mass density in the reference configuration and $\mathcal{C}^{\text{me}} =$ Diag[E, G, G] is the material form of the *elastic constitutive tensor*, with E and G the Young and shear undamaged elastic modulus.

The local form of the *Clausius Planck* inequality for the *mechanical dissipation* is valid [144, 155] and can be written as

$$\dot{\Xi}_m = \left(\frac{1}{\rho_0}\hat{P}_1^{\text{m}} - \frac{\partial\Psi}{\partial\hat{\mathcal{E}}_n}\right)\cdot\dot{\hat{\mathcal{E}}}_n - \frac{\partial\Psi}{\partial d}\dot{d} \geq 0, \quad (57)$$

where $\dot{\Xi}_m$ is the dissipation rate. Considering the fulfillment of the Clausius Planck inequality and the Coleman's principle, we have that the arbitrary variation $\dot{\hat{\mathcal{E}}}_n$ must be null [144]. Then, the following constitutive relation is obtained:

$$\hat{P}_1^{\text{m}} = (1-d)\mathcal{C}^{\text{me}}\hat{\mathcal{E}}_n = \mathcal{C}^{\text{ms}}\hat{\mathcal{E}}_n = (1-d)\hat{P}_{01}^{\text{m}}, \quad (58)$$

where $\mathcal{C}^{\text{ms}} = (1-d)\mathcal{C}^{\text{me}}$ and $\hat{P}_{01}^{\text{m}} = \mathcal{C}^{\text{me}}\hat{\mathcal{E}}_n$ are the material form of the *secant constitutive tensor* and the *elastic* FPK stress vector, respectively.

Inserting the result of (58) into (57) the following expression is obtained for the dissipation rate

$$\dot{\Xi}_m = -\frac{\partial\Psi}{\partial d}\dot{d} = \Psi_0\dot{d} \geq 0. \quad (59)$$

The internal state variable $d \in [0, 1]$ measures the lack of secant stiffness of the material as it can be seen in Fig. 12. Moreover, (59) shows that the temporal evolution of $d$ is always positive due to the fact that $\Psi_0 \geq 0$.

### *4.2.2 Damage Yield Criterion*

By analogy with the developments presented in Refs. [25, 95, 178], the damage yield criterion denoted by the scalar value $\mathcal{F}$ is defined as a function of the undamaged elastic

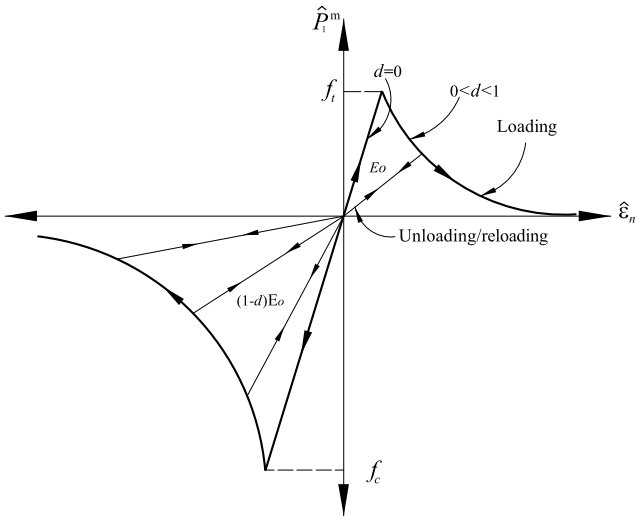


**Fig. 12** Differentiated traction/compression behavior and evolution of the internal variable

[10]For a detailed treatment of this topics, consult [12, 174, 176] and references therein.

free energy density and written in terms of the components of the material form of the undamaged principal stresses, $\hat{P}^{\mathrm{m}}_{p0}$, as

$$\mathcal{F} = \mathcal{P} - f_c = [1 + r(n-1)]\left[\sum_{i=1}^{3} (P^{\mathrm{m}}_{p0i})^2\right]^{1/2} - f_c \leq 0, \quad (60a)$$

where $\mathcal{P}$ is the equivalent (scalar) stress and the parameters $r$ and $n = f_c/f_t$ are given in function of the tension and compression strengths $f_c = \sqrt{(2\rho\Psi^0_c E_0)_L}$ and $f_t = \sqrt{(2\rho\Psi^0_t E_0)_L}$, respectively; $(\Psi^0_t)_L$ and $(\Psi^0_c)_L$ are the parts of the free energy density developed when the tension or compression limits are reached, respectively. These quantities are defined as

$$(\Psi^0_{t,c})_L = \sum_{i=1}^{3} \frac{\langle \pm P^{\mathrm{m}}_{p0i} \rangle \mathcal{E}_{ni}}{2\rho_0}, \quad r = \frac{\sum_{i=1}^{3} \langle P^{\mathrm{m}}_{p0i} \rangle}{\sum_{i=1}^{3} |P^{\mathrm{m}}_{p0i}|}, \quad (60b)$$

with $\Psi^0_L = (\Psi^0_t)_L + (\Psi^0_c)_L$ and $|u|$ is the absolute value function and $\langle \pm u \rangle$ is the McAuley's function. As it has been shown by Oliver *et al.* in [175], other kind of damage yield criteria can be used in substitution of $\mathcal{P}$, *e.g.* Mohr–Coulomb, Drucker–Prager, Von Mises etc. [95].

A more general expression equivalent to that given in (60a) [25] was originally proposed by Simo and Ju [216]: $\bar{\mathcal{F}} = \mathcal{G}(\mathcal{P}) - \mathcal{G}(f_c)$, where $\mathcal{G}(\bullet)$ is a scalar monotonic function to be defined ensuring that the energy dissipated by the material on an specific integration point is limited to the specific energy fracture of the material [175].

### 4.2.3 Evolution of the Damage Variable

The evolution law for $d$ is given by

$$\dot{d} = \dot{\mu} \frac{\partial \bar{\mathcal{F}}}{\partial \mathcal{P}} = \dot{\mu} \frac{\partial \mathcal{G}}{\partial \mathcal{P}}, \quad (61)$$

where $\dot{\mu} \geq 0$ is the *damage consistency* parameter. Additionally, the damage yield condition $\bar{\mathcal{F}} = 0$ and consistency condition $\dot{\bar{\mathcal{F}}} = 0$ are defined analogously as in plasticity theory [215]. The yield condition implies that

$$\mathcal{P} = f_c, \qquad \frac{\mathrm{d}\mathcal{G}(\mathcal{P})}{\mathrm{d}\mathcal{P}} = \frac{\mathrm{d}\mathcal{G}(f_c)}{\mathrm{d}f_c}, \quad (62)$$

and the consistency condition, along with a suitable definition of the damage variable expressed in terms of $\mathcal{G}$ *i.e.* $d = \mathcal{G}(f_c)$, allows to obtain the following expression for the damage consistency parameter:

$$\dot{\mu} = \dot{\mathcal{P}} = \dot{f}_c = \frac{\partial \mathcal{P}}{\partial \hat{P}^{\mathrm{m}}_{01}} \cdot \dot{\hat{P}}^{\mathrm{m}}_{01} = \frac{\partial \mathcal{P}}{\partial \hat{P}^{\mathrm{m}}_{01}} \cdot \boldsymbol{\mathcal{C}}^{\mathrm{me}} \dot{\hat{\mathcal{E}}}_n. \quad (63)$$

These results allow to rewrite (59) and (61) [25, 95] as

$$\dot{d} = \frac{\mathrm{d}\mathcal{G}}{\mathrm{d}\mathcal{P}} \dot{\mathcal{P}}, \qquad \dot{\Xi}_m = \Psi_0 \left[\frac{\mathrm{d}\mathcal{G}}{\mathrm{d}\mathcal{P}} \frac{\partial \mathcal{P}}{\partial \hat{P}^{\mathrm{m}}_{01}}\right] \cdot \boldsymbol{\mathcal{C}}^{\mathrm{me}} \dot{\hat{\mathcal{E}}}_n. \quad (64)$$

Finally, the Kuhn-Thucker relations: (a) $\dot{\mu} \geq 0$, (b) $\bar{\mathcal{F}} \leq 0$, (c) $\dot{\mu}\bar{\mathcal{F}} = 0$ have to be employed to derive the unloading–reloading conditions *i.e.* if $\bar{\mathcal{F}} < 0$ the condition (c) imposes $\dot{\mu} = 0$, on the contrary, if $\dot{\mu} > 0$ then $\mathcal{F} = 0$. The following expression is used for $\mathcal{G}$ [25, 175]:

$$\mathcal{G}(\chi) = 1 - \bar{\mathcal{G}}(\chi)/\chi = 1 - \chi^*/\chi e^{\kappa(1-\chi/\chi^*)}, \quad (65)$$

where $\bar{\mathcal{G}}(\chi)$ gives the initial yield stress for certain value of $\chi = \chi^*$ and $\chi \to \infty$ the final strength is zero.

The parameter $\kappa$ of (65) is calibrated to obtain an amount of dissipated energy equal to the specific fracture energy of the material when all the deformation path is followed.

Integrating (57) for an uniaxial tension process with a monotonically increasing load, and considering $\Psi_0 = \mathcal{P}^2/(2n^2E_0)$ [25], it is possible to obtain that the total energy dissipated is $\Xi^{\max}_t = (\mathcal{P}^{*2}/2\rho_0 E^0)[1/2 - 1/\kappa]$ [175]. Therefore, the expression for $\kappa$ is

$$\kappa = \frac{1}{\frac{\Xi^{\max}_t n^2 \rho_0 E^0}{f_c^2} - \frac{1}{2}} \geq 0, \quad (66)$$

where it has been assumed that the equivalent stress tension $\mathcal{P}^*$ is equal to the initial damage stress $f_c$. The value of $\Xi^{\max}_t$ corresponds to the fracture energy density $g_f$, which is derived from the fracture mechanics as $g^d_f = G^d_f/l_c$, where $G^d_f$ the tensile fracture energy and $l_c$ is the characteristic length of the fractured domain employed in the regularization process [146].

An identical procedure gives the fracture energy density $g^d_c$ for a compression process. Due to the fact that the value of $\kappa$ have to be the same for a compression or tension test, we have that $\Xi^{\max}_c = n^2 \Xi^{\max}_t$.

### 4.2.4 Tangential Constitutive Tensor

Starting from (58) and after several algebraic manipulations which can be reviewed in [25, 95], we obtain that the material form of the *tangent constitutive* tensor $\boldsymbol{\mathcal{C}}^{\mathrm{mt}}$ can be calculated as

$$\begin{aligned} \delta \hat{P}^{\mathrm{m}}_1 &= \boldsymbol{\mathcal{C}}^{\mathrm{ms}} \delta \hat{\mathcal{E}}_n + \delta \boldsymbol{\mathcal{C}}^{\mathrm{ms}} \hat{\mathcal{E}}_n = \boldsymbol{\mathcal{C}}^{\mathrm{mt}} \delta \hat{\mathcal{E}}_n \\ &= \left[(1-d)\mathbf{I} - \frac{\mathrm{d}\mathcal{G}}{\mathrm{d}\mathcal{P}} \hat{P}^{\mathrm{m}}_{01} \otimes \frac{\partial \mathcal{P}}{\partial \hat{P}^{\mathrm{m}}_{01}}\right] \boldsymbol{\mathcal{C}}^{\mathrm{me}} \delta \hat{\mathcal{E}}_n, \end{aligned} \quad (67)$$

where $\mathbf{I}$ is the identity tensor. It is worth noting that $\boldsymbol{\mathcal{C}}^{\mathrm{mt}}$ is nonsymmetric and depends on the elastic FPK stress vector. A backward Euler scheme used for the numerical integration of the constitutive damage model, can be consulted in Ref. [163].

### 4.3 Rate Dependent Effects

In this section, the rate independent damage model previously presented is extended to consider viscosity; the same formulation can be applied to visco elasticity neglecting the damage variable. For the case of materials with a visco plastic constitutive behavior, Ref. [214] can be consulted.

Viscosity is considered by means of *Maxwell*'s model [95, 177]; then, the FPK stress vector is obtained as the sum of a rate independent part $\hat{P}_1^{\mathrm{m}}$ (see (58)) and a viscous part $\hat{P}_1^{\mathrm{mv}}$ as

$$\hat{P}_1^{\mathrm{mt}} = \hat{P}_1^{\mathrm{m}} + \hat{P}_1^{\mathrm{mv}} = (1-d)\boldsymbol{\mathcal{C}}^{\mathrm{me}}\left(\hat{\mathcal{E}}_n + \frac{\eta}{\mathrm{E}}\hat{\mathcal{S}}_n\right), \tag{68}$$

where $\hat{P}_1^{\mathrm{mt}}$ is the material form of the *total* FPK stress vector, $\hat{\mathcal{S}}_n$ is the material strain rate vector and $\boldsymbol{\eta}^{\mathrm{sm}}$ is the material description of the *secant viscous* constitutive tensor defined as $\boldsymbol{\eta}^{\mathrm{sm}} = \eta/\mathrm{E}\boldsymbol{\mathcal{C}}^{\mathrm{ms}}$, where the scalar parameter $\eta$ is the *viscosity*. It is worth to note that in (68) for $\boldsymbol{\mathcal{C}}^{\mathrm{ms}} = \boldsymbol{\mathcal{C}}^{\mathrm{me}}$ the pure visco elastic behavior is recovered.

The dissipative power is given by

$$\dot{\Xi}_m = \left[\Psi_0 + \frac{\tau}{\rho_0}\dot{\hat{\mathcal{E}}}_n \cdot \boldsymbol{\mathcal{C}}^{\mathrm{me}}\hat{\mathcal{E}}\right]\frac{\mathrm{d}\mathcal{G}}{\mathrm{d}\mathcal{P}^{\mathrm{m}}}\frac{\partial \mathcal{P}^{\mathrm{m}}}{\partial \hat{P}_1^{\mathrm{m}}} \cdot \boldsymbol{\mathcal{C}}^{\mathrm{ms}}\dot{\hat{\mathcal{E}}}_n. \tag{69}$$

The linearized increment of the material form of the FPK stress vector is calculated as

$$\delta\hat{P}_1^{\mathrm{mt}} = \delta\hat{P}_1^{\mathrm{m}} + \delta\hat{P}_1^{\mathrm{mv}} = \boldsymbol{\mathcal{C}}^{\mathrm{mv}}\delta\hat{\mathcal{E}}_n + \boldsymbol{\eta}^{\mathrm{sm}}\delta\hat{\mathcal{S}}_n, \tag{70}$$

where $\hat{P}_{01}^{\mathrm{mv}}$ is the material form of the FPK visco elastic stress vector, $\delta\hat{\mathcal{S}}_n$ is the linearized increment of the strain rate vector and the material tangent constitutive tensor which considers the viscous effects is

$$\boldsymbol{\mathcal{C}}^{\mathrm{mv}} = \left[\mathbf{I} - \left(d\mathbf{I} + \frac{\mathrm{d}G}{\mathrm{d}\mathcal{P}^{\mathrm{m}}}(\hat{P}_{01}^{\mathrm{m}} + \hat{P}_{01}^{\mathrm{mv}}) \otimes \frac{\partial \mathcal{P}}{\partial \hat{P}_{01}^{\mathrm{m}}}\right)\right]\boldsymbol{\mathcal{C}}^{\mathrm{me}}. \tag{71}$$

The co-rotated form of the linearized increment of the total FPK stress vector is then obtained according to

$$\delta\,[\overset{\triangledown}{\hat{P}_1^{\mathrm{t}}}] = \boldsymbol{\Lambda}\delta\hat{P}_1^{\mathrm{mt}} = \boldsymbol{\mathcal{C}}^{\mathrm{sv}}\delta\,[\overset{\triangledown}{\hat{\epsilon}_n}] + \boldsymbol{\eta}^{\mathrm{ss}}\delta\,[\overset{\triangledown}{\hat{s}_n}], \tag{72}$$

where $\boldsymbol{\mathcal{C}}^{\mathrm{sv}} = \boldsymbol{\Lambda}\boldsymbol{\mathcal{C}}^{\mathrm{mv}}\boldsymbol{\Lambda}^T$ and $\boldsymbol{\eta}^{\mathrm{ss}} = \boldsymbol{\Lambda}\boldsymbol{\eta}^{\mathrm{sm}}\boldsymbol{\Lambda}^T$ are the spatial descriptions of the rate dependent tangent and secant viscous constitutive tensors, respectively.

### 4.4 Plastic Materials

For materials undergoing *non-reversible deformations*, the plasticity model formulated in the material configuration is used for predicting the corresponding mechanical response [181]. Assuming a thermally stable process, small elastic and finite plastic deformations, the free energy density $\Psi$ is given by [146]

$$\Psi = \Psi^e + \Psi^P = \frac{1}{2\rho_0}(\hat{\mathcal{E}}_n^e \cdot \boldsymbol{\mathcal{C}}^{\mathrm{me}}\hat{\mathcal{E}}_n^e) + \Psi^P(k_p), \tag{73}$$

where the $\hat{\mathcal{E}}_n^e$ is the elastic strain vector calculated subtracting the plastic strain vector $\hat{\mathcal{E}}_n^P$ from $\hat{\mathcal{E}}_n$, $\Psi^e$ and $\Psi^P$ are the elastic and plastic parts of the free energy density, $\rho_0$ is the density in the material configuration and $k_p$ is the *plastic damage* internal variable.

#### 4.4.1 Secant Constitutive Equation and Dissipation

Employing the Clausius Planck inequality and Coleman's principle [144, 155], the secant constitutive equation and the mechanical dissipation take the following form

$$\hat{P}_1^{\mathrm{m}} = \rho_0\frac{\partial\Psi(\hat{\mathcal{E}}_n^e, k_p)}{\partial\hat{\mathcal{E}}_n^e} = \boldsymbol{\mathcal{C}}^{\mathrm{ms}}\left(\hat{\mathcal{E}}_n - \hat{\mathcal{E}}_n^P\right) = \boldsymbol{\mathcal{C}}^{\mathrm{me}}\hat{\mathcal{E}}_n^e. \tag{74a}$$

$$\dot{\Xi}_m = \frac{\hat{P}_1^{\mathrm{m}} \cdot \dot{\hat{\mathcal{E}}}_n^P}{\rho_0} - \frac{\partial\Psi^P}{\partial k_p}\dot{k}_p \geq 0, \tag{74b}$$

where the material description of the secant constitutive tensor $\boldsymbol{\mathcal{C}}^{\mathrm{ms}}$ coincides with the elastic one $\boldsymbol{\mathcal{C}}^{\mathrm{me}}$.

#### 4.4.2 Plastic Yielding and Potential Functions

Both, the yield function, $\mathcal{F}_p$, $\mathcal{G}_p$, for the plasticity model, are formulated in terms of the material FPK stress vector $\hat{P}_1^{\mathrm{m}}$ and the plastic damage internal variable $k_p$ as

$$\mathcal{F}_p(\hat{P}_1^{\mathrm{m}}, k_p) = \mathcal{P}_p(\hat{P}_1^{\mathrm{m}}) - f_p(\hat{P}_1^{\mathrm{m}}, k_p) = 0, \tag{75a}$$

$$\mathcal{G}_p(\hat{P}_1^{\mathrm{m}}, k_p) = \mathcal{K}, \tag{75b}$$

where $\mathcal{P}_p(\hat{P}_1^{\mathrm{m}})$ is the (scalar) equivalent stress, which is compared with the *hardening* function $f_p(\hat{P}_1^{\mathrm{m}}, k_p)$ depending on the damage plastic internal variable $k_p$ and on the current stress state, and $\mathcal{K}$ is a constant value [147, 181].

According to the evolution of the plastic damage variable, $k_p$, it is possible to treat materials considering *isotropic* hardening as in Refs. [92, 185, 217]. It constitutes a measure of the energy dissipated during the plastic process and, therefore, is well suited for materials with *softening* [146, 180]; it can be defined by

$$0 \leq \left[k_p = \frac{1}{g_f^P}\int_0^t \hat{P}_1^{\mathrm{m}} \cdot \dot{\mathcal{E}}_n^P\, dt\right] \leq 1, \tag{76}$$

where $g_f^P = \int_0^\infty \hat{P}_1^{\mathrm{m}} \cdot \dot{\mathcal{E}}_n^P \mathrm{d}t = G_f^P/l_c$, $G_f^P$ is the specific plastic fracture energy of the material in tension and $l_c$ is the length of the fractured domain defined in analogous manner as for the damage model. Similarly, the normalized plastic damage variable for the case of a compressive test depends on $g_c^P$.

#### 4.4.3 Evolution Laws for the Internal Variables

The flow rules for $\hat{\mathcal{E}}_n^P$ and $k_p$ are defined as usual for plastic models in the material configuration [143, 146] *i.e.*

$$\dot{\hat{\mathcal{E}}}_n^P = \dot{\lambda}\frac{\partial \mathcal{G}_p}{\partial \hat{P}_1^{\mathrm{m}}}, \qquad \dot{k}_p = \dot{\lambda}\hat{\varrho}\cdot\frac{\partial \mathcal{G}_p}{\partial \hat{P}_1^{\mathrm{m}}} = \hat{\varrho}\cdot\dot{\hat{\mathcal{E}}}_n^P, \tag{77}$$

where $\dot{\lambda}$ is the plastic consistency parameter and $\hat{\varrho}$ is the following *hardening* vector [146, 181]

$$\dot{k}_p = \left[\frac{r}{g_f^P} + \frac{1-r}{g_c^P}\right]\hat{P}_1^{\mathrm{m}}\cdot\dot{\hat{\mathcal{E}}}_n^P = \widehat{\varrho}\cdot\dot{\hat{\mathcal{E}}}_n^P, \tag{78}$$

where $\hat{P}_1^{\mathrm{m}}\cdot\dot{\hat{\mathcal{E}}}_n^P$ is the plastic dissipation and $r$ is given in (60b). It is interesting to note that the proposed evolution rule allows to differentiate between tensile and compressive properties of the material.

In what regards the hardening function of (75a), the following evolution equation has been proposed [147]:

$$f_p(\hat{P}_1^{\mathrm{m}}, k_p) = r\sigma_t(k_p) + (1-r)\sigma_c(k_p), \tag{79}$$

where the (scalar) functions $\sigma_t(k_p)$ and $\sigma_c(k_p)$ represent the evolution of the yielding threshold in uniaxial tension and compression tests, respectively.

The loading/unloading conditions are derived in the standard form from the Kuhn-Tucker relations formulated for problems with unilateral restrictions, *i.e.*, (a) $\dot{\lambda} \geq 0$, (b) $\mathcal{F}_p \leq 0$ and (c) $\dot{\lambda}\mathcal{F}_p = 0$.

Starting from the plastic consistency condition $\dot{\mathcal{F}}_p = 0$ and considering the flow rules of (77), it is possible to deduce $\dot{\lambda}$ as [180, 181]

$$\dot{\lambda} = -\frac{\frac{\partial \mathcal{F}_p}{\partial \hat{P}_1^{\mathrm{m}}}\cdot(\mathcal{C}^{\mathrm{me}}\dot{\hat{\mathcal{E}}}_n)}{\left\{\frac{\partial \mathcal{F}_p}{\partial \hat{P}_1^{\mathrm{m}}}\cdot(\mathcal{C}^{\mathrm{me}}\frac{\partial \mathcal{G}_p}{\partial \hat{P}_1^{\mathrm{m}}}) - \frac{\partial f_p}{\partial k_p}\hat{\varrho}\cdot\frac{\partial \mathcal{G}_p}{\partial \hat{P}_1^{\mathrm{m}}}\right\}}. \tag{80}$$

#### 4.4.4 Tangent Constitutive Tensor

The material form of the tangent constitutive tensor is calculated taking the time derivative of (74a), considering the flow rules, replacing the plastic consistency parameter of (80) and, after several algebraic manipulations [180, 181] one obtains that $\delta\hat{P}_1^{\mathrm{m}} = \mathcal{C}^{\mathrm{mt}}\delta\hat{\mathcal{E}}_n$ with $\mathcal{C}^{\mathrm{mt}}$ given by

$$\mathcal{C}^{\mathrm{mt}} = \left[\mathcal{C}^{\mathrm{me}} - \frac{(\mathcal{C}^{\mathrm{me}}\frac{\partial \mathcal{G}_p}{\partial \hat{P}_1^{\mathrm{m}}})\otimes(\mathcal{C}^{\mathrm{me}}\frac{\partial \mathcal{F}_p}{\partial \hat{P}_1^{\mathrm{m}}})}{\frac{\partial \mathcal{F}_p}{\partial \hat{P}_1^{\mathrm{m}}}\cdot(\mathcal{C}^{\mathrm{me}}\frac{\partial \mathcal{G}_p}{\partial \hat{P}_1^{\mathrm{m}}}) - \Phi_p}\right], \tag{81}$$

where $\Phi_p$ is the so called *hardening parameter*.

## 4.5 Mixing Theory for Composite Materials

Each material point on the beam cross section is treated as a composite material according to the *mixing theory* [160, 163, 181], considering the following assumptions: (i) Each composite has a finite number of simple materials (see Fig. 11). (ii) Each component influence the mechanical behavior according to its volumetric participation factor defined as $k_q = V_q/V$, $(\sum_q k_q = 1)$ *i.e.* according to its proportional part $V_q$ (in terms of volume) with respect to the total volume $V$ associated to the material point. (iii) All the components are subjected to the same strain field.

Supposing that a generic material point, where coexist $N_c < \infty$ different components (hypothesis i), is subjected to a strain field described by the material strain vector $\hat{\mathcal{E}}_n$, according to hypothesis (iii) we have the following closing equation:

$$\hat{\mathcal{E}}_n \equiv (\hat{\mathcal{E}}_n)^1 = \cdots = (\hat{\mathcal{E}}_n)^j = \cdots = (\hat{\mathcal{E}}_n)^{N_c}, \tag{82}$$

which imposes the strain compatibility between components.

The free energy density of the composite is written for the adiabatic case as the weighted sum of the free energy of the components [181] $\Psi_c \equiv \sum_{q=1}^{N_c} k_q\Psi_q(\hat{\mathcal{E}}_n, \alpha_{p_q})$, where $\Psi_q(\hat{\mathcal{E}}_n, \alpha_{p_q})$ is the free energy of the $q^{\mathrm{th}}$ compounding substance with an associated constitutive model depending on $p$ internal variables, $\alpha_{p_q}$, and $k_q$ is the volumetric fraction of the component.

#### 4.5.1 Secant Constitutive Relation and Dissipation

For a composite material, it is possible to obtain the material form of the secant constitutive equation, the secant constitutive tensor, $\bar{\mathcal{C}}^{\mathrm{ms}}$ and the mechanical dissipation $\dot{\bar{\Xi}}_m$ for the composite in analogous way as for simple materials *i.e.*

$$\hat{P}_1^{\mathrm{m}} \equiv \sum_q^{N_c} k_q(\hat{P}_1^{\mathrm{m}})_q, \qquad \dot{\Xi}_m \equiv -\sum_{q=1}^{N_c} k_q(\dot{\Xi}_m)_q, \tag{83a}$$

where $(\hat{P}_1^{\mathrm{m}})_q$ and $(\dot{\Xi}_m)_q$, are the material form of the FPK stress vector and the mechanical dissipation of the $q$th component, respectively. From the above results it is possible to conclude that $\hat{P}_1^{\mathrm{m}} = \bar{\mathcal{C}}^{\mathrm{ms}}(\hat{\mathcal{E}}_n - \hat{\mathcal{E}}_n^P)$ with

$$\bar{\mathcal{C}}^{\mathrm{ms}} \equiv \sum_{q=1}^{N_c} k_q(\mathcal{C}^{\mathrm{ms}})_q, \qquad \hat{\mathcal{E}}_n^P = \sum_{q=1}^{N_c} k_q(\hat{\mathcal{E}}_n^P)_q, \tag{83b}$$

where $(\mathcal{C}^{\mathrm{ms}})_q$ and $(\hat{\mathcal{E}}_n^P)_q$ are the material form of the secant constitutive tensor and the (fictitious) plastic strain vector, corresponding to the average value of the plastic strain vector of the composite obtained using the mixing theory.

Then, the material form of the tangent constitutive tensor of the composite is estimated as

$$\delta \hat{P}_1^{\mathrm{m}} = \bar{\mathcal{C}}^{\mathrm{mt}} \delta \hat{\mathcal{E}}_n = \sum_{i=1}^{N_c} k_q (\mathcal{C}^{\mathrm{mt}})_q \delta \hat{\mathcal{E}}_n, \tag{84}$$

where $(\mathcal{C}^{\mathrm{mt}})_q$ is the material form of the tangent constitutive tensor of the $q$th component.

#### 4.5.2 Rate Dependent Effects

Using the same reasonings, the participation of rate dependent effects in the composite can be considered in the following way:

$$\begin{aligned} \hat{P}_1^{\mathrm{mt}} &\equiv \sum_{q}^{N_c} k_q (\hat{P}_1^{\mathrm{m}} + \hat{P}_1^{\mathrm{mv}})_q \\ &= \sum_{q}^{N_c} k_q \mathcal{C}_q^{\mathrm{ms}} \hat{\mathcal{E}}_n + k_q \boldsymbol{\eta}_q^{\mathrm{sm}} \hat{\mathcal{S}}_n = \bar{\mathcal{C}}^{\mathrm{ms}} \hat{\mathcal{E}}_n + \bar{\boldsymbol{\eta}}^{\mathrm{sm}} \hat{\mathcal{S}}_n, \end{aligned} \tag{85}$$

where $\bar{\boldsymbol{\eta}}^{\mathrm{sm}}$ corresponds tho the viscous secant tensor of the composite.

By analogy with (70), the linearized relation between material forms of strain and stress vectors is given by $\delta \hat{P}_1^{\mathrm{mt}} = \bar{\mathcal{C}}^{\mathrm{mv}} \delta \hat{\mathcal{E}}_n + \bar{\boldsymbol{\eta}}^{\mathrm{sm}} \delta \hat{\mathcal{S}}_n$, where

$$\bar{\mathcal{C}}^{\mathrm{mv}} = \sum_{q}^{N_c} k_q (\mathcal{C}^{\mathrm{mv}})_q, \qquad \bar{\boldsymbol{\eta}}^{\mathrm{sm}} = \sum_{q}^{N_c} k_q (\boldsymbol{\eta}^{\mathrm{sm}})_q. \tag{86}$$

Again, the co-rotated form of the linearized relation between strains and stresses for the composite material is based on the weighted sum of the spatial form of the tangent constitutive tensors $(\mathcal{C}^{\mathrm{mv}})^i$ plus the rate dependent tensors $(\eta^{\mathrm{ss}})^i$ of (71) for each one of the components and it is given by

$$\delta \overset{\triangledown}{[\hat{P}_1^{\mathrm{t}}]} = \bar{\mathcal{C}}^{\mathrm{sv}} \delta \overset{\triangledown}{[\hat{\varepsilon}_n]} + \bar{\boldsymbol{\eta}}^{\mathrm{ss}} \delta \overset{\triangledown}{[\hat{s}_n]}.$$

#### 4.5.3 Stress Resultant, Couples and Related Reduced Tensors

The distribution of materials on the beam cross sections can be arbitrary (see Fig. 11). Considering (83a) and (84), the material form of the cross sectional stress resultant and couples can be written as

$$\hat{n}^{\mathrm{m}} = \int_{\mathcal{A}_0} \bar{\mathcal{C}}^{\mathrm{ms}} \hat{\mathcal{E}}_n \mathrm{d}\mathcal{A}_0 + \int_{\mathcal{A}_0} \bar{\boldsymbol{\eta}}^{\mathrm{sm}} \dot{\hat{\mathcal{E}}}_n \mathrm{d}\mathcal{A}_0 \hat{\mathcal{S}}_n, \tag{87a}$$

$$\hat{m}^{\mathrm{m}} = \int_{\mathcal{A}_0} \widetilde{\boldsymbol{\varepsilon}} \bar{\mathcal{C}}^{\mathrm{ms}} \hat{\mathcal{E}}_n \mathrm{d}\mathcal{A}_0 + \int_{\mathcal{A}_0} \widetilde{\boldsymbol{\varepsilon}} \bar{\boldsymbol{\eta}}^{\mathrm{sm}} \dot{\hat{\mathcal{E}}}_n \mathrm{d}\mathcal{A}_0. \tag{87b}$$

The numerical computation of $\hat{n}^{\mathrm{m}}$ and $\hat{m}^{\mathrm{m}}$ is explained in detail in Sect. 7.

#### 4.5.4 Fiber Reinforcements and Structural Damping

The mixing rule provides an adequate framework for simulating the mechanical behavior of some advanced composed materials such as reinforced concrete [181]. In this case, the concrete is simulated as a *matrix* component which is reinforced with oriented fibres corresponding to the steel bars which are usually simulated by means of suitable one–dimensional constitutive laws (plasticity).

Due to the limitations imposed by the assumption that plane cross sections remain plane during the motion, the incorporation of stirrups or other kind of transversal reinforcements is not possible in the present formulation. However, the simulation of the effect of this kind of reinforcement is carried out by means of modifying the fracture energy and the limit stress of the matrix material for increasing the cross sectional ductility, deformability, resistance and so on [163–165].

The global structural damping is included in the terms corresponding to the stress resultant and stress couples throughout the cross sectional integration of inelastic stress fields, according to (87a) and (87b). Some branches of engineering are focused on the dynamic response of damped system but considering that the material behavior remains within the linear elastic range. Therefore, with this objective, several *ad hoc* approximations have been developed, most of them based on adding a damping term to the equilibrium equations, which is considered to be a function of the strain rates [108].

### 4.6 Linearization of the Stress Resultants and Stress Couples: Inelastic Case

The linearized form of $\delta \hat{P}_1^{\mathrm{mt}}$ can be expressed as

$$\delta \hat{P}_1^{\mathrm{mt}} = \delta \hat{P}_1^{\mathrm{m}} + \delta \hat{P}_1^{\mathrm{mv}} = \bar{\mathcal{C}}^{\mathrm{mv}} \delta \hat{\mathcal{E}}_n + \bar{\boldsymbol{\eta}}^{\mathrm{ms}} \delta \hat{\mathcal{S}}_n, \tag{88}$$

where $\bar{\mathcal{C}}^{\mathrm{mv}}$ and $\bar{\boldsymbol{\eta}}^{ms}$ are the material form of the rate dependent and viscous tangent constitutive tensors. The term $\delta \hat{\mathcal{S}}_n$ is given in (29a). The co-rotated form of (88) is obtained as

$$\delta \overset{\triangledown}{[\hat{P}_1^{\mathrm{t}}]} = \boldsymbol{\Lambda} \delta \hat{P}_1^{\mathrm{mt}} = \bar{\mathcal{C}}^{\mathrm{sv}} \delta \overset{\triangledown}{[\hat{\varepsilon}_n]} + \bar{\boldsymbol{\eta}}^{\mathrm{ss}} \delta \overset{\triangledown}{[\hat{s}_n]},$$

where $\bar{\mathcal{C}}^{\mathrm{sv}} = \boldsymbol{\Lambda} \bar{\mathcal{C}}^{\mathrm{mv}} \boldsymbol{\Lambda}^T$ and $\bar{\boldsymbol{\eta}}^{\mathrm{ss}} = \boldsymbol{\Lambda} \bar{\boldsymbol{\eta}}^{\mathrm{sv}} \boldsymbol{\Lambda}^T$ are the spatial form of the corresponding constitutive tensors.

On the other hand, the components of the spatial version of the total FPK stress vector can be expressed in the local (time varying) frame $\{\hat{t}_i\}$ as $\hat{P}_1^{\mathrm{t}} = P_{1i}^{\mathrm{t}} \hat{t}_i$ and in the case of its material form $\hat{P}_1^{\mathrm{mt}} = P_{1i}^{\mathrm{mt}} \hat{E}_i$; taking an admissible variation in both cases, one obtains

$$\delta \hat{P}_1^{\mathrm{mt}} = \delta P_{1i}^{\mathrm{mt}} \hat{E}_i, \qquad \delta \hat{P}_1^{\mathrm{t}} = \delta P_{1i}^{\mathrm{t}} \hat{t}_i + \delta \widetilde{\boldsymbol{\theta}} \hat{P}_1^{\mathrm{t}}. \tag{89}$$

Then, the co-rotated version of the linearized increment of the FPK stress vector is obtained according to $\delta\,[\overset{\triangledown}{\hat{P}}{}^{\mathrm{t}}_1]=\boldsymbol{\Lambda}\delta\hat{\mathbf{P}}^{\mathrm{mt}}_1=\delta P^{\mathrm{t}}_{1i}\hat{t}_i$ and, therefore, it is possible to deduce that

$$\delta\hat{P}^{\mathrm{t}}_1=\delta\,[\overset{\triangledown}{\hat{P}}{}^{\mathrm{t}}_1]+\delta\widetilde{\boldsymbol{\theta}}\,\hat{P}^{\mathrm{t}}_1=\boldsymbol{\mathcal{C}}^{\mathrm{sv}}\delta\,[\overset{\triangledown}{\hat{\varepsilon}}_n]+\boldsymbol{\eta}^{\mathrm{ss}}\delta\,[\overset{\triangledown}{\hat{s}}_n]+\delta\widetilde{\boldsymbol{\theta}}\,\hat{P}^{\mathrm{t}}_1. \tag{90}$$

As it has been previously explained, explicit expressions for the linearized forms of $\hat{n}^{\mathrm{m}}$ and $\hat{m}^{\mathrm{m}}$ can be estimated starting from the results provided in (86) and (90) and integrating over the cross sectional area as

$$\begin{aligned}
\delta\hat{n}^{\mathrm{m}}&=\int_{\mathcal{A}_0}\bar{\boldsymbol{\mathcal{C}}}^{\mathrm{mv}}\delta\hat{\mathcal{E}}_n\mathrm{d}\mathcal{A}_0+\int_{\mathcal{A}_0}\bar{\boldsymbol{\eta}}^{\mathrm{sm}}\delta\hat{\mathcal{S}}_n\mathrm{d}\mathcal{A}_0\\
&=\Big[\int_{\mathcal{A}_0}\bar{\boldsymbol{\mathcal{C}}}^{\mathrm{mv}}\mathrm{d}\mathcal{A}_0\Big]\delta\hat{\Gamma}_n-\Big[\int_{\mathcal{A}_0}\bar{\boldsymbol{\mathcal{C}}}^{\mathrm{mv}}\widetilde{\boldsymbol{\mathcal{E}}}\mathrm{d}\mathcal{A}_0\Big]\delta\hat{\Omega}_n\\
&\quad+\Big[\int_{\mathcal{A}_0}\bar{\boldsymbol{\eta}}^{\mathrm{sm}}\mathrm{d}\mathcal{A}_0\Big]\delta\dot{\hat{\Gamma}}_n-\Big[\int_{\mathcal{A}_0}\bar{\boldsymbol{\eta}}^{\mathrm{sm}}\widetilde{\boldsymbol{\mathcal{E}}}\mathrm{d}\mathcal{A}_0\Big]\delta\dot{\hat{\Omega}}_n\\
&=\bar{\mathbf{C}}^{\mathrm{mv}}_{nn}\delta\hat{\Gamma}_n+\bar{\mathbf{C}}^{\mathrm{mv}}_{nm}\delta\hat{\Omega}_n+\bar{\boldsymbol{\Upsilon}}^{\mathrm{sm}}_{nn}\delta\dot{\hat{\Gamma}}_n+\bar{\boldsymbol{\Upsilon}}^{\mathrm{sm}}_{nm}\delta\dot{\hat{\Omega}}_n,
\end{aligned}\tag{91a}$$

$$\begin{aligned}
\delta\hat{m}^{\mathrm{m}}&=\Big[\int_{\mathcal{A}_0}\widetilde{\boldsymbol{\mathcal{E}}}\bar{\boldsymbol{\mathcal{C}}}^{\mathrm{mv}}\mathrm{d}\mathcal{A}_0\Big]\delta\hat{\mathcal{E}}_n+\Big[\int_{\mathcal{A}_0}\widetilde{\boldsymbol{\mathcal{E}}}\bar{\boldsymbol{\eta}}^{\mathrm{sm}}\mathrm{d}\mathcal{A}_0\Big]\delta\hat{\mathcal{S}}_n\\
&=\Big[\int_{\mathcal{A}_0}\widetilde{\boldsymbol{\mathcal{E}}}\bar{\boldsymbol{\mathcal{C}}}^{\mathrm{mv}}\mathrm{d}\mathcal{A}_0\Big]\delta\hat{\Gamma}_n-\Big[\int_{\mathcal{A}_0}\widetilde{\boldsymbol{\mathcal{E}}}\bar{\boldsymbol{\mathcal{C}}}^{\mathrm{mv}}\widetilde{\boldsymbol{\mathcal{E}}}\mathrm{d}\mathcal{A}_0\Big]\delta\hat{\Omega}_n\\
&\quad+\Big[\int_{\mathcal{A}_0}\widetilde{\boldsymbol{\mathcal{E}}}\bar{\boldsymbol{\eta}}^{\mathrm{sm}}\mathrm{d}\mathcal{A}_0\Big]\delta\dot{\hat{\Gamma}}_n-\Big[\int_{\mathcal{A}_0}\widetilde{\boldsymbol{\mathcal{E}}}\bar{\boldsymbol{\eta}}^{\mathrm{sm}}\widetilde{\boldsymbol{\mathcal{E}}}\mathrm{d}\mathcal{A}_0\Big]\delta\dot{\hat{\Omega}}_n\\
&=\bar{\mathbf{C}}^{\mathrm{mv}}_{mn}\delta\hat{\Gamma}_n+\bar{\mathbf{C}}^{\mathrm{mv}}_{mm}\delta\hat{\Omega}_n+\bar{\boldsymbol{\Upsilon}}^{\mathrm{sm}}_{mn}\delta\dot{\hat{\Gamma}}_n+\bar{\boldsymbol{\Upsilon}}^{\mathrm{sm}}_{mm}\delta\dot{\hat{\Omega}}_n,
\end{aligned}\tag{91b}$$

where the *material* and *viscous* cross sectional tangential tensors $\bar{\mathbf{C}}^{\mathrm{mv}}_{ij}$ and $\bar{\boldsymbol{\Upsilon}}^{\mathrm{sm}}_{ij}$ $(i,j\in\{n,m\})$ are calculated in an completely analogous manner as for the elastic case but replacing the components of the elastic constitutive tensor by their tangent and viscous tangent counterparts.

The co-rotated variation of the stress resultant and couples are obtained as

$$\begin{aligned}
\delta\,[\overset{\triangledown}{\hat{n}}]=\boldsymbol{\Lambda}\delta\hat{n}^{\mathrm{m}}&=\bar{\mathbf{C}}^{\mathrm{sv}}_{nn}\delta\,[\overset{\triangledown}{\hat{\gamma}}_n]+\bar{\mathbf{C}}^{\mathrm{sv}}_{nm}\delta\,[\overset{\triangledown}{\hat{\omega}}_n]\\
&\quad+\bar{\boldsymbol{\Upsilon}}^{\mathrm{ss}}_{nn}\delta\,[\overset{\triangledown}{\dot{\hat{\gamma}}}_n]+\bar{\boldsymbol{\Upsilon}}^{\mathrm{ss}}_{nm}\delta\,[\overset{\triangledown}{\dot{\hat{\omega}}}_n],
\end{aligned}\tag{91c}$$

$$\begin{aligned}
\delta\,[\overset{\triangledown}{\hat{m}}]=\boldsymbol{\Lambda}\delta\hat{m}^{\mathrm{m}}&=\bar{\mathbf{C}}^{\mathrm{sv}}_{mn}\delta\,[\overset{\triangledown}{\hat{\gamma}}_n]+\bar{\mathbf{C}}^{\mathrm{sv}}_{mm}\delta\,[\overset{\triangledown}{\hat{\omega}}_n]\\
&\quad+\bar{\boldsymbol{\Upsilon}}^{\mathrm{ss}}_{mn}\delta\,[\overset{\triangledown}{\dot{\hat{\gamma}}}_n]+\bar{\boldsymbol{\Upsilon}}^{\mathrm{ss}}_{mm}\delta\,[\overset{\triangledown}{\dot{\hat{\omega}}}_n],
\end{aligned}\tag{91d}$$

where the spatial form of the cross sectional tangential tensors $\bar{\mathbf{C}}^{\mathrm{sv}}_{ij}$ and $\bar{\boldsymbol{\Upsilon}}^{\mathrm{ss}}_{ij}$ $i,j\in\{n,m\}$ are obtained applying the push–forward by $\boldsymbol{\Lambda}$ on their material counterparts *i.e.* $\bar{\mathbf{C}}^{\mathrm{sv}}_{ij}=\boldsymbol{\Lambda}\bar{\mathbf{C}}^{\mathrm{mv}}_{ij}\boldsymbol{\Lambda}^T$ and $\bar{\boldsymbol{\Upsilon}}^{\mathrm{ss}}_{ij}=\boldsymbol{\Lambda}\bar{\boldsymbol{\Upsilon}}^{\mathrm{sm}}_{ij}\boldsymbol{\Lambda}^T$, respectively.

Taking into account (90) and repeating the procedures for (91a) to (91d), one obtains

$$\delta\hat{\boldsymbol{\Psi}}_\star=\bar{\mathbf{C}}^{\mathrm{sv}}\begin{bmatrix}\delta\,[\overset{\triangledown}{\hat{\gamma}}_n]\\ \delta\,[\overset{\triangledown}{\hat{\omega}}_n]\end{bmatrix}+\bar{\boldsymbol{\Upsilon}}^{\mathrm{ss}}\begin{bmatrix}\delta\,[\overset{\triangledown}{\dot{\hat{\gamma}}}_n]\\ \delta\,[\overset{\triangledown}{\dot{\hat{\omega}}}_n]\end{bmatrix}+\boldsymbol{\mathcal{N}}\hat{\eta}^{\mathrm{s}}. \tag{92}$$

The above results can be rewritten, along with expressions for the linearized form of the material and co-rotated versions of the stress resultant and couples, as

$$\delta\,[\overset{\triangledown}{\hat{\Psi}}]=(\bar{\mathbf{C}}^{\mathrm{sv}}\boldsymbol{B}+\bar{\boldsymbol{\Upsilon}}^{\mathrm{ss}}\boldsymbol{\mathcal{V}})\hat{\eta}^{\mathrm{s}}, \tag{93a}$$

$$\delta\hat{\Psi}^{\mathrm{m}}=(\bar{\mathbf{C}}^{\mathrm{mv}}\bar{\boldsymbol{B}}^{\mathrm{s}}+\bar{\boldsymbol{\Upsilon}}^{\mathrm{ms}}\bar{\boldsymbol{\mathcal{V}}}^{\mathrm{s}})\hat{\eta}^{\mathrm{s}}, \tag{93b}$$

$$\delta\hat{\Psi}=(\bar{\mathbf{C}}^{\mathrm{sv}}\boldsymbol{B}+\bar{\boldsymbol{\Upsilon}}^{\mathrm{ss}}\boldsymbol{\mathcal{V}}+\boldsymbol{\mathcal{N}})\hat{\eta}^{\mathrm{s}}. \tag{93c}$$

In the deduction of (93a) to (93c) it also has been used the results of (22a) to (22c) and (31).

### 4.7 Damage Indices

Several criteria have been defined for estimating the damage level of structures [95, 119, 179]; some of them are defined for the global behavior of the structure, others can be applied to individual members or subparts of the structure [61]. The damage index here described is based on an analogy with the problem at the micro-scale, *i.e.* at the constitutive level.

A measure of the damage level of a material point can be obtained as the ratio of the real stress level, obtained applying the mixing rule, to its undamaged elastic counter part. Following this idea, it is possible to define the fictitious damage variable $\check{D}$ as follows:

$$\check{D}_p=1-\frac{\sum_{i=1}^{3}|P^{\mathrm{mt}}_{1i}|}{\sum_{i=1}^{3}|P^{\mathrm{mt}}_{1i0}|}, \tag{94}$$

where $|P^{\mathrm{mt}}_{1i}|$ and $|P^{\mathrm{mt}}_{1i0}|$ are the absolute values of the components of the existing and visco elastic stress vectors in material form, respectively. It is worth to note that $\check{D}$ considers any kind inelasticity (damage, plasticity, etc.) by means of the mixing rule. Initially, for low loading levels, the material remains elastic and $\check{D}_p=0$, but when the entire fracture energy of the material has been dissipated $|P^{\mathrm{m}}_{1i}|\to 0$ and, therefore, $\check{D}_p\to 1$.

Equation (94) can be extended to consider particular elements or even the whole structure by means of integrating the stresses over a finite volume of the structure. It allows defining the local and global damage indices as follows:

$$\check{D}_v=1-\frac{\int_{V_p}\big(\sum_i|P^{\mathrm{m}}_{1i}|\big)\mathrm{d}V_p}{\int_{V_p}\big(\sum_i|P^{\mathrm{m}}_{1i0}|\big)\mathrm{d}V_p}, \tag{95}$$

where $V_p$ is the volume of the part of the structure in consideration. The local/global damage index defined in (95) is

a force-based criterium as it has been explained in Ref. [95]. Considering (95) a *cross sectional* damage index, $\check{D}_{\mathcal{A}}(S)$, can be expressed restricting the integrations to the cross sectional area as

$$\check{D}_{\mathcal{A}}(S) = 1 - \frac{\int_{\mathcal{A}} \left( \sum_i |P^{\mathrm{m}}_{1i}| \right) \mathrm{d}\mathcal{A}}{\int_{\mathcal{A}} \left( \sum_i |P^{\mathrm{m}}_{1i0}| \right) \mathrm{d}\mathcal{A}} \quad \forall S \in [0, L]. \tag{96}$$

Then, (95) can be rewritten as $\check{D} = \int_0^L \check{D}_{\mathcal{A}}(S) \mathrm{d}S$. The cross sectional damage index has the virtue of being a dimensionally reduced quantity that capture in a scalar value the degradation level of the rod at the arch-length coordinate $S \in [0, L]$.

### 4.8 Numerical Model for EDDs

An EDD can be seen as a *dissipative nucleus* connecting two degree of freedom of the structure. A suitable numerical model can be obtained from the beam model releasing the rotational degrees of freedom and concentrating the mechanical behavior of the device in a unique material point in the middle of the resulting bar. Then, the position of a point in the EDD is obtained from (3) as $\hat{\varphi}(S, t)$ (considering that $\xi_\beta = 0$). The current orientation of the EDD bar of initial length $L^*$ is $\mathbf{\Lambda}^*(t)$ and the position of the dissipative nucleus is obtained as $\hat{\varphi}(L^*/2, t)$ where $L^*/2$ is the arch-length coordinate of the middle point in the bar element and the axial strain and strain rate in the dissipative point is

$$\mathcal{E}_{d_1}(t) = \left\{ (\mathbf{\Lambda}^{*T} \hat{\varphi}_{,S}) \cdot \hat{E}_1 \right\} \Big|_{(L^*/2,t)} - 1, \tag{97a}$$

$$\dot{\mathcal{E}}_{d_1}(t) = \left\{ (\mathbf{\Lambda}^{*T} (\dot{\hat{\varphi}}_{,S} - \tilde{\mathbf{v}}_n \hat{\varphi}_{,S})) \cdot \hat{E}_1 \right\} \Big|_{(L^*/2,t)}. \tag{97b}$$

#### 4.8.1 Constitutive Relations for EDDs

A versatile strain-stress relationship for EDDs has been proposed in Ref. [162]. It has the following general form:

$$P^{\mathrm{m}}_d(\mathcal{E}_{d_1}, \dot{\mathcal{E}}_{d_1}, t) = P^{\mathrm{m}}_{d_1}(\mathcal{E}_{d_1}, t) + P^{\mathrm{m}}_{d_2}(\dot{\mathcal{E}}_{d_1}, t), \tag{98}$$

where $P^{\mathrm{m}}_d$ is the average stress in the EDD, $\mathcal{E}_{d_1}$ the strain level, $t$ the time, $\dot{\mathcal{E}}_{d_1}$ the strain rate, $P^{\mathrm{m}}_{d_1}$ and $P^{\mathrm{m}}_{d_2}$ are the strain dependent and rate dependent parts of the stress, respectively. From the experimental results carried out on different types of devices, it is possible to state that $P^{\mathrm{m}}_{d_1}$ should include the following characteristics: *hysteretic* behavior, *hardening* and *variable* elastic modulus among others.

#### 4.8.2 Rate Dependent Part

The following general form can be used for $P^{\mathrm{m}}_{d_2}$:

$$P^{\mathrm{m}}_{d_2}(\dot{\mathcal{E}}_{d_1}, t) = c_d(\dot{\mathcal{E}}_{d_1}) \dot{\mathcal{E}}_{d_1}, \tag{99}$$

where $c_d$ is the (nonlinear) viscous coefficient of the device which is obtained fitting a polynomial to experimental data [162] using, for example, cyclic sinusoidal tests on a EDD at different maximum displacements and frequencies.

Let $\Delta E$ be the dissipated energy increment, corresponding to two cyclic tests carried out at the same maximum displacement, $u$, but for different consecutive frequencies $\varpi_{i+1}$ and $\varpi_i$, ($i$ is the frequency index). The following expression for the viscous component of the force in the device can be used:

$$A_t P^{\mathrm{m}}_{d_2} = h_t c_d(\varpi) \dot{\mathcal{E}}_{d_1} = h_t c_d(\dot{\mathcal{E}}_{d_1}) \dot{\mathcal{E}}_{d_1}, \tag{100}$$

where $A_t$ and $h_t$ are the average area and the average thickness of the test specimen. If the values of the two loading frequencies are close (numbered as $i$ and $j$, respectively), it is possible to suppose that the coefficients $c_{dij}$ of the viscous coefficient are

$$c_{dij} = \frac{\Delta E}{u_j^2 \left[ \varpi_{i+1}^2 \lambda_{i+1} - \varpi_i^2 \lambda_i \right]}, \tag{101}$$

where $\lambda_i = \int_0^{T_i} \cos^2(\varpi_i t) \mathrm{d}t$. Then, it is possible to fit a polynomial to the values of all the obtained coefficients $c_{dij}$ [162] in function of the frequency. For example, for the case of elastomeric devices, it is possible to consider that (99) is approximately equivalent to

$$P^{\mathrm{m}}_d = P^{\mathrm{m}}_{d_1} + h_t A_t^{-1} \overline{c}_d \dot{\mathcal{E}}_{d_1}, \tag{102}$$

where $\overline{c}_d \in \mathbb{R}$ is experimental.

#### 4.8.3 Rate Independent Part

Hardening can be simulated by means of an appropriated nonlinear elastic curve added to the non viscous hysteretic cycles which is defined numerically by means of a polynomial, whose coefficients are fitted to experimental data obtained from the specific device to be modeled.

Rate independent hysteretic behavior is obtained solving the following system of equations [162]:

$$P^{\mathrm{m}}_{d_1}(\mathcal{E}_{d_1}, t) = K_y(\varsigma^{\flat}) \mathcal{E}_{d_1} + [K_e(\varsigma^{\flat}) - K_y(\varsigma^{\flat})] e \tag{103a}$$

$$\text{if } \dot{\mathcal{E}}_{d_1} e \geqslant 0 \rightarrow \dot{e} = \left[ 1 - \left| \frac{e}{d_y(\varsigma^{\flat})} \right|^{n(\varsigma^{\flat})} \right] \dot{\mathcal{E}}_{d_1}, \tag{103b}$$

$$\text{else} \qquad \rightarrow \dot{e} = \dot{\mathcal{E}}_{d_1},$$

where $K_e$, $K_y$ are the elastic and post yielding stiffness, $d_y$ is the yielding strain level and $e \in [-d_y, d_y]$ represents an internal variable of plastic strain. The parameter $n$ in the associated flow rule of (103b) describes the degree of smoothness exhibited by the transition zone between the pre and the post yielding branches.

The model solves the system of equations (103a) and (103b) taking into account that $K_e$, $K_y$, $d_y$, and $n$ are function of $\varsigma^\flat = (\mathcal{E}^\flat_{d_1}, P^{\mathrm{m}\flat}_d)$ the point in the $\mathcal{E}_{d_1} - P^{\mathrm{m}}_{d_1}$ space where the last change of sign of $\dot{\mathcal{E}}_{d_1}$ has occurred. The algorithm updates the parameters of the model for each change of sign of the strain rate; on the contrary, the parameters are maintained constants.

Explicit expressions for $K_e = \wp_1(\varsigma^\flat)$, $K_y = \wp_2(\varsigma^\flat)$, $d_y = \wp_3(\varsigma^\flat)$, $n = \wp_4(\varsigma^\flat)$ are determined from experimental data. With this model it is possible to simulate the mechanical behavior of a wide variety of devices *e.g.*

1. Linear elastic spring, $c_d = 0$, $\wp_1 = \wp_2 =$ constant, $\wp_3 \sim \infty$ and $\wp_4 = 1$.
2. Viscous dashpot, $c_d =$ constant, $\wp_1 = \wp_2 = 0$, $\wp_3 \sim \infty$ and $\wp_4 = 1$.
3. Maxwell's model, $c_d =$ constant, $\wp_1 = \wp_2 =$ constant, $\wp_3 \sim \infty$ and $\wp_4 = 1$.
4. Visco-plastic device, $c_d =$ constant, $\wp_1 \geqslant \wp_2 > 0$, $n \in [1, 100]$ and $\mathcal{E}_y > 0$. Particularly, if $c_d = \wp_2 = 0$ and $n = 1$ a bilinear model is obtained.
5. Nonlinear viscous dashpot, $c_d = (\dot{\mathcal{E}}_{d_1})^{K_c}$ $(0 < K_c < 1)$, $\wp_1 = \wp_2 = 0$, $\wp_3 \sim \infty$ and $\wp_4 = 1$ (see *e.g.* [223]).

A particular calibration of the parameters for the case of elastomeric materials can be found in [162]).

### 4.9 Integration Algorithm

The flow chart of the algorithm that integrates the system of (103b) is shown in Fig. 13. The algorithm starts by assigning initial values to the parameters of the model. For each strain level $\mathcal{E}^i_{d_1}$ the algorithm verifies if the strain rate, changes of sign. If this is the case, an updating procedure for the parameters $\wp_k$ $(k = 1, \ldots, 4)$ is carried out. On the contrary, the parameters are maintained. Then plastic strain and stress are then estimated. The same algorithm is used for calculating the tangential stiffness as it will be explained in following.

*Tangent Stiffness* The tangent relation for the EDDs is obtained numerically using the *perturbation* method described in Ref. [52]. It consists in applying a small increment[11] to the strain $\mathcal{E}_{d_1}$, denoted by $\delta\mathcal{E}_{d_1}$; after solving the system of (103b) for the total strain $(\mathcal{E}_{d_1} + \delta\mathcal{E}_{d_1})$, the new stress level $P^{\mathrm{m}}_{d_1}$ is determined. Further, the hardening and viscous contributions have to be added to obtain the new total stress $P^{\mathrm{m}}_d(\mathcal{E}_{d_1} + \delta\mathcal{E}_{d_1})$. The tangential stiffness of the device, $K^t$, is then calculated as

$$K^t = \frac{\delta P^{\mathrm{m}}_d}{\delta\mathcal{E}_{d_1}} = \frac{P^{\mathrm{m}}_d(\mathcal{E}_{d_1} + \delta\mathcal{E}_{d_1}) - P^{\mathrm{m}}_d(\mathcal{E}_{d_1})}{\delta\mathcal{E}_{d_1}}. \tag{104}$$

[11] Here the notion of smallness corresponds to the precision of the machine used in the numerical simulations.

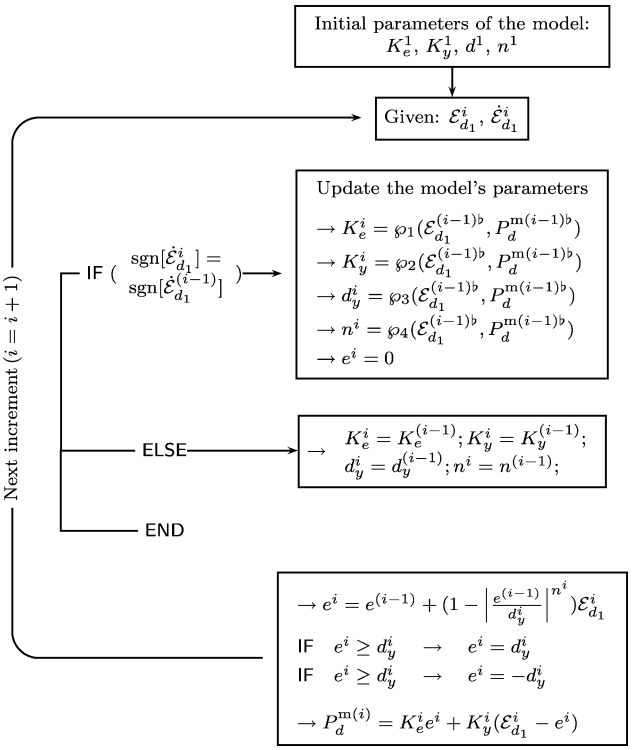


**Fig. 13** Flowchart of the constitutive relation for EDDs

It is important to note that the sign of the perturbation has to be the same as $\dot{\mathcal{E}}_{d_1}$ to obtain a tangential stiffness consistent with the sign of the loading process in the device when cyclic actions are considered.

## 5 Linearization of the Virtual Work Principle

As stated by Marsden (see Chap. 5 of [159]), nonlinear problems in continuum mechanics are invariably solved by linearizing a suitable form of nonlinear equilibrium equations and iteratively solving the resulting linear systems until a solution to the nonlinear problem is found. The Newton-Raphson method is the most popular example of such a technique [31]. Correct linearization of the nonlinear equations is fundamental for the success of such techniques. This section is concerned with the linearization of the virtual work principle to obtain the linearized equilibrium equation, in a manner consistent with the geometry of the configurational manifold where the involved kinetic and kinematical quantities belong.

Considering $\hat{\eta}^{\mathrm{s}} \in T\mathcal{C}_t$ and denoting by $\mathcal{L}[G]$ the linear part of the functional $G(\hat{\Phi}, \hat{\eta}^{\mathrm{s}})$ at the configuration defined by $\hat{\Phi}_* \equiv (\hat{\varphi}_*, \mathbf{\Lambda}_*) \in \mathcal{C}_t$; by definition we have

$$\mathcal{L}[G(\hat{\Phi}_*, \hat{\eta}^{\mathrm{s}})] \triangleq G(\hat{\varphi}_*, \hat{\eta}^{\mathrm{s}}) + DG(\hat{\Phi}_*, \hat{\eta}^{\mathrm{s}}) \cdot \hat{p}^{\mathrm{s}}, \tag{105}$$

where the Frêchet differential $DG(\hat{\Phi}_*, \hat{\eta}^{\mathrm{s}}) \cdot \hat{p}^{\mathrm{s}}$ is obtained throughout the directional derivative formula

$$DG(\hat{\Phi}_*, \hat{\eta}^{\mathrm{s}}) \cdot \hat{p}^{\mathrm{s}} = \frac{\mathrm{d}}{\mathrm{d}\beta}\Big|_{\beta=0} G(\hat{\Phi}_*, \hat{\eta}^{\mathrm{s}}, \beta\hat{p}^{\mathrm{s}}),$$

and $\hat{p}^{\mathrm{s}} \equiv (\Delta\hat{\varphi}, \Delta\hat{\theta}) \in T_{\Phi}\mathcal{C}_t$ is an admissible variation as described in Sect. 3.2. The physical interpretation of (105) is standard [219]. The term $G(\hat{\Phi}_*, \hat{\eta}^{\mathrm{s}})$ supplies the *unbalanced force* at the configuration $\hat{\Phi}_*$ and the term $DG(\hat{\Phi}_*\hat{\eta}^{\mathrm{s}}) \cdot \hat{p}^{\mathrm{s}}$, linear in $\hat{p}^{\mathrm{s}}$, yields the so called *tangential stiffness*. If $\hat{\Phi}_*$ is an equilibrium configuration, we must have that $G(\hat{\Phi}_*, \hat{\eta}^{\mathrm{s}}) = 0$ for any $\hat{\eta}^{\mathrm{s}}$.

### 5.1 Linearization of $G_{\mathrm{int}}$

Before to develop the linearization of the internal force term, (45), it is necessary to obtain the linear part of the co–rotated variations of the reduced strain vectors, $\delta\,\overset{\triangledown}{[\hat{\mathbb{E}}]}_*$, given in matrix form in (22c), *i.e.*

$$\Delta\delta\,\overset{\triangledown}{[\hat{\mathbb{E}}]}_* = \Delta(\boldsymbol{B}_*\hat{\eta}^{\mathrm{s}}) = \begin{bmatrix} 0 & \Delta\widetilde{\boldsymbol{\varphi}}_{,S} \\ 0 & 0 \end{bmatrix}\hat{\eta}^{\mathrm{s}} = \mathbb{E}^T\hat{\eta}^{\mathrm{s}}, \tag{106}$$

where $\delta\,\overset{\triangledown}{[\hat{\mathbb{E}}]}_* = [\delta\,\overset{\triangledown}{[\hat{\gamma}]}_n, \delta\,\overset{\triangledown}{[\hat{\omega}]}_n]^T$ and it has been neglected the terms of order $\Delta\delta(\bullet) \approx 0$. Moreover, considering the previous result, employing (93a) to (93c) for the linearized increment of the internal cross sectional force and moment vectors and (22c) for the co-rotated variations of the reduced strain vectors, it is possible to express the linearization of $G_{\mathrm{int}*}$ as

$$\begin{aligned}
\Delta G_{\mathrm{int}*} &= \int_0^L \Delta(\delta\,\overset{\triangledown}{[\hat{\mathbb{E}}]}_* \cdot \hat{\Psi}_*)\mathrm{d}S, \\
&= \int_0^L \big(\Delta\delta\,\overset{\triangledown}{[\hat{\mathbb{E}}]}_* \cdot \hat{\Psi}_* + \delta\,\overset{\triangledown}{[\hat{\mathbb{E}}]}_* \cdot \Delta\hat{\Psi}_*\big)\mathrm{d}S, \\
&= \int_0^L \hat{\eta}^{\mathrm{s}T}\big(\mathbb{E}\hat{\Psi}_* \\
&\quad + \boldsymbol{B}_*^T(\bar{\mathbf{C}}_*^{\mathrm{sv}}\boldsymbol{B}_* + \bar{\boldsymbol{\Upsilon}}_*^{\mathrm{ss}}\boldsymbol{\mathcal{V}}_* + \boldsymbol{\mathcal{N}}_*)\hat{p}^{\mathrm{s}}\big)\mathrm{d}S.
\end{aligned} \tag{107}$$

It is necessary to note that

$$\mathbb{E}\hat{\Psi}_* = \begin{bmatrix} 0 & 0 \\ \widetilde{\boldsymbol{n}}_*[\frac{\mathrm{d}}{\mathrm{d}S}\mathbf{I}] & 0 \end{bmatrix}\hat{p}^{\mathrm{s}} = \boldsymbol{\mathcal{F}}_*\hat{p}^{\mathrm{s}}, \tag{108}$$

which allows to rewrite (107) as

$$\begin{aligned}
\Delta G_{\mathrm{int}*} &= \underbrace{\int_0^L \hat{\eta}^{\mathrm{s}T}\big(\boldsymbol{\mathcal{F}}_* + \boldsymbol{B}_*^T\boldsymbol{\mathcal{N}}_*\big)\hat{p}^{\mathrm{s}}\mathrm{d}S}_{K_{G*}} \\
&\quad + \underbrace{\int_0^L \hat{\eta}^{\mathrm{s}T}\big(\boldsymbol{B}_*^T\bar{\mathbf{C}}_*^{\mathrm{sv}}\boldsymbol{B}_*\big)\hat{p}^{\mathrm{s}}\mathrm{d}S}_{K_{M*}} \\
&\quad + \underbrace{\int_0^L \hat{\eta}^{\mathrm{s}T}\big(\boldsymbol{B}_*^T\bar{\boldsymbol{\Upsilon}}_*^{\mathrm{ss}}\boldsymbol{\mathcal{V}}_*\big)\hat{p}^{\mathrm{s}}\mathrm{d}S}_{K_{V*}}, \\
&= K_{M*} + K_{G*} + K_{V*},
\end{aligned} \tag{109}$$

where the scalars $K_{M*}$ $K_{G*}$ and $K_{V*}$ correspond to the *material* (constitutive), *geometric* (stress dependant) and *viscous* tangential stiffness.

Two observations can be made about (109):

(i) The linear part $\Delta G_{\mathrm{int}}(\hat{\Phi}_*, \hat{\eta}^{\mathrm{s}})$ constitutes a bilinear operator on $TC_{t_*}$.
(ii) The matrix $[\boldsymbol{B}^T\bar{\mathbf{C}}^{\mathrm{sv}}\boldsymbol{B}]_*$ of $K_{M*}$ is always symmetric although configuration dependent; in contrast with the matrices $[\boldsymbol{\mathcal{F}} + \boldsymbol{B}^T\boldsymbol{\mathcal{N}}]_*$ and $[\boldsymbol{B}^T\bar{\boldsymbol{\Upsilon}}^{\mathrm{ss}}\boldsymbol{\mathcal{V}}]_*$ of $K_{G*}$ $K_{V*}$ respectively, which are always nonsymmetric away from equilibrium.

### 5.2 Linearization of $G_{\mathrm{ine}}$

Considering the results of (49a) and (49b), the inertial term of the virtual work functional, (44), can be expressed as

$$G_{\mathrm{ine}} = \int_0^L \hat{\eta}^{\mathrm{s}T}\begin{bmatrix} \mathcal{A}_{\rho_0}\ddot{\hat{\varphi}}_* \\ \boldsymbol{\Lambda}(\mathbf{I}_{\rho_0}\hat{A}_{n*} + \widetilde{\hat{\boldsymbol{V}}}_{n*}\mathbf{I}_{\rho_0}\hat{V}_{n*}) \end{bmatrix}\mathrm{d}S, \tag{110}$$

where the spatial form of the rotational terms is phrased in terms of the material angular acceleration and velocity by convenience. Employing the same procedure as for the internal virtual work, the linearized increment of $G_{\mathrm{ine}}$ is

$$\begin{aligned}
\Delta G_{\mathrm{ine}} &= \int_0^L \hat{\eta}^{\mathrm{s}T}\begin{bmatrix} \Delta(\mathcal{A}_{\rho_0}\ddot{\hat{\varphi}}_*) \\ \Delta(\boldsymbol{\Lambda}_*\{\mathbf{I}_{\rho_0}\hat{A}_{n*} + \widetilde{\hat{\boldsymbol{V}}}_{n*}\mathbf{I}_{\rho_0}\hat{V}_{n*}\}) \end{bmatrix}\mathrm{d}S, \\
&= \int_0^L \hat{\eta}^{\mathrm{s}T}\begin{bmatrix} \mathcal{A}_{\rho_0}\Delta\ddot{\hat{\varphi}}_* \\ \hat{\Xi}_{\theta_1} + \hat{\Xi}_{\theta_2} \end{bmatrix}\mathrm{d}S
\end{aligned} \tag{111}$$

with $\hat{\Xi}_{\theta_1}$ and $\hat{\Xi}_{\theta_2}$ given by

$$\begin{aligned}
\hat{\Xi}_{\theta_1} &= -\boldsymbol{\Pi}[\boldsymbol{\mathcal{I}}_{\rho_0*}\hat{\alpha}_{n*} + \widetilde{\hat{\boldsymbol{v}}}_{n*}\boldsymbol{\mathcal{I}}_{\rho_0*}\hat{v}_{n*}]\Delta\hat{\theta}, \\
\hat{\Xi}_{\theta_2} &= \boldsymbol{\mathcal{I}}_{\rho_0*}\Delta\ddot{\hat{\theta}} \\
&\quad + (\widetilde{\hat{\boldsymbol{v}}}_{n*}\boldsymbol{\mathcal{I}}_{\rho_0*} - \boldsymbol{\mathcal{I}}_{\rho_0*}\widetilde{\hat{\boldsymbol{v}}}_{n*} - \boldsymbol{\Pi}[\boldsymbol{\mathcal{I}}_{\rho_0*}\hat{v}_{n*}])\Delta\dot{\hat{\theta}}.
\end{aligned} \tag{112}$$

This last results allow to rewrite $\Delta G_{\mathrm{ine}}$ as

$$\begin{aligned}
\Delta G_{\mathrm{ine}} &= \int_0^L \hat{\eta}^{\mathrm{s}T}\big[\boldsymbol{M}_*\ddot{\hat{\eta}}^{\mathrm{s}} + \boldsymbol{C}_{\mathrm{gyr}*}\dot{\hat{\eta}}^{\mathrm{s}} + \boldsymbol{K}_{\mathrm{cent}*}\hat{\eta}^{\mathrm{s}}\big]\mathrm{d}S, \\
&= M_* + K_{\mathrm{gyr}*} + K_{\mathrm{cent}*},
\end{aligned} \tag{113}$$

where the *mass*, *gyroscopic* and *centrifugal* stiffness matrices are [53]

$$\big[\boldsymbol{M}\big] = \begin{bmatrix} \mathcal{A}_{\rho_0}\mathbf{I} & 0 \\ 0 & \boldsymbol{\mathcal{I}}_{\rho_0} \end{bmatrix}, \tag{114a}$$

$$\big[\boldsymbol{C}_{\text{gyr}}\big] = \begin{bmatrix} 0 & 0 \\ 0 & \{\widetilde{\boldsymbol{v}}_n\boldsymbol{\mathcal{I}}_{\rho_0} - \boldsymbol{\mathcal{I}}_{\rho_0}\widetilde{\boldsymbol{v}}_n - \boldsymbol{\Pi}[\boldsymbol{\mathcal{I}}_{\rho_0}\hat{\upsilon}_n]\} \end{bmatrix}, \tag{114b}$$

$$\big[\boldsymbol{K}_{\text{cent}}\big] = \begin{bmatrix} 0 & 0 \\ 0 & -\boldsymbol{\Pi}[\boldsymbol{\mathcal{I}}_{\rho_0}\hat{\alpha}_n + \widetilde{\boldsymbol{v}}_n(\boldsymbol{\mathcal{I}}_{\rho_0}\hat{\upsilon}_n)] \end{bmatrix}, \tag{114c}$$

and $M_*$, $K_{\text{gyr}*}$ and $K_{\text{cent}*}$ are the corresponding *translational*, *gyroscopic* and *centrifugal* terms of the tangential stiffness, respectively.

From the previous equations it is possible to appreciate the mass matrix $\boldsymbol{M}$ is always symmetric; the gyroscopic matrix depends linearly on the angular velocity and the centrifugal stiffness matrix depends linearly on the angular acceleration and quadratically on the angular velocity.

### 5.3 Linearization of $G_{\text{ext}}$

Following the same procedure as before, the external contribution to $G$ can be written as

$$G_{\text{ext}} = \int_0^L \hat{\eta}^{\text{s}T} \begin{bmatrix} \mathrm{d}\hat{f}_g \\ \mathrm{d}\hat{m}_g \end{bmatrix} + \int_0^L \hat{\eta}^{\text{s}T} \begin{bmatrix} \hat{\mathcal{N}}_{\text{b}} \\ \hat{\mathcal{M}}_{\text{b}} \end{bmatrix} \mathrm{d}S + \sum_{k=1}^{Np} \hat{\eta}_k^{\text{s}T} \begin{bmatrix} \hat{P}_f^k \\ \hat{M}_f^k \end{bmatrix}, \tag{115}$$

where $Np$ is the number of points where external loads are applied. In the case of earthquake loading, the external body moment contribution can be neglected remaining only the force body loads due to the base acceleration $\ddot{\hat{a}}$ which is configuration independent and it vanish in the linearization process for obtaining the tangential stiffness tensor. The corresponding linearization simply produces $DG_{\text{ext}} \cdot \hat{p}^{\text{s}} = 0$.

Finally, (115) can be rewritten as

$$\mathcal{L}[G] = G_* + [K_M + K_V + K_G + M + K_{\text{gyr}} + K_{\text{cent}}]_*. \tag{116}$$

The discretization of (116) by using the FE method will be explained in detail in Sect. 7.

### 5.4 Contribution of the EDDs

The contribution of a EDD to the functional of (48) is given by

$$\mathbf{G}_{\text{D}} = \int_{L^*} P_d^{\text{m}}\delta\mathcal{E}_{d_1} dS + (\delta\hat{\varphi}^T\mathbf{M}_d\ddot{\hat{\varphi}})\Big|_{(L^*/2,t)}, \tag{117}$$

where $P_d^{\text{m}} = P_{1d}^{\text{m}}\hat{E}_1$; it was also assumed that $\boldsymbol{\mathcal{I}}_{\rho_0} \approx 0$, *i.e.* the contribution of the EDDs to the rotational mass of the system is negligible and $\mathbf{M}_d$ is the EDD's *translational inertia* matrix, *i.e.* the mass of the control system is supposed to be concentrated on the middle point of the bar. The term $\delta\mathcal{E}_{d_1}$ is given by

$$\delta\mathcal{E}_{d_1} = (\boldsymbol{\Lambda}^{*T}(\delta\hat{\varphi}_{,S} - \delta\widetilde{\boldsymbol{\theta}}\hat{\varphi}_{,S})) \cdot \hat{E}_1, \tag{118}$$

which corresponds to the linearized form (variation) of the material form of the axial strain in the EDD.

The spatial form of (118) is simply

$$\delta\epsilon_{d_1} = (\delta\hat{\varphi}_{,S} - \delta\widetilde{\boldsymbol{\theta}}\hat{\varphi}_{,S}) \cdot \hat{e}_1. \tag{119}$$

Consistently, one has that the spatial form of the linear increment in the axial stress of the EDD is $\delta P_d^{\text{s}} = K^{ts}\delta\epsilon_{d_1}$. Additionally, the linear part of $\delta\epsilon_{d_1}$ is obtained as

$$\Delta\delta\epsilon_{d_1} = \boldsymbol{\Pi}[\Delta\hat{\varphi}_{,S}]\delta\hat{\theta} \cdot \hat{e}_1. \tag{120}$$

Then, the linearization of the contribution of the EDDs to the total virtual work is obtained as

$$\delta\mathbf{G}_{\text{D}} = \int_0^{L^*} (K^{ts}\delta\epsilon_{d_1}^2 + P_d^{\text{s}}\Delta\delta\mathcal{E}_{d_1})\mathrm{d}S + \delta\hat{\varphi}^T\mathbf{M}_d\delta\ddot{\hat{\varphi}}. \tag{121}$$

## 6 Time-Stepping Scheme

An important effort has been devoted to develop time-stepping schemes for the integration of the nonlinear dynamic equations of motion involving finite rotations. As in the static case, the basic difficulty arises in the noncommutative nature of the group $SO(3)$ [220]. Simo and Vu-Quoc in [220] develop an implicit transient algorithm that extends the classical Newmark formulae, stated in $\mathbb{R}^3$, to $SO(3)$, obtaining a formulation similar to that of the linear case.[12] Alternatively, Rubin [201] provides a simplified implicit Newmark integration scheme for finite rotations. A comparison among implicit time-stepping schemes according to different choices of rotational parameters can be reviewed in [107, 108]. Recently, Mata *et al.* [164] have included the viscous and rate independent dissipation in the Reissner–Simo rod model providing updating rules for the kinetic and kinematical variables according to Newmark's scheme.

On the other hand, Newmark's family of implicit schemes fails to preserve certain conservation laws of the motion, such as the total energy and momentum of nonlinear Hamiltonian systems, producing numerical dissipation [48]. Algorithms which inherit the conservation properties are attractive due to the fact that conserved quantities often capture

[12] Mäkinen states in [149, 150] that it only constitutes an approximated version of the corrected formulae, which are given in his work for the spatial and material descriptions.

important qualitative characteristics of the long-term dynamics and numerically, conservation the total energy lead to convenient notions of algorithmic stability [88]. Simo *et al.* [217, 218] provide a detailed formulation and the numerical implementation of a time-stepping algorithm designed to conserve exactly the total energy, the linear and the angular momentum for 3D rods.

Some additional enhancements can be found: for example, Armero and Romero develop an energy-dissipating momentum-conserving time-stepping algorithms for nonlinear rods in Ref. [17]. Second order methods for high-frequency dissipative algorithms are given by the same authors in [16]. In [36] an energy-decaying scheme for beams is developed. In [199] an objective FE approach for the energy-momentum conserving dynamics of rods is developed and in Ref. [42] the same objective is achieved regarding nonlinear beams from the outset as constrained mechanical systems. An energy-decaying scheme based on [217] is presented in [107].

Bottasso *et al.* [44, 45] develop conserving/dissipating numerical schemes for the integration of elastic multi-body systems including rods. In [131] energy preserving implicit and explicit integrators for constrained multi-body systems are developed. A survey about non-linear dynamics of flexible multi-body systems is given in [109].

Recently, attention has been turned towards *variational integrators i.e.* algorithms formed from a discrete version of Hamilton's variational principle [132]. For conservative systems, usual variational principles of mechanics are used while for dissipative or forced systems, the Lagrange-d'Alembert principle is preferred.[13] A complete survey about variational integrators can be reviewed in [133, 157, 158]. Additionally, Kane *et al.* [116] discus about variational integrators and the Newmark algorithm for conservative and dissipative mechanical systems. An application to the design of variational integrators on the Lie group for the full body problem is given in Ref. [129]. At the author's knowledge, this type of methods have not been formally applied to the Reissner–Simo's rod theory.

The time-stepping scheme chosen herein for the updating procedure corresponds to the *classical Newmark* algorithm for the translational part of the motion and can be consulted in [31, 101]. To this end, time is considered as a set of discrete instants. The problem consists in determining $\hat{\boldsymbol{\Phi}} \in \mathcal{C}$ and $\dot{\hat{\boldsymbol{\Phi}}}$, $\ddot{\hat{\boldsymbol{\Phi}}} \in T_{\hat{\boldsymbol{\Phi}}}\mathcal{C}$ at these instants, which fulfills the equilibrium equations. As usual, at each time step the linearized problem is solved by means of an iterative scheme until convergency is achieved. Therefore, consistent updating procedures for strains, strain rates, stresses, etc. have to be developed. The approach here presented corresponds to an *Eulerian* updating procedure. Other works prefer to carry out the updating, as well as the consistent linearization, on the last converged configuration [108] yielding to an *updated Lagrangian* procedure or work directly on the initial configuration yielding to a *total Lagrangian* formulation [53, 151]. Even when both, the updated Lagrangian and the total one, can present some advantages, the algebraic processes required for obtaining consistent updating procedures as well as tangential stiffness tensors are much more involved.

[13] The main properties that make these algorithms attractive are: for the conservative case variational integrators are, *symplectic* [157] and momentum conserving. They also permit the systematic construction of higher order integrators with remarkably good energy behavior.

### 6.1 Formulation of the Problem

The method described herein employs the discrete counterparts of the exponential map and the *parallel transport* in $SO(3)$ as it will be explained in the next sections.

Let the subscript $n$ to denote the temporal discrete approximation of a given time–varying quantity at time $t_n \in \mathbb{R}^+$. Thus, for the field corresponding to the translational part of the motion one has $\hat{\varphi}_n(S) \triangleq \hat{\varphi}(S, t_n)$ and the same rule applies for $\dot{\hat{\varphi}}_n$ and $\ddot{\hat{\varphi}}_n(S)$. For the rotational field one has $\boldsymbol{\Lambda}_n(S) \triangleq \boldsymbol{\Lambda}(S, t_n)$ and analogously for the corresponding kinetic variables $\hat{v}_n(S)$, $\hat{\alpha}_n(S)$, $\hat{V}_n(S)$ and $\hat{A}_n(S)$. The corresponding angular velocity and angular acceleration tensors can be obtained as usual using the $\boldsymbol{\Pi}[\bullet] = \widetilde{\bullet}$ operator.

The basic problem consists in: Given a configuration $\hat{\boldsymbol{\Phi}}_n \in \mathcal{C}_{t_n}$, its associated linear and angular velocity and acceleration vectors, $(\dot{\hat{\varphi}}_n, \hat{v}_n)$ and $(\ddot{\hat{\varphi}}_n, \hat{\alpha}_n)$, respectively, obtain the *updated* configuration $\hat{\boldsymbol{\Phi}}_{n+1} \in \mathcal{C}_{t_{n+1}}$ and the corresponding linear and angular velocity and acceleration vectors $(\dot{\hat{\varphi}}_{n+1}, \hat{v}_{n+1})$ and $(\ddot{\hat{\varphi}}_{n+1}, \hat{\alpha}_{n+1})$, in a manner that is consistent with the virtual work principle.

The corresponding relations in spatial and material form have been summarized in Table 1.

The classical Newmark [31, 62, 101] algorithm for nonlinear elastodynamics [220] is employed to update the translational part of the configuration and its associated dynamic variables. In the case of the rotational part, Simo and Vu-Quoc [220] purpose to use a modified form of Newmark's time-stepping algorithm formulated in material form which is given in Table 2, where $\beta \in [0, \frac{1}{2}]$, $\gamma \in [0, 1]$ are the classical (scalar) parameters of the algorithm and $\Delta t$ is the time step.

A geometric interpretation of the algorithm can be consulted in Ref. [219]. For the rotational part the procedure

**Table 1** Discrete relations between angular velocity and acceleration vectors at times $t_n$ and $t_{n+1}$

| Material | | Spatial | |
|---|---|---|---|
| $t_n$ | $t_{n+1}$ | $t_n$ | $t_{n+1}$ |
| $\hat{V}_n$ | $\hat{V}_{n+1}$ | $\hat{v}_n = \boldsymbol{\Lambda}_n \hat{V}_n$ | $\hat{v}_{n+1} = \boldsymbol{\Lambda}_{n+1} \hat{V}_{n+1}$ |
| $\hat{A}_n$ | $\hat{A}_{n+1}$ | $\hat{\alpha}_n = \boldsymbol{\Lambda}_n \hat{A}_n$ | $\hat{\alpha}_{n+1} = \boldsymbol{\Lambda}_{n+1} \hat{A}_{n+1}$ |

**Table 2** Newmark algorithm on $\mathbb{R}^3 \times SO(3)$

Translation

$\hat{\varphi}_{n+1} = \hat{\varphi}_n + \hat{u}_n$

$\hat{u}_n = \Delta t \dot{\hat{\varphi}}_n + (\Delta t)^2\big[(\frac{1}{2} - \beta)\ddot{\hat{\varphi}}_n + \beta \ddot{\hat{\varphi}}_{n+1}\big]$

$\dot{\hat{\varphi}}_{n+1} = \dot{\hat{\varphi}}_n + \Delta t\big[(1-\gamma)\ddot{\hat{\varphi}}_n + \gamma \ddot{\hat{\varphi}}_{n+1}\big]$

Rotation

$\boldsymbol{\Lambda}_{n+1} = \exp[\widetilde{\boldsymbol{\theta}}_n]\boldsymbol{\Lambda}_n$

$\hat{\Theta}_n = \Delta t \hat{V}_n + (\Delta t)^2\big[(\frac{1}{2} - \beta)\hat{A}_n + \beta \hat{A}_{n+1}\big]$

$\hat{V}_{n+1} = \hat{V}_n + \Delta t\big[(1-\gamma)\hat{A}_n + \gamma \hat{A}_{n+1}\big]$

takes place in $SO(3)$. Given $\boldsymbol{\Lambda}_n$, it is updated by means of exponentiating the incremental rotation $\hat{\theta}_n \in \mathbb{R}^3$ to obtain $\boldsymbol{\Lambda}_{n+1} = \exp[\widetilde{\boldsymbol{\theta}}_n]\boldsymbol{\Lambda}_n$. This procedure ensures $\boldsymbol{\Lambda}_{n+1}$ remains in $SO(3)$. The spatial angular velocity and acceleration tensors can be obtained as

$$\widetilde{\boldsymbol{v}}_{n+1} = \boldsymbol{\Lambda}_{n+1}\widetilde{\boldsymbol{V}}_{n+1}\boldsymbol{\Lambda}_{n+1}^T \quad \text{and} \quad \widetilde{\boldsymbol{\alpha}}_{n+1} = \boldsymbol{\Lambda}_{n+1}\widetilde{\boldsymbol{A}}_{n+1}\boldsymbol{\Lambda}_{n+1}^T.$$

If material the form of the angular velocity and acceleration vectors are considered as independent variables using the Newmark scheme of Table 2, the obtained solution procedure yields to the case where the rotational and translational parts are integrated in similar way. This appears as a contradiction with the fact that the rotational part develops on $SO(3)$, however, more precise Newmark algorithms can be developed following the procedure of Ref. [149] and employing a tangential transformation to obtain an additive approximation between two consecutive rotation vectors. In this work only the approximated version of the Newmark algorithm on rotational manifold (as originally proposed in Ref. [220]) will be explained, due to the fact that it concerns with structures which dissipate most of the energy throughout inelastic mechanisms and therefore, no great advantages are obtained by means of using more sophisticated formulations for time-stepping algorithms.

### 6.2 Iterative Configuration Update

The linearized form of (105) is solved in a Newton–Raphson scheme for each time step $t_{n+1}$. Usually, each time step require several iterations to converge; lets denote generically by $(i)$ to the $i$th iteration. Assuming that the configuration $\hat{\boldsymbol{\Phi}}_{n+1}^{(i)} \in \mathcal{C}_{t_{n+1}}$ is known, by solving the linearized system it is possible to obtain an *incremental field* $\hat{p}_{n+1}^{\mathrm{s}} = (\Delta\hat{\varphi}_{n+1}^{(i)}, \Delta\hat{\theta}_{n+1}^{(i)})$ such as

$$\mathcal{L}[G_{n+1}^{(i)}] = G_{n+1}^{(i)} + DG_{n+1}^{(i)} \cdot \hat{p}_{n+1}^{\mathrm{s}(i)} \approx 0, \tag{122}$$

which is approximately zero for a new family of configuration variables in equilibrium. Then, the basic setup [220] is: Given $\hat{\boldsymbol{\Phi}}_{n+1}^{(i)} \in \mathcal{C}_{t_{n+1}}$ and the incremental field $\hat{p}_{n+1}^{(i)} \in$

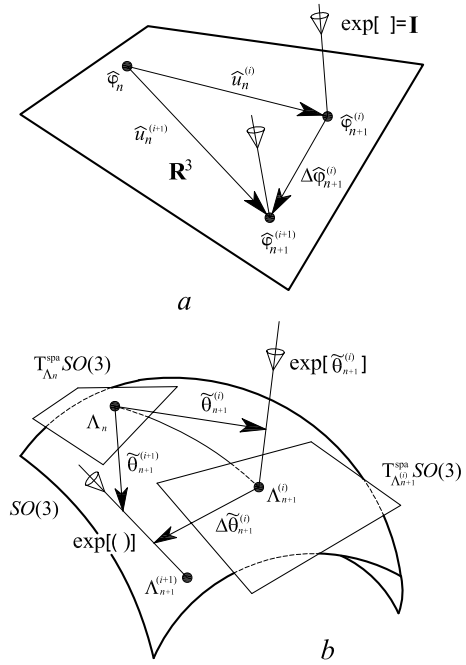


**Fig. 14** Iterative configuration updating in spatial form. (**a**): Translational part in $\mathbb{R}^3$. (**b**): Rotational part in $SO(3)$

$T\mathcal{C}_{t_{n+1}}$. Update $\hat{\boldsymbol{\Phi}}_{n+1}^{(i)}$ to $\hat{\boldsymbol{\Phi}}_{n+1}^{(i+1)}$ in a manner consistent with the time-stepping algorithm given in Table 2.

The translational part is updated as usual in $\mathbb{R}^3$. In this case, the exponential map reduces to the identity and parallel transport reduces to *shift* the base point (see Fig. 14a). The central issue concerns the update of incremental rotation.

On one hand, one has

$$\boldsymbol{\Lambda}_{n+1}^{(i)} = \exp[\widetilde{\boldsymbol{\theta}}_n^{(i)}]\boldsymbol{\Lambda}_n \quad \text{and} \quad \boldsymbol{\Lambda}_{n+1}^{(i+1)} = \exp[\widetilde{\boldsymbol{\theta}}_n^{(i+1)}]\boldsymbol{\Lambda}_n, \tag{123}$$

where $\widetilde{\boldsymbol{\theta}}_n^{(i)}$ and $\widetilde{\boldsymbol{\theta}}_n^{(i+1)}$ are the skew-symmetric tensors associated to the spatial form of the vectors which parameterize the rotation from $\boldsymbol{\Lambda}_n$ to $\boldsymbol{\Lambda}_{n+1}^{(i)}$ and $\boldsymbol{\Lambda}_{n+1}^{(i+1)}$ corresponding to the iterations $(i)$ and $(i+1)$, respectively. Note that the incremental rotation $\Delta\hat{\theta}_{n+1}^{(i)}$ is non-additive to $\hat{\theta}_{n+1}^{(i)}$ but

$$\boldsymbol{\Lambda}_{n+1}^{(i+1)} = \exp[\Delta\widetilde{\boldsymbol{\theta}}_{n+1}^{(i)}]\boldsymbol{\Lambda}_{n+1}^{(i)}. \tag{124}$$

On the other hand, it is interesting to note the fact that both $\widetilde{\boldsymbol{\theta}}_n^{(i)}\boldsymbol{\Lambda}_n$ and $\widetilde{\boldsymbol{\theta}}_n^{(i+1)}\boldsymbol{\Lambda}_n$ are elements of the same tangent space $\in T^{\mathrm{spa}}_{\boldsymbol{\Lambda}_n}SO(3)$ and $\Delta\widetilde{\boldsymbol{\theta}}_{n+1}^{(i)}\boldsymbol{\Lambda}_n^{(i)} \in T^{\mathrm{spa}}_{\boldsymbol{\Lambda}_{n+1}}SO(3)$, therefore, the updating procedure described in (124) makes perfect sense (see Fig. 14b).

The second formula in (123) requires the estimation of $\hat{\theta}_n^{(i+1)}$ from $\hat{\theta}_n^{(i)}$ and $\Delta\hat{\theta}_{n+1}^{(i)}$; which is obtained as

$$\hat{\theta}_n^{(i+1)} = \hat{\theta}_n^{(i)} + \mathbf{T}(\hat{\theta}_n^{(i)})\Delta\hat{\theta}_{n+1}^{(i)}, \tag{125}$$

where $\mathbf{T}(\hat{\theta}_n^{(i)}) = \mathbf{T}_n^{(i)}$ is a linearizing operator and it can be consulted in [220]. Other authors [104, 107] prefer to use

($123_2$) and (125) *i.e.* the total incremental rotation vector is the main independent variable selected for describing rotations. This last choice of parametrization for rotations produce symmetric tangential stiffness matrices but the deduction and implementation of the resulting numerical problem become much more complicated and time consuming during calculations.

### 6.3 Updating Procedure for the Angular Velocity and Acceleration

Translational velocities $\dot{\hat{\varphi}}^{(i)}_{n+1}$ and accelerations $\ddot{\hat{\varphi}}^{(i+1)}_{n+1}$ can be obtained by means the formulas of Table 2. The iterative version of the time–stepping algorithm is presented in Table 3. The updated angular velocity $\hat{V}^{(i+1)}_{n+1}$ and acceleration $\hat{A}^{(i+1)}_{n+1}$ vectors in material form are obtained assuming the following *approximation* for the time-step $t_{n+1}$ iterations $(i)$ and $(i+1)$:

$$\begin{aligned}\hat{\Theta}^{(i+1)}_n &= \Delta t\,\hat{V}_n + (\Delta t)^2\left[\left(\frac{1}{2}-\beta\right)\hat{A}_n + \beta\,\hat{A}^{(i+1)}_{n+1}\right],\\ \hat{\Theta}^{(i)}_n &= \Delta t\,\hat{V}_n + (\Delta t)^2\left[\left(\frac{1}{2}-\beta\right)\hat{A}_n + \beta\,\hat{A}^{(i)}_{n+1}\right],\end{aligned} \tag{126}$$

where $\hat{\Theta}^{(i)}_n = \mathbf{\Lambda}^T_n\hat{\theta}^{(i)}_n$ and $\hat{\Theta}^{(i+1)}_n = \mathbf{\Lambda}^T_n\hat{\theta}^{(i+1)}_n$. Subtracting the two expressions of (126) one obtains

$$\hat{A}^{(i+1)}_{n+1} = \hat{A}^{(i)}_{n+1} + \frac{1}{(\Delta t)^2\beta}\big[\hat{\Theta}^{(i+1)}_n - \hat{\Theta}^{(i)}_n\big]. \tag{127}$$

Similarly, in the case of the material angular velocities, one has

$$\begin{aligned}\hat{V}^{(i+1)}_n &= \hat{V}_n + \Delta t\big[(1-\gamma)\hat{A}_n + \gamma\,\hat{A}^{(i+1)}_{n+1}\big],\\ \hat{V}^{(i)}_n &= \hat{V}_n + \Delta t\big[(1-\gamma)\hat{A}_n + \gamma\,\hat{A}^{(i)}_{n+1}\big],\end{aligned} \tag{128}$$

subtracting the two expressions of (128) and employing (127) one obtains

$$\hat{V}^{(i+1)}_{n+1} = \hat{V}^{(i)}_{n+1} + \frac{\gamma}{\Delta t\beta}\big[\hat{\Theta}^{(i+1)}_n - \hat{\Theta}^{(i)}_n\big]. \tag{129}$$

Their spatial counterparts are obtained throughout the push-forward relations:

$$\hat{v}^{(i+1)}_{n+1} = \mathbf{\Lambda}^{(i+1)}_{n+1}\hat{V}^{(i+1)}_{n+1};\quad \text{and}\quad \hat{\alpha}^{(i+1)}_{n+1} = \mathbf{\Lambda}^{(i+1)}_{n+1}\hat{A}^{(i+1)}_{n+1}.$$

A geometric interpretation (in spatial description) of the procedure summarized in Table 3 can be formulated taking into account that

$$\begin{aligned}\hat{v}^{(i+1)}_{n+1} &= \mathbf{\Lambda}^{(i+1)}_{n+1}\mathbf{\Lambda}^{(i)T}_{n+1}\hat{v}^{(i)}_{n+1}\\ &\quad + \frac{\gamma}{(\Delta t)^2\beta}\mathbf{\Lambda}^{(i+1)}_{n+1}\mathbf{\Lambda}^T_n\big[\hat{\theta}^{(i+1)}_n - \hat{\theta}^{(i)}_n\big].\end{aligned} \tag{130}$$

**Table 3** Discrete Newmark algorithm

Translation

$\hat{\varphi}^{(i+1)}_{n+1} = \hat{\varphi}^{(i)}_{n+1} + \hat{u}^{(i)}_{n+1}$
$\dot{\hat{\varphi}}^{(i+1)}_{n+1} = \dot{\hat{\varphi}}^{(i)}_{n+1} + \frac{\gamma}{\Delta t\beta}\Delta\hat{\varphi}^{(i)}_{n+1}$
$\ddot{\hat{\varphi}}^{(i+1)}_{n+1} = \ddot{\hat{\varphi}}^{(i)}_{n+1} + \frac{1}{(\Delta t)^2\beta}\Delta\hat{\varphi}^{(i)}_{n+1}$

Rotation

$\mathbf{\Lambda}^{(i+1)}_{n+1} = \exp\big[\Delta\widetilde{\boldsymbol{\theta}}^{(i)}_{n+1}\big]\mathbf{\Lambda}^{(i)}_{n+1}$
$\exp\big[\widetilde{\boldsymbol{\theta}}^{(i+1)}_n\big] = \exp\big[\Delta\widetilde{\boldsymbol{\theta}}^{(i)}_{n+1}\big]\exp\big[\widetilde{\boldsymbol{\theta}}^{(i)}_n\big]$
$\hat{V}^{(i+1)}_{n+1} = \hat{V}^{(i)}_{n+1} + \frac{\gamma}{\Delta t\beta}\big[\hat{\Theta}^{(i+1)}_n - \hat{\Theta}^{(i)}_n\big]$
$\hat{A}^{(i+1)}_{n+1} = \hat{A}^{(i)}_{n+1} + \frac{1}{(\Delta t)^2\beta}\big[\hat{\Theta}^{(i+1)}_n - \hat{\Theta}^{(i)}_n\big]$

Since $\mathbf{\Lambda}^{(i+1)}_{n+1}\mathbf{\Lambda}^{(i)T}_{n+1} : T^{\text{spa}}_{\mathbf{\Lambda}^{(i)}_{n+1}}SO(3) \to T^{\text{spa}}_{\mathbf{\Lambda}^{(i+1)}_{n+1}}SO(3)$ and $\mathbf{\Lambda}^{(i+1)}_{n+1}\mathbf{\Lambda}^T_n : T^{\text{spa}}_{\mathbf{\Lambda}_n}SO(3) \to T^{\text{spa}}_{\mathbf{\Lambda}^{(i+1)}_{n+1}}SO(3)$, the first term in (130) may be interpreted as the *parallel transport* of $\hat{v}^{(i)}_{n+1}$ from $T^{\text{spa}}_{\mathbf{\Lambda}^{(i)}_{n+1}}SO(3)$ to $T^{\text{spa}}_{\mathbf{\Lambda}^{(i+1)}_{n+1}}SO(3)$; whereas the second term is the parallel transport of $[\hat{\theta}^{(i+1)}_n - \hat{\theta}^{(i)}_n]$ from $T^{\text{spa}}_{\mathbf{\Lambda}_n}SO(3)$ to $T^{\text{spa}}_{\mathbf{\Lambda}^{(i+1)}_{n+1}}SO(3)$.

The update procedure summarized in Table 3 applies for $i \geq 1$. For $i = 0$, the *initial guess* in the Newton process, is

$$\hat{\varphi}^{(0)}_{n+1} = \hat{\varphi}_n,\qquad \mathbf{\Lambda}^{(0)}_{n+1} = \mathbf{\Lambda}_n. \tag{131}$$

With this assumption $(\dot{\hat{\varphi}}^{(0)}_{n+1}, \hat{v}^{(0)}_{n+1})$ and $(\ddot{\hat{\varphi}}^{(0)}_{n+1}, \hat{\alpha}^{(0)}_{n+1})$ are computed using the Newmark formulae of Table 2.

### 6.4 Iterative Strain and Strain Rate Updating Procedure

The discrete form, about the configuration $\hat{\boldsymbol{\Phi}}^{(i)}_{n+1} \in \mathcal{C}_{t_{n+1}}$ of the spatial form of the translational and rotational strains (for each $S \in [0, L]$) can be written as

$$\hat{\gamma}^{(i)}_{n(n+1)} = \hat{\varphi}^{(i)}_{,S(n+1)} - \hat{t}^{(i)}_{1(n+1)}, \tag{132a}$$

$$\hat{\omega}^{(i)}_{n(n+1)} = \text{axial}\big[(\mathbf{\Lambda}_{n,S})^{(i)}_{n+1}(\mathbf{\Lambda}^T_n)^{(i)}_{n+1}\big] \tag{132b}$$

and the corresponding material descriptions are

$$\hat{\Gamma}^{(i)}_{n(n+1)} = [\mathbf{\Lambda}^T\hat{\gamma}_n]^{(i)}_{(n+1)},\ \hat{\Omega}^{(i)}_{n(n+1)} = [\mathbf{\Lambda}^T\hat{\omega}_n]^{(i)}_{(n+1)}. \tag{133}$$

Then, displacements are updated as described in Table 3, the vector normal to the cross section $\hat{t}_1$ is updated by means of the application of $\exp[\Delta\hat{\theta}^{(i)}_{n+1}]$ on the previous iterative rotation tensor, to obtain the updated orientation triad $\{\hat{t}_j\}^{(i)}_{n+1}$. Therefore, the spatial form of the updated translational strains vector is calculated as

$$\hat{\gamma}^{(i+1)}_{n(n+1)} = \hat{\varphi}^{(i+1)}_{,S(n+1)} - \hat{t}^{(i+1)}_{1(n+1)}, \tag{134}$$

and $\hat{\Gamma}^{(i+1)}_{n(n+1)} = \mathbf{\Lambda}^{(i+1)T}_{n+1}\hat{\gamma}^{(i+1)}_{n(n+1)}$ for the material description.

An additive updating rule for the spatial form of the curvature tensor can be constructed as follows

$$\widetilde{\boldsymbol{\omega}}^{(i+1)}_{n(n+1)} = \Delta\widetilde{\boldsymbol{\omega}}^{(i)}_{n(n+1)} + \exp[\Delta\widetilde{\boldsymbol{\theta}}^{(i)}_{n+1}]\widetilde{\boldsymbol{\omega}}^{(i)}_{n(n+1)}\exp[\Delta\widetilde{\boldsymbol{\theta}}^{(i)}_{n+1}]^T, \qquad (135)$$

$$\Delta\widetilde{\boldsymbol{\omega}}^{(i)}_{n(n+1)} = \frac{\mathrm{d}(\exp[\Delta\widetilde{\boldsymbol{\theta}}^{(i)}_{n+1}])}{\mathrm{d}S}\exp[-\Delta\widetilde{\boldsymbol{\theta}}^{(i)}_{n+1}],$$

and for the material description one obtains $\widetilde{\boldsymbol{\Omega}}^{(i+1)}_{n(n+1)} = \boldsymbol{\Lambda}^{(i+1)T}_{n+1}\widetilde{\boldsymbol{\omega}}^{(i+1)}_{n(n+1)}$. Finally, the updated rotational strain vectors can be obtained with the aid of the operator $\boldsymbol{\Pi}^{-1}$. In (135) it is necessary to calculate the term $(\mathrm{d}(\exp[\Delta\widetilde{\boldsymbol{\theta}}])/\mathrm{d}S)\exp[-\Delta\widetilde{\boldsymbol{\theta}}]$ which can be done according to the methods described in Ref. [219] or [113].

The spatial and material forms of the iterative strain vector at a given material point on the current cross section are obtained with the aid of the results of (134) and (135) as

$$\hat{\varepsilon}^{(i+1)}_{n(n+1)} = f_0[\hat{\gamma}^{(i+1)}_{n(n+1)} + \widetilde{\boldsymbol{\omega}}^{(i+1)}_{n(n+1)}\hat{\mathcal{T}}^{(i+1)}_{n+1}], \qquad (136a)$$

$$\hat{\mathcal{E}}^{(i+1)}_{n(n+1)} = f_0[\Gamma^{(i+1)}_{n(n+1)} + \widetilde{\boldsymbol{\Omega}}^{(i+1)}_{n(n+1)}\hat{\mathcal{E}}]. \qquad (136b)$$

The vector $\hat{\mathcal{E}}^{(i+1)}_{n(n+1)} = \boldsymbol{\Lambda}^{(i+1)T}_{n+1}\hat{\varepsilon}^{(i+1)}_{n(n+1)}$ is used for the numerical integration of the constitutive equations.

Having estimated $\hat{\varphi}^{(i+1)}_{n+1}$, $\dot{\hat{\varphi}}^{(i+1)}_{n+1}$ and $\hat{v}^{(i+1)}_{n+1}$ from Newmark's algorithm, it is possible to construct the discrete form of the co-rotated strain rate vector as

$$\hat{s}^{(i+1)}_{n(n+1)} = \dot{\hat{\varphi}}^{(i+1)}_{,S(n+1)} - \widetilde{\boldsymbol{v}}^{(i+1)}_{n(n+1)}\hat{\varphi}^{(i+1)}_{,S(n+1)} + \widetilde{\boldsymbol{v}}^{(i+1)}_{n,S(n+1)}\hat{\mathcal{E}}^{(i+1)}_{n+1}, \qquad (137)$$

with the material form given by $\hat{\mathcal{S}}^{(i+1)}_{n+1} = \boldsymbol{\Lambda}^{(i+1)T}_{n+1}\hat{s}^{(i+1)}_{n(n+1)}$.

It has been supposed in (137) that the angular velocity tensor is interpolated at the integration point bye means of using the following approximation:

$$\widetilde{\boldsymbol{v}}^{(i+1)}_{n(n+1)}(S) = \sum_{I}^{N_\mathrm{d}} N_I(S)\widetilde{\boldsymbol{v}}^I_n, \qquad \sum_{I}^{N_\mathrm{d}} N_I(S)_{,S}\,\widetilde{\boldsymbol{v}}^I_n,$$

where $N_\mathrm{d}$ is the number of nodal points on a beam element and the functions $N(s)$ are the standard isoparametric shape functions.

### 6.5 Discrete Form of the Linearized Functional

In order to give an explicit expression of the term $DG^{(i)}_{n+1}$, entering in the iterative Newton–Raphson scheme one has to write the discrete version of the linear forms of Sect. 5 in terms of the incremental (iterative) field $\hat{p}^{(i)}_{n+1} \in T\mathcal{C}_{t_{n+1}}$.

First, it is necessary to calculate the discrete counterpart of a curve onto the *perturbed configurations* in $\mathcal{C}_{t_{n+1}}$ by setting

$$\hat{\varphi}^{(i)}_{\varepsilon(n+1)} \triangleq \hat{\varphi}^{(i)}_{n+1} + \varepsilon\Delta\hat{\varphi}^{(i)}_{n+1}, \qquad (138a)$$

$$\boldsymbol{\Lambda}^{(i)}_{\varepsilon(n+1)} \triangleq \exp[\varepsilon\Delta\widetilde{\boldsymbol{\theta}}^{(i)}_{n+1}]\exp[\widetilde{\boldsymbol{\theta}}^{(i)}_{n+1}]\boldsymbol{\Lambda}_n, \qquad (138b)$$

which provides the following expressions for the linearized increments:

$$\Delta\hat{\varphi}^{(i)}_{n+1} \triangleq \frac{\mathrm{d}}{\mathrm{d}\varepsilon}\Big|_{\varepsilon=0}\hat{\varphi}^{(i)}_{\varepsilon(n+1)} = \Delta\hat{\varphi}^{(i)}_{n+1}, \qquad (139a)$$

$$\Delta\boldsymbol{\Lambda}^{(i)}_{n+1} \triangleq \frac{\mathrm{d}}{\mathrm{d}\varepsilon}\Big|_{\varepsilon=0}\boldsymbol{\Lambda}^{(i)}_{\varepsilon(n+1)} = \Delta\widetilde{\boldsymbol{\theta}}^{(i)}_{n+1}\boldsymbol{\Lambda}^{(i)}_n. \qquad (139b)$$

To proceed further with the linearization of the incremental rotational vector, we make use of representations of $\boldsymbol{\Lambda}^{(i)}_{\varepsilon(n+1)}$ and $\boldsymbol{\Lambda}^{(i)}_{n+1}$ in terms of exponential maps with base point at $\boldsymbol{\Lambda}_n$. One has that $\boldsymbol{\Lambda}^{(i)}_{\varepsilon(n+1)} = \exp[\widetilde{\boldsymbol{\theta}}^{(i)}_{\varepsilon(n)}]\boldsymbol{\Lambda}_n$ and, hence,

$$\exp\big[\widetilde{\boldsymbol{\theta}}^{(i)}_{\varepsilon(n)}\big] = \exp\big[\varepsilon\Delta\widetilde{\boldsymbol{\theta}}^{(i)}_{n+1}\big]\exp\big[\widetilde{\boldsymbol{\theta}}^{(i)}_{n}\big]. \qquad (140)$$

With this relation in mind, we obtain the linearization of the *discrete incremental rotation* $\hat{\theta}^{(i)}_{\varepsilon(n)}$, which is the axial vector of $\widetilde{\boldsymbol{\theta}}^{(i)}_{\varepsilon(n)}$ in (140), as

$$\delta\hat{\theta}^{(i)}_n = \frac{\mathrm{d}}{\mathrm{d}\varepsilon}\Big|_{\varepsilon=0}\hat{\theta}^{(i)}_{\varepsilon(n)} = \mathbf{T}^{(i)}_n\delta\hat{\theta}^{(i)}_{n+1}, \qquad (141)$$

where $\mathbf{T}^{(i)}_n : T^{\mathrm{spa}}_{\Lambda^{(i)}_{n+1}}SO(3) \to T^{\mathrm{spa}}_{\boldsymbol{\Lambda}_n}SO(3)$ is the linear tangential map of (125). From the time-stepping algorithm of Table 3 it is possible to write the linearized forms of the material angular velocity and acceleration as

$$\delta\hat{V}^{(i)}_{n+1} = \frac{\gamma}{\Delta t\beta}\boldsymbol{\Lambda}^T_n\mathbf{T}^{(i)}_n\Delta\hat{\theta}^{(i)}_{n+1}, \qquad (142a)$$

$$\delta\hat{A}^{(i)}_{n+1} = \frac{1}{(\Delta t)^2\beta}\boldsymbol{\Lambda}^T_n\mathbf{T}^{(i)}_n\Delta\hat{\theta}^{(i)}_{n+1}. \qquad (142b)$$

The discrete form of the *out-of-balance force* term of (122), $G^{(i)}_{n+1}$, is obtained from the contribution of the *internal, external* and *inertial* terms as follows:

*Internal Component* The discrete contribution of the internal component to the residual force vector is obtained as

$$G^{\mathrm{int}(i)}_{(n+1)} = \int_0^L \hat{\eta}^{\mathrm{s}T}\boldsymbol{B}^{(i)T}_{n+1}\hat{\Psi}^{(i)}_{n+1}\mathrm{d}S, \qquad (143)$$

where the discrete forms of the operators $\boldsymbol{B}^{(i)}_{n+1}$ is obtained evaluating the expressions of (22c) at the configuration $\hat{\Phi}^{(i)}_{n+1}$. Observe that the internal force and moment vector $\hat{\Psi}^{(i)}_{n+1}$ is evaluated at $t_{n+1}$ iteration $(i)$.

*Inertial Component* The discrete contribution of the inertial forces to $G^{(i)}_{n+1}$ is obtained as

$$G^{\mathrm{ine}(i)}_{(n+1)} = \int_0^L \hat{\eta}^{\mathrm{s}T} \begin{bmatrix} \mathcal{A}_{\rho_0} \ddot{\hat{\varphi}}^{(i)}_{n+1} \\ \{\mathcal{I}_{\rho_0} \hat{\alpha}_n + \tilde{\mathbf{v}}_n \mathcal{I}_{\rho_0} \hat{\mathbf{v}}_n\}^{(i)}_{n+1} \end{bmatrix} \mathrm{d}S, \tag{144}$$

where the time-discrete form of $\mathcal{I}_{\rho_0}$ is obtained from its material counterpart as $\mathcal{I}^{(i)}_{\rho_0(n+1)} = \mathbf{\Lambda}^{(i)}_{n+1} \mathbf{I}_{\rho_0} \mathbf{\Lambda}^{T(i)}_{n+1}$.

*External Component* The discrete contribution of the external loading to the out of balance force vector is obtained as

$$G^{\mathrm{ext}(i)}_{(n+1)} = \int_0^L \hat{\eta}^{\mathrm{s}T} \begin{bmatrix} \hat{\mathcal{N}}_g \\ \hat{\mathcal{M}}_g \end{bmatrix} \mathrm{d}S + \sum_{k=1}^{Np} \hat{\eta}^{\mathrm{s}\,T}_k \begin{bmatrix} \hat{P}^k_g \\ \hat{M}^k_g \end{bmatrix}, \tag{145}$$

which is obtained evaluating at $\hat{\mathbf{\Phi}}^{(i)}_{n+1}$ the configuration dependent terms.

### 6.6 Discrete Tangential Stiffness

If the configuration $\hat{\mathbf{\Phi}}^{(i)}_{n+1} \in \mathcal{C}_{t_{n+1}}$ is an equilibrium configuration, it follows that $G^{(i)}_{n+1} \approx 0 \ \forall \hat{\eta}^{\mathrm{s}} \in T\mathcal{C}_{n+1}$. On the contrary, a next iteration has to be performed using the discrete form of the tangential stiffness $DG^{(i)}_{n+1} \cdot \hat{p}^{\mathrm{s}(i)}_{n+1}$ of (122), which is obtained as

$$\begin{aligned} &DG^{(i)}_{n+1} \cdot \hat{p}^{\mathrm{s}(i)}_{n+1} \\ &\quad = \Delta G^{\mathrm{int}(i)}_{(n+1)} + \Delta G^{\mathrm{ine}(i)}_{(n+1)} + \Delta G^{\mathrm{ext}(i)}_{(n+1)} \\ &\quad = \left[K_M + K_V + K_G + K_P + M + K_{\mathrm{gyr}} + K_{\mathrm{cent}}\right]^{(i)}_{n+1}. \end{aligned} \tag{146}$$

Therefore, according to (109) we have that the discrete version of $[K_M + K_G + K_V]^{(i)}_{n+1}$ is obtained as

$$K^{(i)}_{M(n+1)} = \int_0^L \hat{\eta}^{\mathrm{s}T} \boldsymbol{B}^{(i)T}_{n+1} \bar{\mathbf{C}}^{\mathrm{sv}(i)}_{n+1} \boldsymbol{B}^{(i)}_{n+1} \hat{p}^{\mathrm{s}(i)}_{n+1} \mathrm{d}S, \tag{147a}$$

where $\bar{\mathbf{C}}^{\mathrm{sv}}_{ij} = \mathbf{\Lambda}^{(i)}_{n+1} \bar{\mathbf{C}}^{\mathrm{mv}}_{ij} \mathbf{\Lambda}^{(i)T}_{n+1}$ $i, j \in \{n, m\}$ and $\boldsymbol{B}^{(i)}_{n+1}$ is obtained from (22c) evaluating at $\hat{\varphi},^{(i)}_{S(n+1)}$. On the other hand, the geometric part given by

$$K^{(i)}_{G(n+1)} = \int_0^L \hat{\eta}^{\mathrm{s}T} \left[\boldsymbol{B}^{(i)T}_{n+1} \boldsymbol{\mathcal{N}}^{(i)}_{n+1} + \boldsymbol{\mathcal{F}}^{(i)}_{n+1}\right] \hat{p}^{\mathrm{s}(i)}_{n+1} \mathrm{d}S, \tag{147b}$$

where the stress dependent tensors $\boldsymbol{\mathcal{N}}$ and $\boldsymbol{\mathcal{F}}$ are calculated according to (92) and (108) but the associated values of the stress resultant and couples are those corresponding to $\hat{\mathbf{\Psi}}^{(i)}_{n+1} \in T^*\mathcal{C}_{n+1}$.

The viscous dependent part is obtained as

$$K^{(i)}_{G(n+1)} = \int_0^L \hat{\eta}^{\mathrm{s}} \left[\boldsymbol{B}^{(i)T}_{n+1} \bar{\mathbf{\Upsilon}}^{\mathrm{ss}(i)}_{n+1} \boldsymbol{\mathcal{V}}^{(i)}_{n+1}\right] \hat{p}^{\mathrm{s}(i)}_{n+1} \mathrm{d}S, \tag{147c}$$

where $\bar{\mathbf{\Upsilon}}^{\mathrm{ss}(i)}_{ij(n+1)} = \mathbf{\Lambda}^{(i)}_{n+1} \bar{\mathbf{\Upsilon}}^{\mathrm{ss}}_{ij} \mathbf{\Lambda}^{T(i)}_{n+1}$ $i, j \in \{n, m\}$ are calculated according to (91a) and (91b). The strain rate dependent tensor $\boldsymbol{\mathcal{V}}^{(i)}_{n+1}$ can be calculated considering (142a), along with the discrete form of the result of (26), which allow to establish the following equivalences:

$$\Delta \dot{\hat{\varphi}}^{(i)}_{n+1} = [\gamma/(\Delta t \beta)] \mathbf{I} \Delta \hat{\varphi}^{(i)}_{n+1},$$

$$\Delta \hat{V}^{(i)}_{n+1} = [\gamma/(\Delta t \beta)] \mathbf{\Lambda}^T_n \mathbf{T}^{(i)}_n \Delta \hat{\theta}^{(i)}_{n+1} = \mathbf{\Lambda}^T_n \Delta \dot{\hat{\theta}}^{(i)}_n,$$

identifying the tensors $[\gamma/(\Delta t \beta)]\mathbf{I}$ and $[\gamma/(\Delta t \beta)]\mathbf{T}^{(i)}_n$ with $\boldsymbol{\mathcal{H}}_a$ and $\boldsymbol{\mathcal{H}}_b$ of (30a) and (30b), respectively; Therefore, the following expressions are obtained:

$$\Delta \dot{\hat{\theta}}^{(i)}_n = \frac{\gamma}{\Delta t \beta} \mathbf{T}^{(i)}_n \Delta \hat{\theta}^{(i)}_{n+1}, \tag{148a}$$

$$\Delta \dot{\hat{\theta}},^{(i)}_{S(n)} = \frac{\gamma}{\Delta t \beta} \left[\mathbf{T}^{(i)}_n \Delta \hat{\theta},^{(i)}_{S(n+1)} + \mathbf{T}^{(i)}_n,_S \Delta \hat{\theta}^{(i)}_{n+1}\right], \tag{148b}$$

and $\delta \dot{\hat{\varphi}}^{(i)}_{n+1} = [\gamma/(\Delta t \beta)] \mathbf{I} \Delta \hat{\varphi},^{(i)}_{S(n+1)}$. The explicit expression for $\mathbf{T},_S$ appearing in (148a) and (148b) can be consulted in Ref. [53]. Finally, the discrete form of (28c) and (28d) can be rearranged as

$$\delta \overset{\nabla}{[\hat{\mathbf{\Phi}}]} = \left[\begin{array}{c|c} \boldsymbol{\mathcal{V}}^{\varphi(i)}_{n+1} & \boldsymbol{\mathcal{V}}^{\varphi\theta(i)}_{n+1} \\ \hline 0 & \boldsymbol{\mathcal{V}}^{\theta(i)}_{n+1} \end{array}\right] \hat{p}^{\mathrm{s}(i)}_{n+1} = \boldsymbol{\mathcal{V}}^{(i)}_{n+1} \hat{p}^{\mathrm{s}(i)}_{n+1}, \tag{149}$$

where

$$\boldsymbol{\mathcal{V}}^{\varphi(i)}_{n+1} = \gamma_{t\beta} \mathbf{I} \frac{\mathrm{d}}{\mathrm{d}S} \mathbf{I} - \tilde{\mathbf{v}}^{(i)}_{n+1} \frac{\mathrm{d}}{\mathrm{d}S} \mathbf{I},$$

$$\boldsymbol{\mathcal{V}}^{\varphi\theta(i)}_{n+1} = \dot{\tilde{\boldsymbol{\varphi}}},^{(i)}_{S(n+1)} + \tilde{\boldsymbol{\varphi}},^{(i)}_{S(n+1)} \gamma_{t\beta} \mathbf{T}^{(i)}_n - \tilde{\mathbf{v}}^{(i)}_{n+1} \tilde{\boldsymbol{\varphi}},^{(i)}_{S(n+1)},$$

$$\boldsymbol{\mathcal{V}}^{\theta(i)}_{n+1} = (\gamma_{t\beta} \mathbf{T}^{(i)}_n - \tilde{\mathbf{v}}_n) \frac{\mathrm{d}}{\mathrm{d}S} \mathbf{I} + \gamma_{t\beta} \left[\mathbf{T}^{(i)}_n \frac{\mathrm{d}}{\mathrm{d}S} \mathbf{I} + \mathbf{T}^{(i)}_n,_S\right],$$

and $\gamma_{t\beta} = \frac{\gamma}{\Delta t \beta}$.

Considering the iterative Newmark time-stepping scheme of Table 3, it is possible to rewrite the discrete form of the term $\mathcal{A}_{\rho_0} \ddot{\hat{\varphi}}$ in (111) as

$$\mathcal{A}_{\rho_0} \Delta \ddot{\hat{\varphi}}^{(i)}_{n+1} = \frac{1}{h^2 \beta} \mathcal{A}_{\rho_0} \mathbf{I} \Delta \hat{\varphi}^{(i)}_{n+1} = \boldsymbol{\Xi}_{\varphi} \Delta \hat{\varphi}^{(i)}_{n+1}, \tag{150}$$

where it is possible to see that $\boldsymbol{\Xi}_{\varphi}$ is a configuration independent tensor.

Employing the results of (142a) and (142b), it is possible to rewrite the terms $\hat{\Xi}_{\theta_1}$ and $\hat{\Xi}_{\theta_2}$ of (111) in discrete form as

$$\hat{\Xi}_{\theta_1} = -\boldsymbol{\Pi} \left[\mathbf{\Lambda}^{(i)}_{n+1} (\mathbf{I}_{\rho_0} \hat{A}_n + \tilde{\mathbf{V}}_n \mathbf{I}_{\rho_0} \hat{\mathbf{V}}_n)^{(i)}_{n+1}\right] \Delta \hat{\theta}^{(i)}_{n+1}, \tag{151a}$$

$$\begin{aligned} \hat{\Xi}_{\theta_2} = \frac{1}{(\Delta t)^2 \beta} \mathbf{\Lambda}^{(i)}_{n+1} \big[&\mathbf{I}_{\rho_0} + \Delta t \gamma (\tilde{\mathbf{V}}_n \mathbf{I}_{\rho_0} \\ &- \boldsymbol{\Pi} [\mathbf{I}_{\rho_0} \hat{\mathbf{V}}_n])\big]^{(i)}_{n+1} \mathbf{\Lambda}^T_n \mathbf{T}^{(i)}_n \Delta \hat{\theta}^{(i)}_{n+1}, \end{aligned} \tag{151b}$$

then, the following result is obtained: $(\hat{\Xi}_{\theta_1} + \hat{\Xi}_{\theta_2})^{(i)}_{n+1} = \boldsymbol{\Xi}^{(i)}_{\theta(n+1)} \Delta\hat{\theta}^{(i)}_{n+1}$ where the $\boldsymbol{\Xi}^{(i)}_{\theta(n+1)}$ is a *nonsymmetric* and *configuration dependent* tensor. This last result allows to obtain the discrete form of the inertial contribution to the tangential stiffness as

$$\begin{aligned}\Delta\mathbf{G}^{\text{ine}(i)}_{(n+1)} &= [M + K_{\text{gyr}} + K_{\text{cent}}]^{(i)}_{n+1} = K^{(i)}_{\text{ine}(n+1)} \\ &= \int_0^L \hat{\eta}^{\text{s}T} \begin{bmatrix} \boldsymbol{\Xi}_{\varphi} & 0 \\ 0 & \boldsymbol{\Xi}^{(i)}_{\theta(n+1)} \end{bmatrix} \hat{p}^{\text{s}(i)}_{n+1} \text{d}S \\ &= \int_0^L \hat{\eta}^{\text{s}T} \mathbf{M}^{(i)}_{\varphi\theta(n+1)} \hat{p}^{\text{s}(i)}_{n+1} \text{d}S. \end{aligned} \tag{152}$$

The discrete form of the contribution to the tangential stiffness due to external loading $K_L$ is obtained directly from (145) as

$$\begin{aligned}\Delta\mathbf{G}^{\text{ext}(i)}_{(n+1)} &= \int_0^L \hat{\eta}^{\text{s}T} \begin{bmatrix} \widetilde{\boldsymbol{\mathcal{N}}}^{(i)}_{p(n+1)} \\ \widetilde{\boldsymbol{\mathcal{M}}}^{(i)}_{p(n+1)} \end{bmatrix} \hat{p}^{\text{s}(i)}_{n+1} \text{d}S \\ &\quad + \sum_{k=1}^{Np} \hat{\eta}^{\text{s}T}_k \begin{bmatrix} \widetilde{\boldsymbol{P}}^{k(i)}_{p(n+1)} \\ 0 \end{bmatrix} \hat{p}^{\text{s}(i)}_{k(n+1)}, \end{aligned} \tag{153}$$

where the involved loading quantities have to be evaluated at the configuration $\hat{\boldsymbol{\Phi}}^{(i)}_{n+1}$.

## 7 Finite Element Implementation

A Galerkin discretization [101] of the linearized form of the virtual work functional, consistent with the time discretization previously discussed, is presented in this section. As usual in the FE method, the applied procedure yields to a system of nonlinear algebraic equations well suited for the application of the Newton iterative method.

Numerical procedures based on the spatial form of the iterative incremental rotation vector are preferred to others due to the fact that it makes the expressions for the internal, external and inertial vectors and the tangential matrices concise and explicit, as opposed to the case when using the incremental rotation vector. This choice seems to be more efficient and robust for computations and more convenient for programming. See *e.g.* Ibrahimbegović Ref. [104] for the employment of an updated *additive* rotation vector or Cardona *et al.* Ref. [53] for the total Lagrangian formulation.

Consider a FE discretization of the one–dimensional domain $[0, L]$:

$$[0, L] = \bigcup_{e=1}^{\text{N}_e} \text{I}^h_e; \quad (\text{I}^h_i \cap \text{I}^h_j = \emptyset, \forall i, j \in \{1 \cdots \text{N}_e\}), \tag{154}$$

where $\text{I}^h_e$ denotes a typical element with length $h > 0$, and $\text{N}_e$ is the total number of elements. The space of admissible variations $T\mathcal{C}_t$ is approximated by a finite dimensional subspace $V^h \subset T\mathcal{C}_t$.

Accordingly, let $\hat{\eta}^{sh}$ be the restriction to a typical element $\text{I}^h_e$ of the incremental displacement field/rotation field $\hat{\eta}^{sh} \equiv (\Delta\hat{\varphi}^h, \Delta\hat{\theta}^h) \in V^h$ superposed onto the configuration $\hat{\boldsymbol{\Phi}}_*$ (at $t = t_*$).

The conventional *Lagrangian interpolation* [31] is used for describing the reference rod curve $\hat{\varphi}_{0(e)}$, the current rod position vector $\hat{\varphi}_{(e)}$, the displacement vector, $\hat{u}_{(e)}$ and the linearized increments $\Delta\hat{\varphi}_{(e)}$ and $\Delta\hat{\theta}_{(e)}$, *i.e.*

$$s \in [-1, 1] \mapsto \begin{cases} \hat{\varphi}_{0(e)}(s) = \sum_{I=1}^{\text{N}_d} N_I(s) \hat{\varphi}_{0I(e)}, \\ \hat{\varphi}_{(e)}(s) = \sum_{I=1}^{\text{N}_d} N_I(s) \hat{\varphi}_{I(e)}, \\ \Delta\hat{\theta}_{(e)}(s) = \sum_{I=1}^{\text{N}_d} N_I(s) \Delta\hat{\theta}_{I(e)}, \\ \Delta\hat{\varphi}_{(e)}(s) = \sum_{I=1}^{\text{N}_d} N_I(s) \delta\hat{\varphi}_{I(e)}; \end{cases} \tag{155}$$

where $\text{N}_d$ is the number of nodes on a given element and $N_I(s)$, $I = 1 \cdots \text{N}_d$ are the local (elemental) shape functions. Therefore, the value at $s \in [-1, 1]$ of any vectorial quantity, denoted generically by $\hat{\text{H}}(s)^{(e)}$, is obtained from the values at the nodes as

$$\begin{aligned}\hat{\text{H}}_{(e)}(s) &= \left[\begin{array}{ccc|c|ccc} N_{11} & \cdots & 0 & & N_{\text{N}_d 1} & \cdots & 0 \\ \vdots & \ddots & \vdots & \cdots & \vdots & \ddots & \vdots \\ 0 & \cdots & N_{16} & & 0 & \cdots & N_{\text{N}_d 6} \end{array}\right] \\ &\quad \times \begin{bmatrix} \hat{\text{H}}_1 \\ \vdots \\ \hat{\text{H}}_{\text{N}_d 1} \end{bmatrix}_{(e)}, \\ &= [\,\mathbf{N}_1 | \cdots | \mathbf{N}_{\text{N}_d 1}\,] \hat{\text{H}}^{(e)} = [\mathbf{N}] \hat{\text{H}}_{(e)}, \end{aligned} \tag{156}$$

where $\hat{\text{H}}_{(e)I}$ is the value of the vectorial quantity $\hat{\text{H}}_{(e)}$ at the node $I$; $[\mathbf{N}(s)_I] = \text{Diag}[N(s)_{Ii}]$, $(i = 1, \ldots, 6)$ is the diagonal matrix with the values of the shape function corresponding to the node $I$ evaluated at $s$.

A possibility for calculating the interpolated values of the skew-symmetric tensor $\widetilde{\boldsymbol{\theta}}(s)_{(e)}$ is given by calculating $\hat{\theta}(s)_{(e)}$ using (156) and then applying the operator $\boldsymbol{\Pi}[\bullet]$. Other possibility is the direct interpolation using the matrix $\mathbf{N}$ of the values of the skew-symmetric tensors $\widetilde{\boldsymbol{\Theta}}(s)_{(e)I}$ at the nodes, taking advantages of the linearity of $so(3)$. By contrast, if the rotation tensor $\boldsymbol{\Lambda}(S)$ has to be determined, we have

$$\boldsymbol{\Lambda}(s)_{(e)} = \exp[\widetilde{\boldsymbol{\theta}}(s)_{(e)}] \neq [\mathbf{N}]_{(4-6)\bullet} \exp[\widetilde{\boldsymbol{\theta}}_{I(e)}] = \overline{\boldsymbol{\Lambda}}, \tag{157}$$

where $[\mathbf{N}]_{(4-6)\bullet}$ is the matrix corresponding to the rows 4 to 6 of the matrix $\mathbf{N}$. In general, $\overline{\boldsymbol{\Lambda}}\overline{\boldsymbol{\Lambda}}^T \neq \mathbf{I}$ due to the fact that $SO(3)$ is not a linear space.

The derivative with respect to $S \in [0, L]$ of the quantities defined by in (155) can be calculated starting from (156) as

$$\hat{\text{H}}(S)_{(e),S} = \left[\,\mathbf{N}_{1,S} | \cdots | \mathbf{N}_{\text{N}_d,S}\,\right] \hat{\text{H}}^{(e)} = [\mathbf{N}_{,S}\,] \hat{\text{H}}^{(e)}, \tag{158}$$

where it has been used the generic notation $\hat{\mathrm{H}}(S)_{(e)}$ and $[\mathbf{N}_{I,S}] = \mathrm{Diag}[N(S)_{Ii,S}]$, $(i = 1, \ldots, 6)$ corresponds to the diagonal matrix constructed from the derivatives with respect to $S$ of the shape functions $N_I$ corresponding to the node $I$ of the element.

As usual in FE implementations, shape functions normalized with respect to a curvilinear coordinate $s \in [-1, 1]$ are used; and, in this case, (158) is rewritten as $\hat{\mathrm{H}}(s)_{(e),S} = J_s^{-1}[\boldsymbol{N}_{,s}]\hat{\mathrm{H}}^{(e)}$, with $J_s = \|\hat{\varphi}_{0,S}\|$ being the Jacobian of the transformation between $S$ and $s$.

### 7.1 FE Approximation of the Out of Balance Force Vector

The FE approximation of the internal component of the virtual work principle, $G_{(e)}^{\mathrm{int}(h)}$, with

$$\hat{\eta}^{sh} = [(\delta\hat{\varphi}_1, \delta\hat{\theta}_1) \cdots (\delta\hat{\varphi}_{\mathrm{N}_d}, \delta\hat{\theta}_{\mathrm{N}_d})]^T \in V^h$$

being the vector containing nodal values of the admissible variation of $\hat{\boldsymbol{\Phi}}_{(e)}$ is

$$G_{(e)}^{\mathrm{int}(h)} = \int_0^{L_e} [\hat{\eta}_1^{\mathrm{s}} \cdots \hat{\eta}_{\mathrm{N}_d}^{\mathrm{s}}][\mathbf{N}_1 \cdots \mathbf{N}_{\mathrm{N}_d}]^T [\boldsymbol{B}]^T \hat{\Psi}\, \mathrm{d}S, \tag{159}$$

where (22c) has been considered and the following expression is obtained for the generic term $\mathbf{N}_I^T \boldsymbol{B}^T$:

$$\mathbf{N}_I^T \boldsymbol{B}^T = \begin{bmatrix} N_{I,S}\mathbf{I} & 0 \\ -N_I\widetilde{\boldsymbol{\varphi}}_{,S} & N_{I,S}\mathbf{I} \end{bmatrix}, \tag{160}$$

with $\widetilde{\boldsymbol{\varphi}}_{,S} = J_s^{-1}\boldsymbol{\Pi}\big[[\boldsymbol{N}_{(1-3)\bullet,s}]\hat{\varphi}_{(e)}\big]$ according to (158). In this way , it is possible to rewrite (159) as

$$\begin{aligned} G_{(e)}^{\mathrm{int}(h)} &= \sum_{I=1}^{\mathrm{N}_d} \begin{bmatrix} \delta\hat{\varphi}_I \\ \delta\hat{\theta}_I \end{bmatrix} \\ &\quad \times \int_0^{L_{(e)}} \left( J_s^{-1} \begin{bmatrix} N_{I,s}\,\hat{n} \\ N_{I,s}\,\hat{m} - N_I\widetilde{\boldsymbol{\varphi}}_{,s}\,\hat{n} \end{bmatrix} \right) \mathrm{d}S, \\ &= \hat{\eta}^{shT} \sum_{I=1}^{\mathrm{N}_d} \hat{q}_{\mathrm{int}(e)I}^h. \end{aligned} \tag{161}$$

Here, $\hat{q}_{\mathrm{int}(e)I}^h$ denotes the internal force vector related to the node $I$ in a typical element $I_e^h$. The integral appearing in this equation can be calculated using a standard numerical procedure selecting a set of $N_{ip}$ integration points on the element and using the corresponding weighting factors $W_J$ $(J = 1, \ldots, N_{ip})$ [101]. Therefore, $\hat{q}_{\mathrm{int}(e)I}^h$ is

$$\hat{q}_{\mathrm{int}(e)I}^h = \sum_{J=1}^{N_{ip}} \left. \begin{bmatrix} J_s^{-1}N_{I,s}\,\hat{n} \\ J_s^{-1}(N_{I,s}\,\hat{m} - N_I\widetilde{\boldsymbol{\varphi}}_{,s}\,\hat{n}) \end{bmatrix} \right|_J J_s W_J, \tag{162}$$

where $(\bullet)|_J$ denotes the evaluation of the given quantity at the integration point number $J$. The evaluation of the spatial form of the cross sectional forces and moments, $\hat{n}$ and $\hat{m}$, at the integration points is carried out by means of suitable cross sectional analysis as it will be explained in following.

In the same way, the FE approximation of the external component of the virtual work principle, $G_{(e)}^{\mathrm{ext}(h)}$ is

$$\begin{aligned} G_{\mathrm{ext}(e)}^h &= \hat{\eta}^{shT} \sum_{J=1}^{N_{ip}} N_I \left. \begin{bmatrix} \hat{\mathcal{N}} \\ \hat{\mathcal{M}} \end{bmatrix} \right|_J J_s W_J \\ &= \hat{\eta}^{shT} \sum_{I=1}^{\mathrm{N}_d} \hat{q}_{\mathrm{ext}(e)I}^h, \end{aligned} \tag{163}$$

where $\hat{q}_{\mathrm{ext}(e)I}^h$ is the external load vector at the node $I$.

The inertial contribution, $G_{(e)}^{\mathrm{ine}(h)}$, can be calculated as

$$\begin{aligned} G_{(e)}^{\mathrm{int}(h)} &= \sum_{I=1}^{\mathrm{N}_d} \hat{\eta}_I^{shT} \cdot \sum_{J=1}^{N_{ip}} \left. \begin{bmatrix} N_I A_{\rho_0} \ddot{\hat{\varphi}} \\ N_I[\boldsymbol{\mathcal{I}}_{\rho_0}\hat{\alpha}_n + \widetilde{\boldsymbol{v}}_n\boldsymbol{\mathcal{I}}_{\rho_0}\hat{v}_n] \end{bmatrix} \right|_J J_s W_J, \\ &= \hat{\eta}^{shT} \sum_{I=1}^{\mathrm{N}_d} \hat{q}_{\mathrm{ine}(e)I}^h, \end{aligned} \tag{164}$$

where $\hat{q}_{\mathrm{ext}(e)I}^h$ is the inertial force load vector at the node $I$.

Finally, considering the results of (162), (163) and (164), the *unbalanced force* term is written as

$$G_{(e)}^h = \hat{\eta}^{shT} \sum_{I=1}^{\mathrm{N}_d} (\hat{q}_{\mathrm{int}(e)I}^h + \hat{q}_{\mathrm{ine}(e)I}^h - \hat{q}_{\mathrm{ext}(e)I}^h). \tag{165}$$

#### 7.1.1 FE Approximation of the Tangential Stiffness

The FE discretization of the tangent stiffness matrix is obtained from the linearized form of the virtual work principle [104, 117, 134, 219]. Considering $\hat{\eta}^{sh} = \mathbf{N}\hat{\eta}_{(e)}^{sh}$ and $\hat{p}^{sh} = \mathbf{N}\hat{p}_{(e)}^{sh}$, it is possible to consider the FE approximation of the linearized form of the internal contribution to the virtual work principle, (109), relative to the element $I_e^h$ at a given configuration, as

$$\begin{aligned} \Delta G_{\mathrm{int}(e)}^h = \hat{\eta}^{shT} & \underbrace{\left[ \int_0^{L_e} (\mathbf{N}^T \boldsymbol{B}^T \bar{\mathbf{C}}^{\mathrm{sv}} \boldsymbol{B}\mathbf{N})\mathrm{d}S \right]}_{\mathbf{K}_{M(e)}} \hat{p}^{sh} \\ + \hat{\eta}^{shT} & \underbrace{\left[ \int_0^{L_e} (\mathbf{N}^T (\boldsymbol{\mathcal{F}} + \boldsymbol{B}^T \boldsymbol{\mathcal{N}})\mathbf{N})\mathrm{d}S \right]}_{\mathbf{K}_{G(e)}} \hat{p}^{sh} \\ + \hat{\eta}^{shT} & \underbrace{\left[ \int_0^{L_e} (\mathbf{N}^T (\boldsymbol{B}^T \bar{\boldsymbol{\Upsilon}}^{\mathrm{ss}} \boldsymbol{\mathcal{V}})\mathbf{N})\mathrm{d}S \right]}_{\mathbf{K}_{V(e)}} \hat{p}^{sh}, \end{aligned} \tag{166}$$

where $\mathbf{K}_{M(e)}$, $\mathbf{K}_{G(e)}$ and $\mathbf{K}_{V(e)}$ are the *material*, *geometric* and *viscous* components of the element stiffness matrix at the current configuration.

Then, we have that the material stiffness matrix can be written as

$$\mathbf{K}_{M(e)} = \sum_{I,J}^{\mathrm{N}_d} \int_0^L \mathbf{N}_I^T \boldsymbol{B}^T \bar{\mathbf{C}}^{\mathrm{sv}} \boldsymbol{B} \mathbf{N}_J \mathrm{d}S = \sum_{I,J}^{\mathrm{N}_d} \mathbf{K}_{M(e)IJ}, \quad (167)$$

where $[\mathbf{K}_{M(e)}]_{IJ}$ denote the sub-matrix coupling the nodes $I$ and $J$ of the finite element with explicit expression, after the numerical integration procedure, given by

$$\mathbf{K}_{M(e)IJ} = \sum_{K}^{N_{ip}} J_s^{-1} \left[ \begin{array}{c|c} \mathbf{K}^{nn}_{M(e)IJ} & \mathbf{K}^{nm}_{M(e)IJ} \\ \hline \mathbf{K}^{mn}_{M(e)IJ} & \mathbf{K}^{mm}_{M(e)IJ} \end{array} \right]\Bigg|_K W_K, \quad (168)$$

where

$$\begin{aligned}
\mathbf{K}^{nn}_{M(e)IJ} &= N_{I,s}\, N_{J,s}\, \mathbf{C}^{\mathrm{sv}}_{nn}, \\
\mathbf{K}^{nm}_{M(e)IJ} &= N_{I,s}\, (\mathbf{C}^{\mathrm{sv}}_{nn} \widetilde{\boldsymbol{\varphi}}_{,s} + \mathbf{C}^{\mathrm{sv}}_{nm} N_{J,s}), \\
\mathbf{K}^{mn}_{M(e)IJ} &= \mathbf{C}^{\mathrm{sv}}_{mn} N_{I,s}\, N_{J,s} - N_I N_{J,s}\, \mathbf{C}^{\mathrm{sv}}_{nn} \widetilde{\boldsymbol{\varphi}}_{,s}, \\
\mathbf{K}^{mm}_{M(e)IJ} &= N_{I,s}\, (\mathbf{C}^{\mathrm{sv}}_{mn} \widetilde{\boldsymbol{\varphi}}_{,s}\, N_J + \mathbf{C}^{\mathrm{sv}}_{mm} N_{J,s}), \\
&\quad - N_I \widetilde{\boldsymbol{\varphi}}_{,s}\, (\mathbf{C}^{\mathrm{sv}}_{nn} \widetilde{\boldsymbol{\varphi}}_{,s}\, N_J + \mathbf{C}^{\mathrm{sv}}_{nm} N_{J,s}),
\end{aligned}$$

which is always symmetric.

In an analogous manner, for the term $\mathbf{K}_{G(e)IJ}$, taking into account (160), one has

$$\begin{aligned}
\mathbf{K}_{G(e)IJ} &= \sum_{K}^{N_{ip}} (\mathbf{N}_I \boldsymbol{\mathcal{F}} \mathbf{N}_J + \mathbf{N}_I^T \boldsymbol{B}^T \boldsymbol{\mathcal{N}} \mathbf{N}_J)\Big|_K W_K, \\
&= \sum_{K}^{N_{ip}} \left[ \begin{array}{c|c} 0 & \mathbf{K}^{nm}_{G(e)IJ} \\ \hline \mathbf{K}^{mn}_{G(e)IJ} & \mathbf{K}^{mm}_{G(e)IJ} \end{array} \right]\Bigg|_K W_K, \quad (169)
\end{aligned}$$

$$\begin{aligned}
\mathbf{K}^{nm}_{G(e)IJ} &= -N_{I,s}\, \widetilde{\boldsymbol{n}} N_J, \\
\mathbf{K}^{mn}_{G(e)IJ} &= N_I \widetilde{\boldsymbol{n}} N_{J,s}, \\
\mathbf{K}^{mm}_{G(e)IJ} &= (N_I (\hat{n} \otimes \hat{\varphi}_{,s} - \hat{n} \cdot \hat{\varphi}_{,s}\, \mathbf{I}) + N_{I,s}\, \widetilde{\boldsymbol{m}}) N_J,
\end{aligned}$$

which is not necessarily symmetric. A deep analysis about this and other aspects was provided by Simo in Ref. [213].

Analogously, the FE discretization of the viscous component off the tangential stiffness is computed as

$$\begin{aligned}
\mathbf{K}_{V(e)} &= \sum_{IJ}^{\mathrm{N}_d} \int_0^{L_e} \mathbf{N}_I^T (\boldsymbol{B}^T \bar{\boldsymbol{\Upsilon}}^{\mathrm{ss}} \boldsymbol{\mathcal{V}}) \boldsymbol{N}_J \mathrm{d}S, \\
&= \sum_{IJ}^{\mathrm{N}_d} \mathbf{K}_{V(e)IJ}, \quad (170)
\end{aligned}$$

where the sub-matrix $I$–$J$ of the viscous component of the tangential stiffness matrix is given by

$$\mathbf{K}_{V(e)IJ} = J_s^{-1} \sum_{K}^{N_{ip}} \left[ \begin{array}{c|c} \mathbf{K}^{nn}_{V(e)IJ} & \mathbf{K}^{nn}_{V(e)IJ} \\ \hline \mathbf{K}^{nn}_{V(e)IJ} & \mathbf{K}^{nn}_{V(e)IJ} \end{array} \right]\Bigg|_K W_K, \quad (171)$$

with

$$\begin{aligned}
\mathbf{K}^{nn}_{V(e)IJ} &= N_{I,s}\, \bar{\boldsymbol{\Upsilon}}^{\mathrm{ss}}_{nn} N_{J,s}\, (\gamma_{t\beta} \mathbf{I} - \widetilde{\boldsymbol{v}}), \\
\mathbf{K}^{nm}_{V(e)IJ} &= N_{I,s} \left\{ \bar{\boldsymbol{\Upsilon}}^{\mathrm{ss}}_{nn} N_J (\hat{\boldsymbol{\varphi}}_{,s} + \widetilde{\boldsymbol{\varphi}}_{,s}\, \gamma_{t\beta} \mathbf{T} - \widetilde{\boldsymbol{v}} \widetilde{\boldsymbol{\varphi}}_{,s}) \right. \\
&\quad \left. + \bar{\boldsymbol{\Upsilon}}^{\mathrm{ss}}_{nm} ((2\gamma_{t\beta} \mathbf{T} - \widetilde{\boldsymbol{v}}_n) N_{J,s} + \gamma_{t\beta} \mathbf{T}_{,s}\, N_J) \right\}, \\
\mathbf{K}^{mn}_{V(e)IJ} &= N_{J,s}\, (\gamma_{t\beta} \mathbf{I} - \widetilde{\boldsymbol{v}}) (N_{I,s}\, \bar{\boldsymbol{\Upsilon}}^{\mathrm{ss}}_{mn} - N_I \widetilde{\boldsymbol{\varphi}}_{,s}\, \bar{\boldsymbol{\Upsilon}}^{\mathrm{ss}}_{nn}), \\
\mathbf{K}^{mm}_{V(e)IJ} &= (N_{I,s}\, \bar{\boldsymbol{\Upsilon}}^{\mathrm{ss}}_{mm} - N_I \widetilde{\boldsymbol{\varphi}}_{,s}\, \bar{\boldsymbol{\Upsilon}}^{\mathrm{ss}}_{nn}) N_J (\hat{\boldsymbol{\varphi}}_{,s} \\
&\quad + \widetilde{\boldsymbol{\varphi}}_{,s}\, \gamma_{t\beta} \mathbf{T} - \widetilde{\boldsymbol{v}} \widetilde{\boldsymbol{\varphi}}_{,s}) + (N_{I,s}\, \bar{\boldsymbol{\Upsilon}}^{\mathrm{ss}}_{nm} \\
&\quad - N_I \widetilde{\boldsymbol{\varphi}}_{,s}\, \bar{\boldsymbol{\Upsilon}}^{\mathrm{ss}}_{nn}) ((\gamma_{t\beta} 2\mathbf{T} - \widetilde{\boldsymbol{v}}_n) N_{J,s} + \gamma_{t\beta} \mathbf{T}_{,s}\, N_J).
\end{aligned}$$

The FE discretization of the inertial contribution to the elemental tangent stiffness $K_{\mathrm{ine}(e)}$, (152), is obtained as

$$\begin{aligned}
K_{\mathrm{ine}(e)} &= \hat{\eta}^{shT} \Big[ \int_0^{L_e} \mathbf{N}^T \mathbf{M}_{\varphi\theta} \mathbf{N} \mathrm{d}S \Big] \hat{p}^{sh}, \\
&= \hat{\eta}^{shT} \sum_{IJ}^{\mathrm{N}_d} \mathbf{K}_{\mathrm{ine}(e)IJ}\, \hat{p}^{sh}, \quad (172)
\end{aligned}$$

where $\mathbf{K}_{\mathrm{ine}(e)IJ}$, coupling the degree of freedom of node $I$ and of node $J$, is given by

$$\begin{aligned}
\mathbf{K}_{\mathrm{ine}(e)IJ} &= \int_0^{L_e} \mathbf{N}_I^T \begin{bmatrix} \boldsymbol{\Xi}_\varphi & 0 \\ 0 & \boldsymbol{\Xi}_\theta \end{bmatrix} \mathbf{N}_J \mathrm{d}S, \\
&= \sum_{k}^{N_{ip}} \left[ \begin{array}{c|c} \mathbf{K}^{\varphi}_{\mathrm{ine}(e)IJ} & 0 \\ \hline 0 & \mathbf{K}^{\theta}_{\mathrm{ine}(e)IJ} \end{array} \right]\Bigg|_K J_s W_K, \quad (173)
\end{aligned}$$

with

$$\begin{aligned}
\mathbf{K}^{\varphi}_{\mathrm{ine}(e)IJ} &= \frac{1}{(\Delta t)^2 \beta} \mathcal{A}_{\rho_0} N_I N_J, \\
\mathbf{K}^{\theta}_{\mathrm{ine}(e)IJ} &= \Big[ -\boldsymbol{\Lambda} \Pi [\mathbf{I}_{\rho_0} \hat{A}_n + \hat{V}_n \times \mathbf{I}_{\rho_0} \hat{V}_n] \\
&\quad + \frac{1}{(\Delta t)^2 \beta} \boldsymbol{\Lambda} (\boldsymbol{I}_{\rho_0} + \Delta t \gamma (\widetilde{V}_n \mathbf{I}_{\rho_0} - \Pi [\mathbf{I}_{\rho_0} \hat{V}_n]) \Big] \\
&\quad \times \boldsymbol{\Lambda}^{*T} \mathbf{T} N_I N_J,
\end{aligned}$$

where $\boldsymbol{\Lambda}^{*T}$ corresponds to the last converged configuration and the remaining $\boldsymbol{\Lambda}$'s are the iterative ones as described in Sect. 6.5. The tangent inertia matrix is *nonsymmetric* and *configuration dependent*. This property concerns only the rotational degrees of freedom.

As it has been explained in Sect. 5.3, the linear part of the external contribution to the virtual work principle is zero.

Finally, the tangent stiffness matrix relating the nodes $I$ and $J$ is given by

$$[\mathbf{K}^h_{(e)}]_{IJ} = \Big[ \mathbf{K}_M + \mathbf{K}_G + \mathbf{K}_V + \mathbf{K}_{\mathrm{ine}} \Big]_{(e)IJ}. \quad (174)$$

## 7.2 Iterative Newton–Raphson Scheme

An iterative form of the Newton–Raphson scheme (122), is used for solving the discrete version of the linearized form of the virtual work functional (for more details see classical textbooks [62, 101]). The *global unbalanced force vector*, the *global stiffness matrix* and the *incremental configuration field* are obtained as

$$\hat{q} = \mathop{\mathbf{A}}_{e,\,I}^{N_e \times N_d} \hat{q}^h_{(e)I}; \qquad \mathbf{K} = \mathop{\mathbf{A}}_{e,\,I,\,J}^{N_e \times N_d} \mathbf{K}^{hIJ}_{(e)}; \qquad \hat{p} = \mathop{\mathbf{A}}_{e,\,I}^{N_e \times N_d} \hat{p}^h_{(e)I}; \tag{175}$$

respectively; where $\mathbf{A}$ denotes the usual *assembly procedure* which runs over the number of elements $N_e$ and their corresponding nodal points $N_d$. Then, solving the following linear systems of equations it is possible to obtain the iterative increments of the configuration variables

$$\hat{\eta}^{\mathrm{s}} \cdot \left[\hat{q}^{\mathrm{s}} + \mathbf{K}\hat{p}^{\mathrm{s}}\right]^{(i)}_{n+1} \approx 0 \rightarrow \hat{p}^{\mathrm{s}(i)}_{n+1} = -\left[\mathbf{K}^{-1}\hat{q}^{\mathrm{s}}\right]^{(i)}_{n+1}, \tag{176}$$

where the super and sub-scripts $(i)$ and $n+1$ corresponds to the iteration and time, respectively. Note that (176) is valid for both the static or dynamic cases. Having obtained an iterative field $\hat{p}^{(i)}_{n+1}$, the previously described updating procedures are used for determining $\hat{\Phi} \in T\mathcal{C}_t$, the related linear and angular velocity and acceleration and the strain and strain rate fields existing on each integration point (see Fig. 15).

This formulation makes use of uniformly reduced integration on the pure displacement and rotation weak form to avoid shear locking [104, 219], however, the inertial terms are integrated in exact manner. It remains to determine the stress field existing on each material point in the cross sections associated to integration points; this is done by means of an adequate cross sectional analysis that will be explained in following.

### 7.2.1 Cross Sectional Analysis

In distributed models for the nonlinear analysis of rod–like structures, the cross sectional analysis (CSA) became a crucial step. The CSA in a *strain driven* numerical method can be defined as the set of procedures used for determining:

(i) The stress distribution in a cross section for a given strain field.
(ii) The stress resultant and stress couples.
(iii) The reduced (cross sectional) tangential stiffness if inelastic materials are considered.

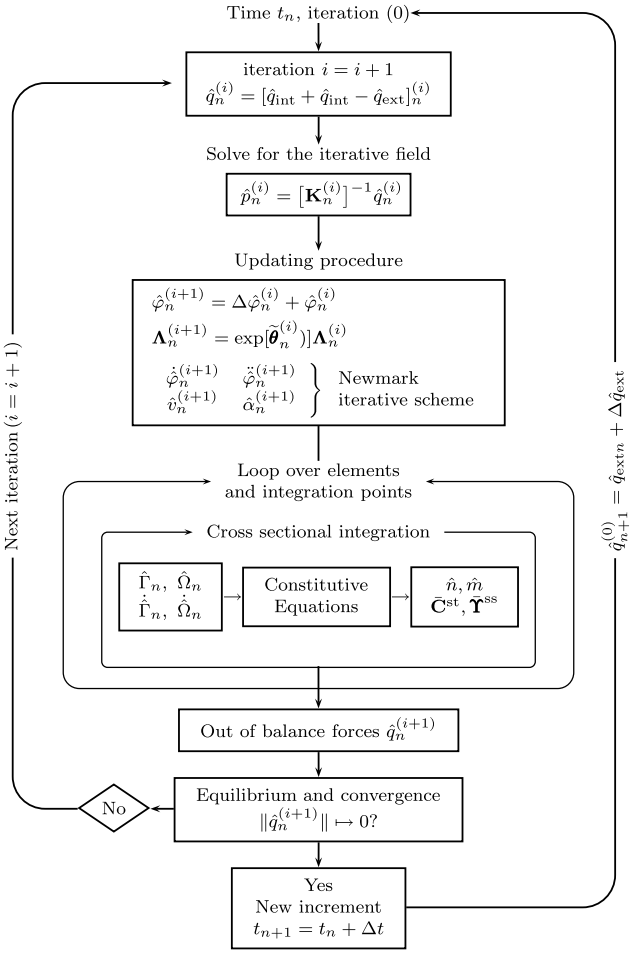


**Fig. 15** Iterative Newton–Raphson scheme (spatial form)

All these procedures are usually dependent on the shape of the cross section and the distribution and the constitutive relation of the involved materials.

A large amount of research has been concentrated on this topic. The significance of the techniques developed for the precise CSA arises on the accuracy of the stress field assigned to point on the rod. Special attention has been directed to the determination of the shear stress and the shear strain distribution on arbitrarily shaped cross sections. Gruttmann *et al.* [91] develop a refined method based on the FE method for shear stresses in prismatic beams. Jiang and Henshall [115] present a FE model coupled with the CRA for the torsion problem in prismatic bars. Similarly, in Ref. [187] a 3D beam element based on the Saint Venant's rod theory is developed.

Specific efforts have been oriented to the case of thin walled (closed or not) cross sections (see *e.g.* [84]) and to beams made of composite materials. For example, Reznikov [194] develops a method for the analysis of the nonlinear deformation of composites including finite rotations. Ovesy *et al.* [183] perform the nonlinear CSA of channel sections using the so called finite strip method. An innovative pro-

cedure for the precise CSA of stresses is given by the *asymptotic variational methods* which take advantage of certain small parameters inherent to beam-like structures [248]. Several works can be quoted in this line of research, *e.g.* [56, 189, 247].

Most of the previous mentioned references are restricted to the infinitesimal deformation or to the elastic case. In several areas of engineering, the inelastic response of the structures is required. Complex phenomena such as the effect of confinement in shear dominated failures of civil engineering structures have received increasing research effort. For example, Thanoon *et al.* [231] propose a method for estimating the inelastic response of composite sections. Ayoub and Filippou [21] employ a mixed formulation for structures with composite steel and concrete cross sections. An attempt to develop a method for the cross sectional analysis is presented by Bentz [39]. Recently, Bairan and Mari [22] present a coupled model for the nonlinear analysis of anisotropic sections.

The CSA procedure here presented combines simplicity and the sophistication required by composite materials. The analysis is carried out expanding each integration point on the beam axis in a set of integration points located on each fiber on cross section. In order to perform this operation, the beam cross section is meshed into a grid of quadrilaterals, each of them corresponding to a fiber oriented along the beam axis (see Fig. 16).

The estimation of the average stress level existing on each quadrilateral is carried out by integrating the constitutive equations of the compounding materials of the composite associated to the corresponding quadrilateral and applying the mixing rule as explained in Sect. 4.5. The geometry of each quadrilateral is described by means of normalized bi-dimensional shapes functions and several integration points can be specified according to a selected integration rule. In the case of the average value of the material form of the FPK stress vector, one has

$$\hat{P}_1^{\mathrm{m}} = \frac{1}{A_c}\int_{A_c} \hat{P}_1^{\mathrm{m}} \mathrm{d}A_c$$

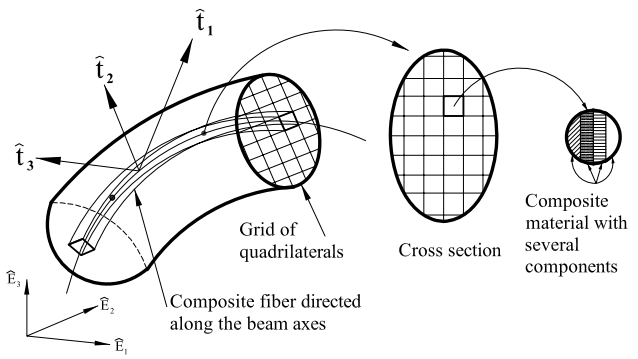


**Fig. 16** Discrete fiber like model of the beam element

$$= \frac{1}{A_c}\sum_{p=1}^{N_p}\sum_{q=1}^{N_q} \hat{P}_1^{\mathrm{m}}(y_p, z_q) J_{pq} W_{pq}, \tag{177}$$

where $A_c$ is the area of the quadrilateral, $N_p$ and $N_q$ are the number of integration points in the two directions of the normalized geometry of the quadrilateral, $\hat{P}_1^{\mathrm{m}}(y_p, z_q)$ is the value of the FPK stress vector on a integration point with coordinates $(y_p, z_q)$ with respect to the reference beam axis, $J_{pq}$ is the Jacobian of the transformation between $(y_p, z_q)$ and $(\xi_1, \xi_2)$ and $W_{pq}$ are the weighting factors.

Analogously, the coefficients of the tangent constitutive tensors, $\bar{\boldsymbol{\mathcal{C}}}^{\mathrm{mt}}(y_p, z_q)$, can be obtained as

$$\bar{\boldsymbol{\mathcal{C}}}^{\mathrm{mt}} = \frac{1}{A_c}\sum_{p=1}^{N_p}\sum_{q=1}^{N_q} \bar{\boldsymbol{\mathcal{C}}}^{\mathrm{mt}}(y_p, z_q) J_{pq} W_{pq}. \tag{178}$$

Finally, the cross sectional forces and moments are obtained by means of the discrete form of (11a) and (11b) as

$$\hat{n}^{\mathrm{m}} = \sum_{k=1}^{N_{\mathrm{fiber}}} A_{c(k)} \hat{P}_{1(k)}^{\mathrm{m}}, \qquad \hat{m}^{\mathrm{m}} = \sum_{k=1}^{N_{\mathrm{fiber}}} A_{c(k)} \hat{\ell}_k \times \hat{P}_{1(k)}^{\mathrm{m}}, \tag{179}$$

were $N_{\mathrm{fiber}}$ is the number of quadrilaterals of the beam cross section, $A_{c(k)}$ is the area of the $k$ quadrilateral, $\hat{P}_{1(k)}^{\mathrm{m}}$ is the average value of the material FPK stress vector and $\hat{\ell}_k = (0, y_k, z_k)$ are the coordinates of the gravity center of the $k$th quadrilateral.

Applying the same procedure, the material form of the reduced tangential tensors of (91a) and (91b) are numerically estimated as

$$\bar{\mathbf{C}}_{nn}^{\mathrm{mt}} = \sum_{k=1}^{N_{\mathrm{fiber}}} A_{ck} \bar{\boldsymbol{\mathcal{C}}}_k^{\mathrm{mt}}, \qquad \bar{\mathbf{C}}_{nm}^{\mathrm{mt}} = -\sum_{k=1}^{N_{\mathrm{fiber}}} A_{ck} \bar{\boldsymbol{\mathcal{C}}}_k^{\mathrm{mt}} \widetilde{\boldsymbol{E}}_{\star k}, \tag{180a}$$

$$\bar{\mathbf{C}}_{mn}^{\mathrm{mt}} = \sum_{k=1}^{N_{\mathrm{fiber}}} A_{ck} \widetilde{\boldsymbol{\ell}}_k \bar{\boldsymbol{\mathcal{C}}}_k^{\mathrm{mt}}, \qquad \bar{\mathbf{C}}_{mm}^{\mathrm{mt}} = -\sum_{k=1}^{N_{\mathrm{fiber}}} A_{ck} \widetilde{\boldsymbol{\ell}}_k \bar{\boldsymbol{\mathcal{C}}}_k^{\mathrm{mt}} \widetilde{\boldsymbol{E}}_{\star k}, \tag{180b}$$

where $\widetilde{\boldsymbol{E}}_{\star k} = (y_k \widetilde{\boldsymbol{E}}_2 + z_k \widetilde{\boldsymbol{E}}_3)$, $\widetilde{\boldsymbol{\ell}}_k$ is the skew-symmetric tensor obtained from $\hat{\ell}_k$ and $(\bar{\boldsymbol{\mathcal{C}}}^{\mathrm{mt}})_k$ is the material form of the tangent constitutive tensor for the composite material of the $k$th quadrilateral.

Analogously, the reduced constitutive tensor $\bar{\boldsymbol{\Upsilon}}^{\mathrm{ss}}$ is obtained as [163]

$$\bar{\boldsymbol{\Upsilon}}_{nn}^{\mathrm{ss}} = \sum_{k=1}^{Nfiber} A_{ck} \bar{\boldsymbol{\eta}}_k^{\mathrm{ss}}, \qquad \bar{\boldsymbol{\Upsilon}}_{nm}^{\mathrm{ss}} = -\sum_{k=1}^{Nfiber} A_{ck} \bar{\boldsymbol{\eta}}_k^{\mathrm{ss}} \widetilde{\boldsymbol{E}}_{\star k}, \tag{181a}$$

$$\bar{\boldsymbol{\Upsilon}}^{\mathrm{ss}}_{mn} = \sum_{k=1}^{Nfiber} A_{ck}\widetilde{\boldsymbol{\ell}}_k\bar{\boldsymbol{\eta}}^{\mathrm{ss}}_k, \qquad \bar{\boldsymbol{\Upsilon}}^{\mathrm{ss}}_{mm} = -\sum_{k=1}^{Nfiber} A_{ck}\widetilde{\boldsymbol{\ell}}_k\bar{\boldsymbol{\eta}}^{\mathrm{ss}}_k\widetilde{\boldsymbol{E}}_{\star k}. \tag{181b}$$

From the point of view of the numerical implementations, in a given loading step and iteration of the global Newton–Raphson scheme, three additional integration loops are required:

(i) The first one is a loop over the quadrilaterals; where, having obtained $\hat{\Gamma}_n$, $\hat{\Omega}_n$ and their time derivatives $\dot{\hat{\Gamma}}_n$ and $\dot{\hat{\Omega}}_n$, the strain measure $\hat{\mathcal{E}}_n$ and the strain rate measure $\hat{\mathcal{S}}_n$ are calculated according to the updating procedure of Sect. 6.4. Then, they are imposed for each simple material associated to the composite of a given fiber.

(ii) The second loop runs over each simple material associated to the composite of the quadrilateral. In this case, the FPK stress vector, $\hat{P}_1^{\mathrm{m}}$, and the tangent constitutive relations, $\bar{\mathcal{C}}^{\mathrm{mt}}$ and $\bar{\boldsymbol{\eta}}^{\mathrm{ms}}$, are determine for each component. The behavior of the composite is recovered with the help of the mixing theory as explained in Sect. 4.5.

(iii) The integration procedure carried out over the fibers allows to obtain the cross sectional forces and moments and the reduced tangential tensors.

Figure 17 shows the flow chart of the CSA procedure for a cross section with $N_{\mathrm{fiber}}$ fibers and $k$ simple components associated to each fiber [163, 164]. As it has been previously explained, the sectional behavior is obtained as the weighted sum of the contribution of the fibers, conversely to other works which develop global sectional integration methods [249, 252]. Material nonlinearity, such as degradation or plasticity, is captured by means of the constitutive laws of the simple materials at each quadrilateral.

It is worth to note that large deformations out of the cross sectional plane can not be reproduced due to the assumed planarity of the cross sections, therefore, the mechanical equilibrium at element level does not implies mechanical equilibrium among fibers.

If materials presenting *softening* are associated to the fibers, the strain localization phenomenon can occur on specific integration points [13, 15, 175, 176]. Softening behavior of fibers imply the induction of a softer response at cross sectional level and, in this manner, the strain localization induced at material point level is translated to the cross sectional force-displacement relationships. The structural response can became dependent on the mesh size. A the mesh independent response can be obtained regularizating the energy dissipated on each fiber and limiting this value to the specific fracture energy of the involved materials. However, other alternative procedures based on con-

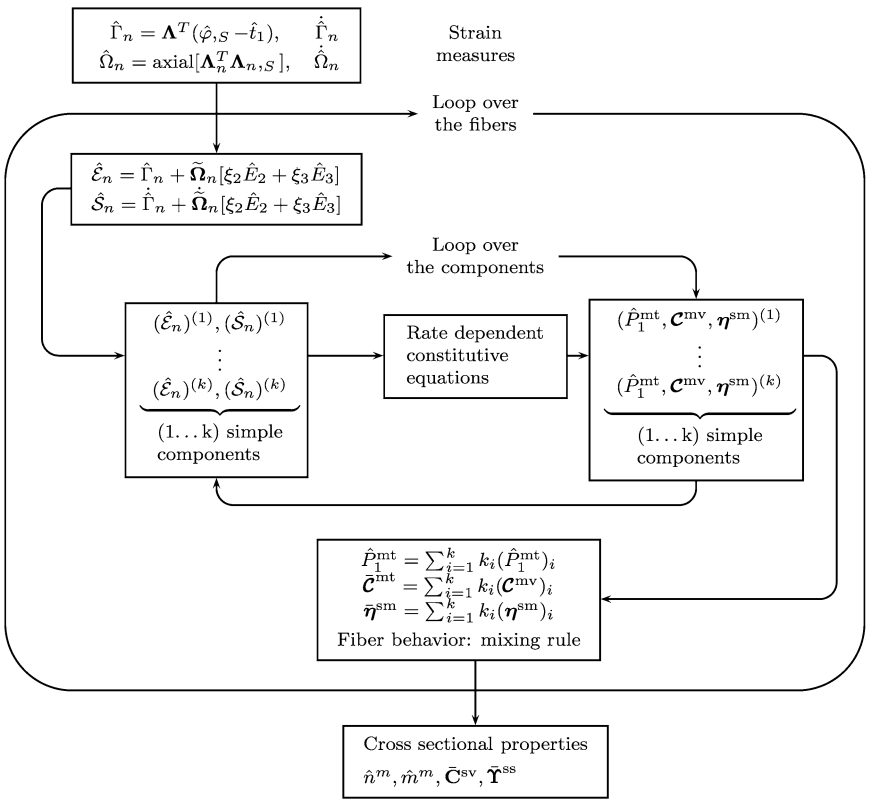


**Fig. 17** Flow chart of the cross sectional integration

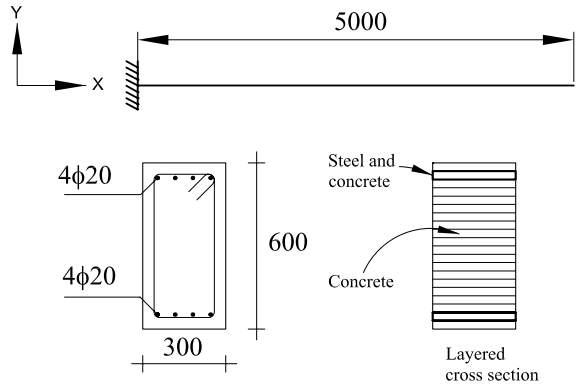


**Fig. 18** RC cantilever beam

sidering *strong discontinuities* in beams can be consulted [13–15].

## 8 Numerical Examples

### 8.1 Mesh Independent Response of a RC Beam

The objective of this example consists into show how the regularization of the energy at constitutive level allows to obtain a mesh objective structural response at global level when including softening materials. The RC cantilever beam shown in Fig. 18 is subjected to forty increments of imposed displacements in the $Y$ direction to obtain the capacity curve [163]. Four meshes of 10, 20, 40 and 80 quadratic elements with the Gauss integration rule where used.

The beam cross section was meshed into 20 equally spaced layers. The steel bars were included as a part of the composite material with a volumetric fraction corresponding to their contributing area to the total area of the layer. The mechanical properties of the concrete and steel are:

(i) Concrete: $E$ =21000 MPa, $\nu = 0.20$, $f_c = 25$ MPa, $n = 8$ and $G_f = 1$ Nmm$^{-2}$.
(ii) Steel: $E = 200000$ MPa, $\nu = 0.15$, $f_c = 500$ MPa, $n = 1$ and $G_f = 500$ Nmm$^{-2}$,

where $E$ and $\nu$ are the elastic modulus and Poisson coefficient, respectively; $G_f$ is the fracture energy, $f_c$ is the ultimate compression limit and $n$ is the ratio of the compression to the tension yielding limits.

Figure 19 shows the capacity curve relating the vertical reaction and displacement of the free end. It is possible to see that the numerical responses converge to that corresponding to the model with the greater number of elements. Figure 20 shows the evolution of the global damage index which allows to appreciate the mesh independent response of the structure.

The previous results allow to affirm that the technique based on regularizating the dissipation according to the specific fracture energy of the material and the characteristic length of the FE mesh permits to obtain a objective structural response.

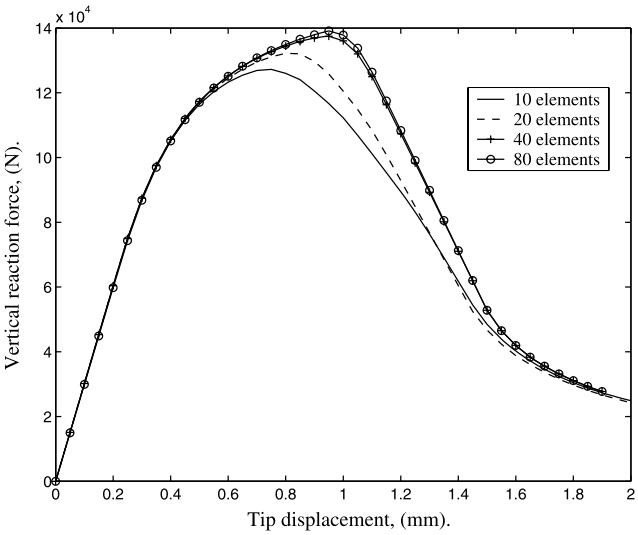


**Fig. 19** Capacity curves (Mata *et al.* [163])

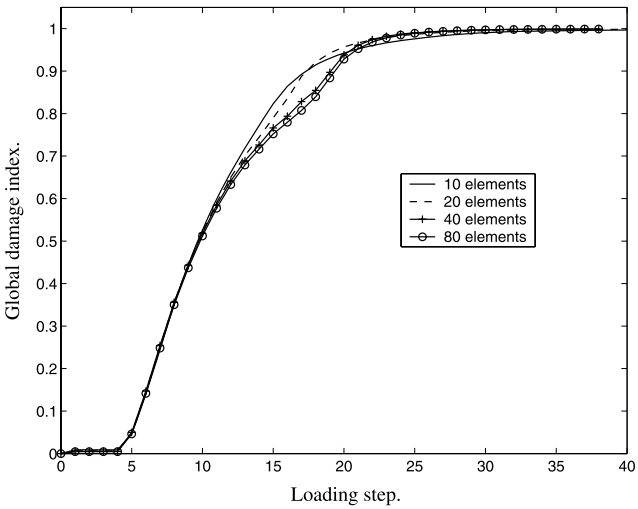


**Fig. 20** Global damage index (Mata *et al.* [163])

### 8.2 Seismic Response of a Precast RC Building with EDDs

The nonlinear seismic response of a typical precast RC building with EDD studied in Ref. [165] is described in this example. The geometry of the building is shown in Fig. 21 along with the location of the devices. The mechanical properties of the materials are: (i) Concrete H-35 ($f_c = 35$ MPa), $E = 290.000$ MPa, $\nu = 0.2$, $n = 10$ and $g_f = 1$ N/mm$^{-2}$. (ii) Steel with a yielding level of $f_c = 510$ MPa, $E =$ 200000 MPa, $\nu = 0.15$, $n = 1$ and $g_f = 500$ N/mm$^{-2}$. This figure also shows some details of the steel reinforcement of the cross sections. In the same figure the cross sectional meshes are depicted. The beam has an initial hight of 40 cm

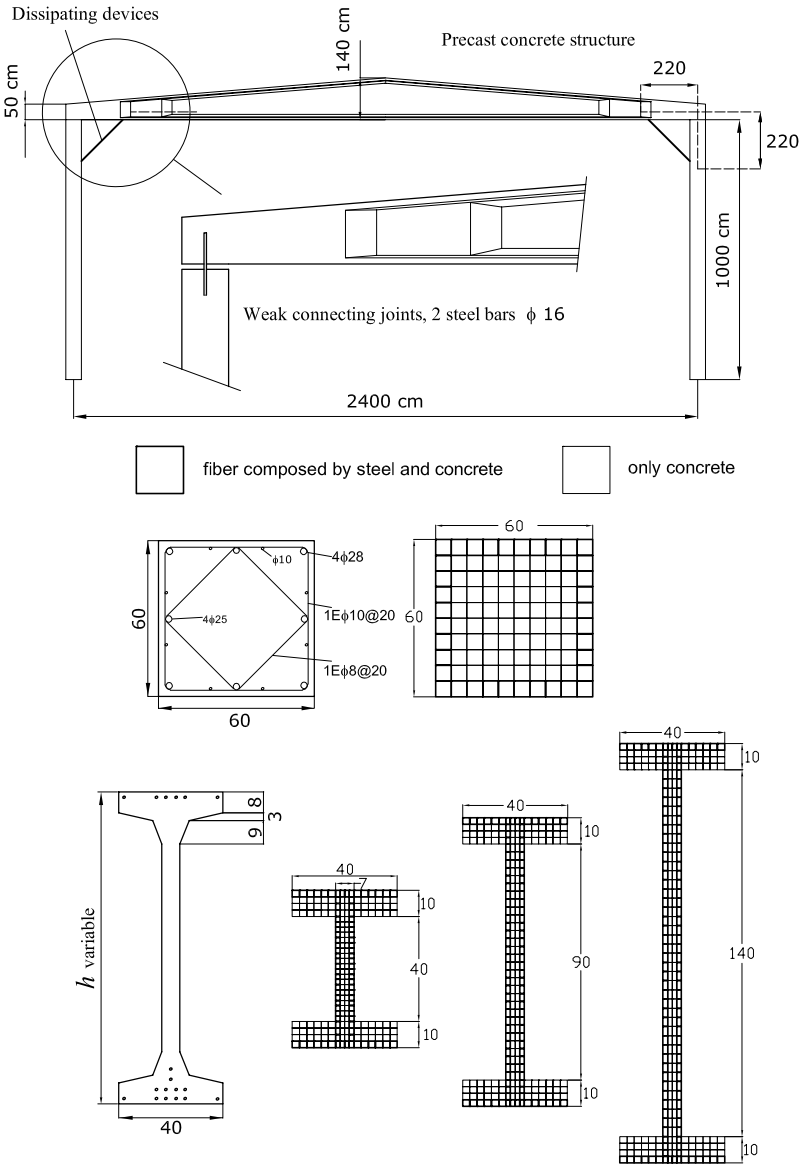


**Fig. 21** Description of the structure

on the supports and of 140 cm in the middle of the span. The permanent loads considered are 1000 N/m$^2$ and the weight of the upper half of the closing walls of 225.000 N. The input acceleration is the N-S component of the El Centro 1940 earthquake with a peak acceleration of $0.3g$.

The two columns and the beam are meshed using 8 quadratic elements with two Gauss integration points per element. A purely plastic EDD was used with $c_d = 0$, $\wp_1 =$ 167000 N/mm, $\wp_2 = 0$, $d_y = 1.2$ mm and $\wp_4 = 1$. The length of the devices is 3.1 m. First, a set of four numerical pushover analysis are performed considering: (1) The bare frame under small displacements assumption. (2) The bare frame in finite deformation. (3) The frame with EDDs and small deformation. (4) Idem as (3) but with finite deformation. The purpose is to establish clearly the importance of considering geometric nonlinearity coupled with inelasticity in the response of the structure.

The corresponding capacity curves are shown in Fig. 22a. It is possible to see that for both cases, with and without EDDs, the small strain assumption overestimates the real capacity of the structure, due to the fact that the vertical loads compress the columns controlling the cracking due to the lateral loading. In the case of finite deformation, the so called $P$–$\Delta$ [242] effect produces an anticipated strength degradation clearly observed for displacements >60 mm. Softening behavior observed in the finite deformation models is not captured in the cases (1) and (3). EDDs also contributes to increases the stiffness and yielding point of the structure.

Figure 22b shows the evolution of the global damage index for the four cases. This index grows quickly for the cases

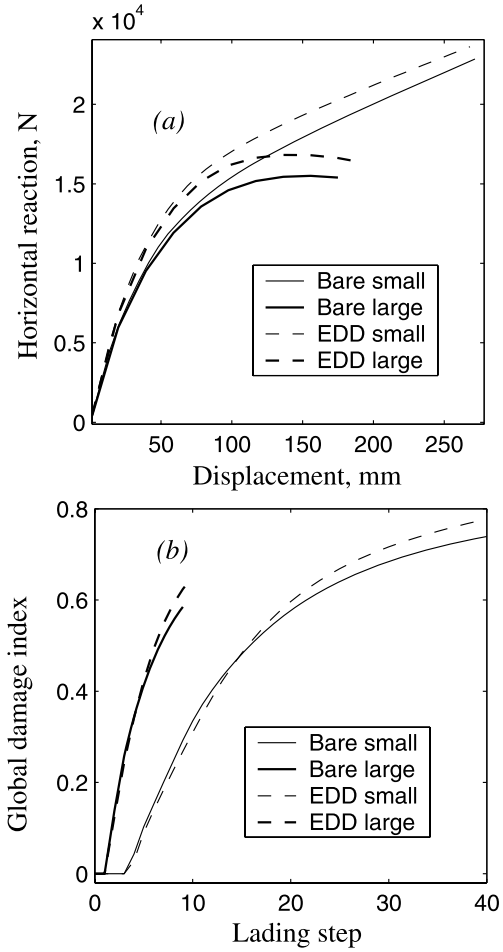


**Fig. 22** (**a**): Capacity curves. (**b**): Evolution of the global damage index (Mata *et al.* [165])

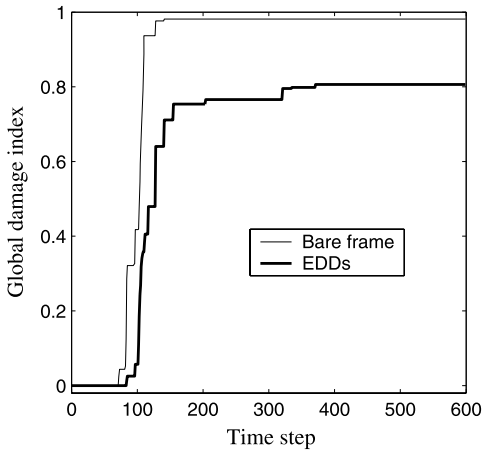


**Fig. 23** Evolution of the global damage index (Mata *et al.* [165])

when finite deformation is considered and the benefits of adding EDDs are not clear due to the fact that the pushover analysis does not take into account energy dissipation criteria [165].

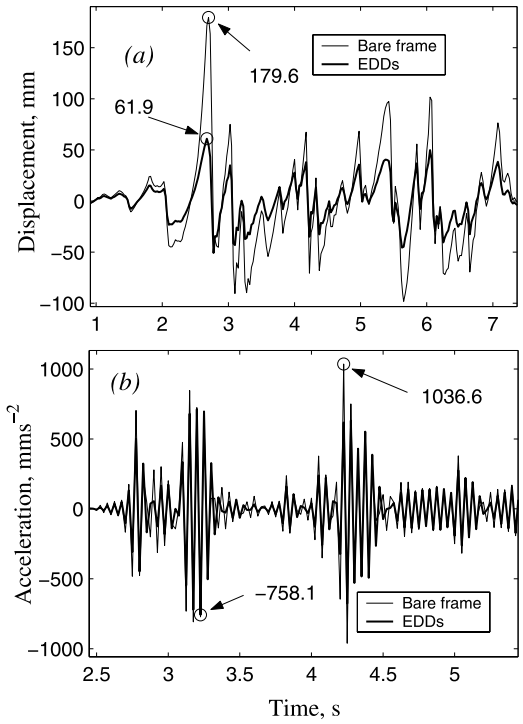


**Fig. 24** Time history responses of the top beam–column joint. (**a**): Horizontal displacement. (**b**): Acceleration (Mata *et al.* [165])

The results of the numerical simulations in the dynamic range confirm that the incorporation of plastic EDDs contributes to improve the seismic behavior of the structure. Figure 23 shows the evolution of the global damage index. The curve corresponding to the structure with EDDs has been estimated without considering the damage in the devices; therefore, it constitutes a measure of degradation in the RC building. On the contrary to the static case, here the benefits of including EDDs are clearly evidenced from the fact that the global level of degradation is higher for the case of the bare structure.

Figure 24 shows the time history response of the horizontal displacement and acceleration of the upper beam–column joint for the uncontrolled and the controlled case. A reduction of approximately 65.5% is obtained for the maximum lateral displacement when compared with the bare frame. Acceleration is controlled in the same way, but only 26.9% of reduction is obtained. A possible explanation for the limited effectiveness of the EDD is that the devices only contribute to increase the ductility of the beam–column joint without alleviating the base shear demand on the columns due to the dimensions of the device and its location in the structure.

### 8.3 Seismic Response of a 3D Building with EDDs

This example corresponds to the study of the seismic response a 3-storey building designed according to the Eu-

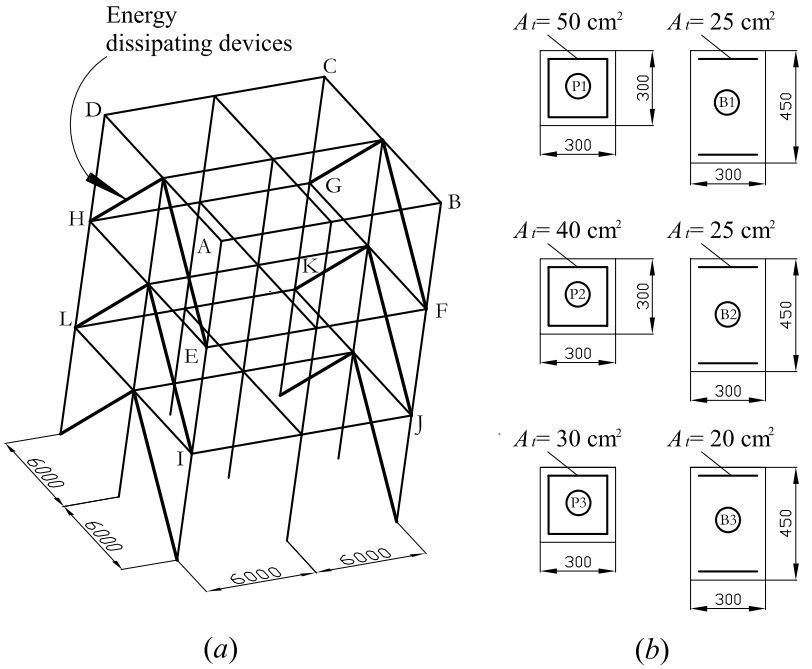


**Fig. 25** (**a**): 3-storey urban building with EDDs. (**b**): RC detailing (Mata *et al.* [165])

rocode 8 [75] for a medium ductility class, a soil profile A and a peak ground acceleration of $0.2g$, see Fig. 25a. It highlights the geometric and constitutive nonlinear behavior of a 3D structure with and without EDDs, including complex phenomena like the torsional response coupled with $P$–$\Delta$ effects [165]. The mechanical properties for steel and concrete as well as the applied acceleration record are the same as in the previous example. The loading is applied according to the axis $A$–$B$ of Fig. 25a.

The inertial forces are derived from the contribution of the mass corresponding to a concrete floor of 130 mm thickness along with the sum of dead and live loads of 2500 N/mm$^2$. Structural torsion is induced adding two point masses in nodes $A$ and $B$ corresponding to the 10% of the total mass of a floor.

Three cases are considered: (1) Bare building. (2) Elastic bare equipped with viscous EDDs. The location of the viscous devices is shown in Fig. 25a and their mechanical properties are: $c_d = 10.000$ Ns$^{-1}$ with an exponent of $n = 0.5$ and $\wp_j = 0$ ($j = 1, \ldots, 4$). (3) Full nonlinear model of the building equipped with viscous EDDs. Case (2) is used to investigate the influence on the structural response of the *a priori* assumption that considers the building's structure remaining elastic when using EDDs.

The displacement time history responses of the nodes $B$ and $C$ of the building in the direction of the applied record are shown in Fig. 26a and 26b, respectively. The difference observed between these figures is due to the fact that the torsional effect induces a rotational motion about the inertial center of the floors. It is possible to appreciate that the use of the viscous EDDs contributes to alleviate the maximum displacement demand about a 25% with respect to the bare frame. Clearly, the *a priori* consideration that the main structure remains elastic underestimates the displacement and ductility demand of the structural elements.

Figures 26c and 26d shows the displacement time history response (torsionally induced) of the nodes $C$ and $D$ in the direction perpendicular to $A$–$B$. It is possible to see that the inclusion of EDDs alleviates significatively the torsional response in the nonlinear range.

The evolution of the global damage index is shown for the full nonlinear controlled and uncontrolled cases in Fig. 27. In the same manner as before, the benefits obtained from the application of EDDs are clearly evidenced.

## 9 Conclusions

In summary, the review of a large amount of works devoted to the modern numerical approach to the structural analysis of RC structures with EDDs allows to affirm that the following aspects constitute current and active branches of research:

(i) *Geometric nonlinearity*. Changes in the configuration of RC beam in structures due to the action of static and/or dynamic actions produces additional stress fields which should be considered.

(ii) *Constitutive nonlinearity*. RC structures invariantly present inhomogeneous distributions of inelastic (probably rate dependent) materials. The success in determining the energy dissipation for softening structures constitutes an excellent point of departure for the application of

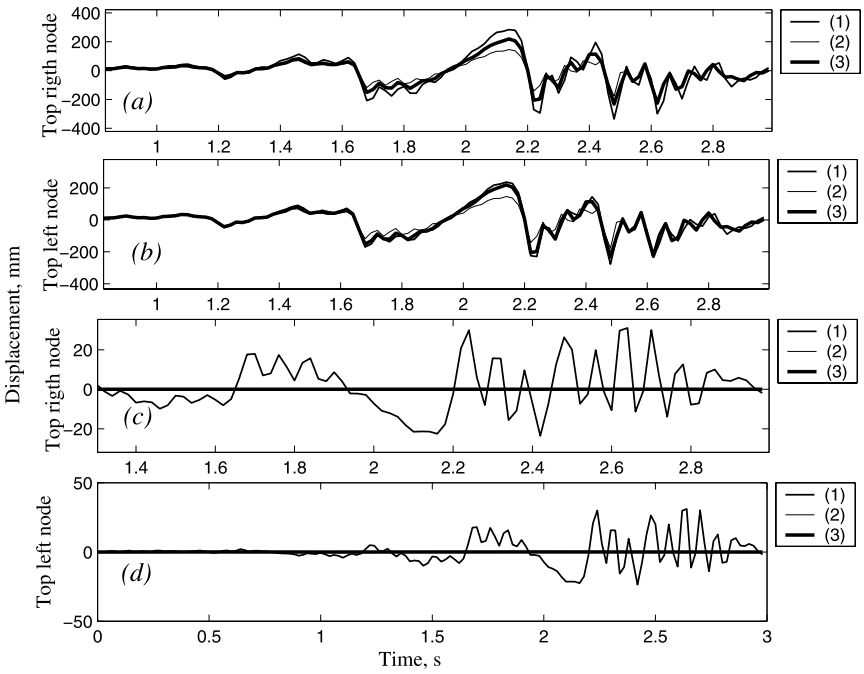


**Fig. 26** Displacement time history response in the direction of the applied record. (**a**): Node $B$. (**b**): Node $C$. (**c**): Node $C$ (perpendicular). (**d**): Node $D$ (perpendicular) (Mata *et al.* [165])

(iii) *Control techniques*, based on the incorporation of EDDs which allows to improve the dynamic response of structures contributing to the control of displacements and alleviating the ductility demand on structural elements.

In most of the cases, finite deformation models for beam structures have been restricted to the elastic case. By the contrary, most of the formulations considering inelasticity are developed under the small strain assumption and the thermodynamical basis of the constitutive laws are violated, limiting the possibility of obtaining good characterizations of the mechanical properties of the structures. Several numerical codes have included special elements for EDDs, however, the obtained formulations commonly are subjected to the mentioned limitations.

A more detailed exposition has been done for the case of beam elements able to consider in a coupled manner geometric and constitutive sources of nonlinearity in both the static and the dynamic ranges and including passive energy dissipating elements as an special element. The described formulation is based on the 3D formulation for rods due to Reissner and Simo but extended to include arbitrary distribution of composite materials in the cross sections. Constitutive laws for the simple materials are based on thermodynamically consistent formulations allowing to obtain more realistic estimations of the energy dissipation. The simple mixing rule for composites is used for modeling complex behaviors at material point level. A detailed cross sectional analysis, consistent with the kinematic hypothesis is also presented. Local and global damage indices have been developed based on the ratio between the visco elastic and nonlinear stresses. An specific element for EDDs is described, based on the rod model but releasing the rotational degrees of freedom. Constitutive relations are given for a wide variety of possible dissipative mechanisms including the corresponding integration algorithms.

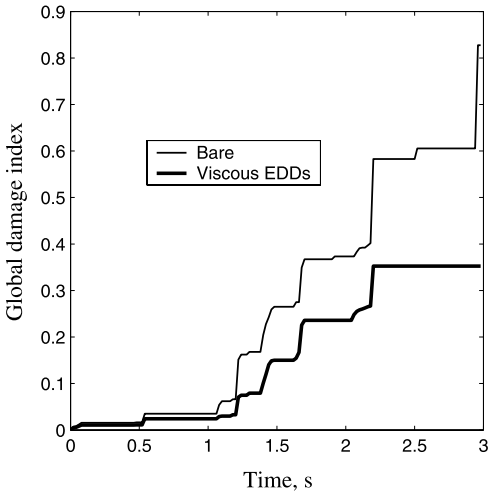


**Fig. 27** Time history response of the global damage index (Mata *et al.* [165])

The linearization of the virtual work functional is consistent with the kinematical hypothesis of the rod's theory and rate dependent inelasticity. The formulation leads to the consistent deduction of the mass and viscous tangent components of the stiffness which are added to the material, geometric terms. A suitable version of Newmark's scheme is

used and details about the numerical implementation of the iterative updating procedure of the involved variables are also addressed. The space discretization of the linearized problem is performed using the standard Galerkin FE approach. A Newton–Raphson type of iterative scheme is used for the step-by-step solution of the discrete problem.

Several numerical examples are provided, which include the verification of the mesh independency of the response for structures presenting softening behavior. The study of a realistic flexible RC framed structures subjected to static and seismic actions is also included.

**Acknowledgements** This research was partially supported by the European Commission, CEE–FP6 Project FP6-50544(GOCE) "Risk Mitigation for Earthquakes and Landslides (LESSLOSS)"; by the Spanish Government (Ministerio de Educación y Ciencia), project BIA2003-08700-C03-02 "Numerical simulation of the seismic behaviour of structures with energy dissipation devices"; project MAT2003-09768-C03-02 "Delamination of reinforced matrix composites (DECOMAR)"; project BIA2005-06952 "Study of composite materials for design, reinforcement and retrofit of civil engineering structures (RECOMP)"; by the Spanish Government (Ministerio de Fomento) "Numerical simulation methodology for the reinforced concrete behavior structures reinforced with composite materials", and by the collaboration framework between CIMNE and AIRBUS, project PBSO-13-06 "Innovative finite element methods for non linear analysis of composite structures (FEMCOM)". The fellowship of the PhD student Pablo Mata A has been provided by International Center for Numerical Methods in Engineering (CIMNE). All this support is gratefully acknowledged.

## References

1. Ahmadi HR, Muhr AH (1997) Modelling dynamic properties of filled rubber. Plast Rubber Compos Process Appl 26:451–461
2. Aiken I (1996) Passive energy dissipation hardware and applications. In: Proceedings, Los Angeles county and SEAOSC symposium on passive energy dissipation systems for new and existing buildings, Los Angeles, July 1996
3. Aiken I (1998) Testing of seismic isolators and dampers—considerations and limitations. In: Proceedings, structural engineering world congress, San Francisco, California, 1998
4. Aiken ID, Kelly JM (1996) Cyclic dynamic testing of fluid viscous dampers. In: Proceedings, Caltrans fourth seismic research workshop, California Department of Transportation, Sacramento, California, USA, July 1996
5. Aiken ID, Kelly JM, Pall AS (1968) Seismic response of a nine-story steel frame with friction damped cross-bracing. In: Proceedings, ninth world conference on earthquake engineering, Tokyo and Kyoto, Japan, August 1988
6. Akiyama H (2003) Metodología de proyecto sismoresistente de edificios basada en el balance energético. Editorial Reverté SA, 2003
7. Antman SS (1991) Nonlinear problems of elasticity. Springer, New York
8. Antman SS (1996) Dynamical problems for geometrically exact theories of nonlinearly viscoelastic rods. J Nonlinear Sci 6:1–18
9. Arfiadi Y, Hadi MNS (2000) Passive and active control of three-dimensional buildings. Earthquake Eng Struct Dyn 29:377–396
10. Argyris J (1982) An excursion into large rotations. Comput Methods Appl Mech Eng 32:85–155
11. Argyris J, Poterasu VF (1993) Large rotations revisited application of Lie algebra. Comput Methods Appl Mech Eng 103:11–42
12. Armero F (1999) Large-scale modeling of localized dissipative mechanisms in a local continuum: applications to the numerical simulation of strain localization in rate-dependent inelastic solids. Mech Cohes-Frict Mater 4:101–131
13. Armero F, Ehrlich D (2004) An analysis of strain localization and wave propagation in plastic models of beams at failure. Comput Methods Appl Mech Eng 193:3129–3171
14. Armero F, Ehrlich D (2005) Numerical modeling of softening hinges in the Euler-Bernoulli beams. Comput Struct 84:641–656
15. Armero F, Ehrlich D (2005) Finite element methods for the analysis of softening plastic hinges in beams and frames. Comput Mech 35:237–264
16. Armero F, Romero I (2001) On the formulation of high-frequency dissipative time-stepping algorithms for nonlinear dynamics. Part II: second-order methods. Comput Methods Appl Mech Eng 190:6783–6824
17. Armero F, Romero I (2003) Energy–dissipating momentum–conserving time–stepping algorithms for the dynamic of nonlinear Cosserat rods. Comput Mech 31:3–26
18. Asano M, Masahiko H, Yamamoto M (2001) The experimental study on viscoelastic material dampers and the formulation of analytical model. In: Proceedings of the 12th world conference on earthquake engineering, Paper no 1535
19. Atluri SN, Cazzani A (1995) Rotations in computational solid mechanics. Arch Comput Methods Eng 2:49–138
20. Atluri SN, Vasudevan S (2001) A consistent theory of finite stretches and finite rotations, in space–curved beams of arbitrary cross section. Comput Mech 27:271–281
21. Ayoub A, Filippou FC (2000) Mixed formulation of nonlinear steel-concrete composite beam element. J Struct Eng 126:0371–0381
22. Bairan Garcia JM, Mari Bernat AR (2006) Coupled model for the non-linear analysis of anisotropic sections subjected to general 3D loading. Part 1: theoretical formulation. Comput Struct 84:2254–2263
23. Barbat AH, Bozzo LM (1997) Seismic analysis of base isolated buildings. Arch Comput Methods Eng 4(2):153–192
24. Barbat AH, Cervera M, Hanganu A, Cirauqui C, Oñate E (1998) Failure pressure evaluation of the containment building of a large dry nuclear power plant. Nucl Eng Des 180:251–270
25. Barbat AH, Oller S, Hanganu A, Oñate E (1997) Viscous damage model for Timoshenko beam structures. Int J Solids Struct 34(30):3953–3976
26. Barbat AH, Oller S, Mata P, Vielma JC (2007) Computational simulation of the seismic response of buildings with energy dissipating devices. In: Proceedings of the COMPDYN 2007, first international conference on computational methods in structural dynamics and earthquake engineering, Rethymno, Crete, Greece, June 13th–15th, 2007
27. Barbat AH, Rodellar J, Ryan E, Molinares N (1993) Comportamiento sísmico de edificios con un sistema no lineal de control hibrido. Rev Int Métodos Numér Cálcy Diseño Ing 9:201–220
28. Barbat AH, Rodellar J, Ryan EP, Molinares N (1995) Active control of nonlinear base-isolated buildings. J Eng Mech 121(6):676–684
29. Barham WS, Aref AJ, Dargush GF (2005) Flexibility-based large increment method for analysis of elastic-perfectly plastic beam structures. Comput Struct 83:2453–2462
30. Barroso LR, Breneman SE, Smith HA (2002) Performance evaluation of controlled steel frames under multilevel seismic loads. J Struct Eng 128(11):1368–1378
31. Bathe KJ (1996) Finite element procedures. Prentice-Hall, Englewood Cliffs
32. Bathe KJ, Bolourchi S (1979) Large displacement analysis of three-dimensional beam structures. Int J Numer Methods Eng 14:961–986

33. Batista Marques de Sousa J Jr, Barreto Caldas R (2005) Numerical analysis of composite steel–concrete columns of arbitrary cross section. J Eng Mech 131(11):1721–1730
34. Battini JM, Pacoste C (2002) Co-rotational beam elements with warping effects in instability problems. Comput Methods Appl Mech Eng 191:1755–1789
35. Bauchau OA, Choi JI (2003) The vector parameterization of motion. Nonlinear Dyn 33:165–188
36. Bauchau OA, Theron NJ (1996) Energy decaying scheme for non-linear beam models. Comput Methods Appl Mech Eng 134:37–56
37. Bauchau O, Trainelli L (2003) The vectorial parametrization of rotation. Nonlinear Dyn 32:71–92
38. Bayrak O, Sheikh SA (2001) Plastic hinge analysis. J Struct Eng 127(9):1092–1100
39. Bentz EC (2000) Sectional analysis of reinforced concrete members. PhD thesis, University of Toronto
40. Betsch P, Menzel A, Stein E (1998) On the parametrization of finite rotations in computational mechanics. A classification of concepts with application to smooth shells. Comput Methods Appl Mech Eng 155:273–305
41. Betsch P, Steinmann P (2002) Frame-indifferent beam finite element based upon the geometrically exact beam theory. Int J Numer Methods Eng 54:1775–1788
42. Betsch P, Steinmann P (2003) Constrained dynamics of geometrically exact beams. Comput Mech 31:49–59
43. Blandford GE (1996) Large deformation analysis of inelastic space truss structures. J Struct Eng 122(4):407–415
44. Bottasso CL, Borri M (1997) Energy preserving/decaying schemes for non-linear beam dynamics using the helicoidal approximation. Comput Methods Appl Mech Eng 143:393–415
45. Bottasso CL, Borri M, Trainelli L (2001) Integration of elastic multibody systems by invariant conserving/dissipating algorithms. II. Numerical schemes and applications. Comput Methods Appl Mech Eng 190:3701–3733
46. Braga F, Faggella M, Gigliotti R, Laterza M (2005) Nonlinear dynamic response of HDRB and hybrid HDRB-friction sliders base isolation systems. Bull Earthquake Eng 3:333–353
47. Bratina S, Saje M, Planinc I (2004) On materially and geometrically non-linear analysis of reinforced concrete planar frames. Int J Solids Struct 41:7181–7207
48. Briseghella L, Majorana CE, Pellegrino C (1999) Conservation of angular momentum and energy in the integration of non-linear dynamic equations. Comput Methods Appl Mech Eng 179:247–263
49. Bruneau M, Vian D Experimental investigation of $P$–$\Delta$ effects to collapse during earthquakes. In: 12th European conference on earthquake engineering, Elsevier Science Ltd., Amsterdam, Paper Ref. 021
50. Budd CJ, Iserles A (1999) Geometric integration: numerical solution of differential equations on manifolds. R Soc 357:945–956
51. Buonsanti M, Royer-Carfagni G (2003) From 3-D nonlinear elasticity theory to 1-D bars with nonconvex energy. J Elast 70:87–100
52. Car E (2000) Modelo constitutivo continuo para el estudio del comportamiento mecánico de los materiales compuestos. PhD thesis, Universidad Politécnica de Cataluña
53. Cardona A, Gerardin M (1988) A beam finite element non-linear theory with finite rotations. Int J Numer Methods Eng 26:2403–2438
54. Cardona A, Huespe A (1999) Evaluation of simple bifurcation points and post-critical path in large finite rotations problems. Comput Methods Appl Mech Eng 175:137–156
55. Celledoni E, Owren B (2003) Lie group methods for rigid body dynamics and time integration on manifolds. Comput Methods Appl Mech Eng 192:421–438
56. Cesnik CES, Sutyrint VG, Hodges DH (1988) Refined theory of composite beams: the role of short-wavelength extrapolation. Int J Solids Struct 33(10):1387–1408
57. Clark P, Aiken I, Ko E, Kasai K, Kimura I (1999) Design procedures for buildings incorporating hysteretic seismic devices. In: Proceedings, 68th annual convention Santa Barbara, California, Structural Engineering Association of California, October 1999
58. Cocchetti G, Maier G (2003) Elastic-plastic and limit-state analyses of frames with softening plastic–hinge models by mathematical programming. Int J Solids Struct 40:7219–7244
59. Coleman J, Spacone E (2001) Localization issues in force-based frame elements. J Struct Eng 127(11):1257–1265
60. Connor JJ, Wada A, Iwata M, Huang YH (1997) Damage-controlled structures. I: preliminary design methodology for seismically active regions. J Struct Eng 123(4):423–431
61. Cosenza E, Manfredy G (2000) Damage indices and damage measures. Progress Struct Eng Mater 2:50–59
62. Crisfield MA (1998) Non-linear finite element analysis of solids and structures, vol 1&2. Willey, New York
63. Crisfield MA, Galvanetto U, Jelenič G (1997) Dynamics of 3-D co-rotational beams. Comput Mech 20:507–519
64. Crisfield MA, Jelenič G (1999) Objectivity of strain measures in the geometrically exact three-dimensional beam theory and its finite-element implementation. R Soc 455:1125–1147
65. Crisfield MA, Wills J (1988) Solution strategies and softening materials. Comput Methods Appl Mech Eng 66:267–289
66. CSI analysis reference manual for SAP200r®, ETABs®, and SAFE™. Computers and Structures, Inc., Berkeley, California, USA, 2004
67. Das S, Hadi MNS (1996) Non-linear finite element analysis of reinforced concrete members using MSC/NASTRAN. In: MSC world users conference, Newport Beach, CA, June 1996
68. Davenne L (2004) Macro-element analysis in earthquake engineering. In: Multi-physics and multi-scale computer models in non-linear analysis and optimal design of engineering structures under extreme conditions, Slovenia, June 13–17, 2004
69. Davenne L, Ragueneau F, Mazar J, Ibrahimbegović A (2003) Efficient approaches to finite element analysis in earthquake engineering. Comput Struct 81:1223–1239
70. De La Llera JC, Vásquez J, Chopra AK, Almazán JL (2000) A macro-element model for inelastic building analysis. Earthquake Eng Struct Dyn 29:1725–1757
71. Dides MA, De La Llera JC (2005) A comparative study of concentrated plasticity models in dynamic analysis of building structures. Earthquake Eng Struct Dyn 34:1005–1026
72. Driemeier L, Baroncini SP, Alves M (2005) A contribution to the numerical non-linear analysis of three-dimensional truss system considering large strains, damage and plasticity. Commun Nonlinear Sci Numer Simul 10:515–535
73. Ehrlich D, Armero F (2005) Finite element methods for the analysis of softening plastic hinges in beams and frames. Comput Mech 35:237–264
74. Ericksen JL, Truesdell C (1957) Exact theory of stress and strain in rods and shells. Arch Ration Mech Anal 1:295–323
75. European Committee for Standardization (1998) Eurocode 8: design of structures for earthquake resistance–Part 1: general rules, seismic actions and rules for buildings. Final Draft, Ref No: prEN 1998-1:2003 E
76. Fajfar P, Fifchinger M, Dolšek M (2004) Macro-models and simplified methods for efficient structural analysis in earthquake engineering. In: Multi-physics and multi-scale computer models in non-linear analysis and optimal design of engineering structures under extreme conditions, Slovenia, June 13–17, 2004
77. Faleiro J, Oller S, Barbat AH (2008) Plastic-damage seismic model for reinforced concrete frames. Comput Struct 86(7–8):581–597

78. Fardis MN (1997) Seismic analysis of RC structures. Constr Res Commun Ltd 1(1):57–67
79. Federal Emergency Management Agency (FEMA) (2000) NEHRP recommended provisions for seismic regulations for new buildings and other structures. Report 368, Washington, DC
80. Federal Emergency Management Agency (FEMA) (2000) Prestandard and commentary for the seismic rehabilitation of buildings. Report 356, Washington, DC
81. Felippa CA, Crivelli LA, Haugen B (1994) A survey of the core-congruential formulation for geometrically nonlinear TL finite elements. Arch Comput Methods Eng 1:1–48
82. Fialko S (2001) Aggregation multilevel iterative solver for analysis of large-scale finite element problems of structural mechanics: linear statics and natural vibrations. In: Parallel processing and applied mathematics: 4th international conference. PPAM 2001, Naleczów, Poland, September 9–12, 2001
83. Fraternali F, Bilotti G (1997) Nonlinear elastic stress analysis in curved composite beams. Comput Struct 62(5):837–859
84. Freddi L, Morassi A, Paroni R (2004) Thin-walled beams: the case of the rectangular cross-section. J Elast 76:45–66
85. Fu Y, Kasai K (1998) Comparative study of frames using viscoelastic and viscous dampers. J Struct Eng 124(5):513–522
86. Gerardin M, Cardona A (1989) Kinematics and dynamics of rigid and flexible mechanisms using finite elements and quaternion algebra. Comput Mech 4:115–135
87. Gluck N, Reinhorn AM, Gluck J, Levy R (1996) Design of supplemental damping for control of structures. J Struct Eng 122(12):1394–1399
88. Gonzalez O, Simo JC (1996) On the stability of symplectic and energy-momentum algorithms for non-linear Hamiltonian systems with symmetry. Comput Methods Appl Mech Eng 134:197–222
89. Grassia FS (1998) Practical parameterization of rotations using the exponential map. J Graphics Tools 3:29–48
90. Gruttmann F, Sauer R, Wagner W (1998) A geometrical nonlinear eccentric 3-D beam element with arbitrary cross sections. Comput Methods Appl Mech Eng 160:383–400
91. Gruttmann F, Sauer R, Wagner W (1998) Shear stresses in prismatic beams with arbitrary cross-sections. Technical Report Universität Karlsruhe (TH), Institut für Baustatik
92. Gruttmann F, Sauer R, Wagner W (2000) Theory and numerics of three-dimensional beams with elastoplastic material behavior. Int J Numer Methods Eng 48:1675–1702
93. Gupta A, Krawinkler H (2000) Dynamic P-Delta effects for flexible inelastic steel structures. J Struct Eng 126(1):145–154
94. Hajjar JF (2000) Concrete-filled steel tube columns under earthquake loads. Progress Struct Eng Mater 2:72–81
95. Hanganu AD, Oñate E, Barbat AH (2002) Finite element methodology for local/global damage evaluation in civil engineering structures. Comput Struct 80:1667–1687
96. Hanson RD, Aiken ID, Nims DK, Ritchter PJ, Batchman RE (1993) State of the art and state of the practice in seismic engineering dissipation. In: Proceedings, ATC-17-1. Seminar on seismic isolation, passive energy dissipation and active control. Applied Technology Council, San Francisco, California, March 1993
97. Highway Innovative Technology Evaluation Center (HITEC) (1996) A service center of the civil engineering research foundation (CERF). Guidelines for the testing of seismic isolation and energy dissipation devices. Technical Evaluation Report No: 96-02
98. Highway Innovative Technology Evaluation Center (HITEC) (1999) A service center of the civil engineering research foundation (CERF). Summary of the evaluation findings for the testing of seismic isolation and passive energy dissipating devices. Technical Evaluation Report No: 40404
99. Hjelmstad KD, Taciroglu E (2003) Mixed variational methods for finite element analysis of geometrically non-linear, inelastic Bernoulli-Euler beams. Commun Numer Methods Eng 19:809–832
100. Hsiao KM, Lin JY, Lin WY (1999) A consistent co-rotational finite element formulation for geometrically nonlinear dynamic analysis of 3-D beams. Comput Methods Appl Mech Eng 169:1–18
101. Hughes TJR (2000) The finite element method. Linear static and dynamic finite element analysis. Dover, New York
102. Hwang JS, Ku SW (1997) Analytical modelling of high damping rubber bearings. J Struct Eng 123:1029–1036
103. Iaura M, Atluri SN (1989) On a consistent theory, and variational formulation of finitely stretched and rotated 3-D space-curved beams. Comput Mech 4:73–78
104. Ibrahimbegović A (1995) On finite element implementation of geometrically nonlinear Reissner's beam theory: three-dimensional curved beam elements. Comput Methods Appl Mech Eng 122:11–26
105. Ibrahimbegović A (1997) On the choice of finite rotation parameters. Comput Methods Appl Mech Eng 149:49–71
106. Ibrahimbegović A, Al Mikdad M (2000) Quadratically convergent direct calculation of critical points for 3D structures undergoing finite rotations. Comput Methods Appl Mech Eng 189:107–120
107. Ibrahimbegović A, Mamouri S (2002) Energy conserving/decaying implicit time-stepping scheme for nonlinear dynamics of three-dimensional beams undergoing finite rotations. Comput Methods Appl Mech Eng 191:4241–4258
108. Ibrahimbegović A, Mazen AM (1998) Finite rotations in dynamics of beams and implicit time-stepping schemes. Int J Numer Methods Eng 41:781–814
109. Ibrahimbegović A, Taylor RL, Lim H (2003) Non-linear dynamics of flexible multibody systems. Comput Struct 81:1113–1132
110. Isobe D, Tsuda M (2003) Seismic collapse analysis of reinforced concrete framed structures using the finite element method. Earthquake Eng Struct Dyn 32:2027–2046
111. Izzuddin BA (2001) Conceptual issues in geometrically nonlinear analysis of 3D framed structures. Comput Methods Appl Mech Eng 191:1029–1053
112. Jelenič G (2004) Different aspects of invariance and shear locking in 3D beam elements. In: Advanced research workshop: multi-physics and multi-scale computer models in non-linear analysis and optimal design of engineering structures under extreme conditions, Bled, Slovenia, June 13–17, 2004
113. Jelenič G, Crisfield MA (1999) Geometrically exact 3D beam theory: implementation of a strain-invariant finite element for static and dynamics. Comput Methods Appl Mech Eng 171:141–171
114. Jelenič G, Saje M (1995) A kinematically exact space finite strain beam model-finite element formulation by generalized virtual work principle. Comput Methods Appl Mech Eng 120:131–161
115. Jiang WG, Henshall JL (2002) A coupling cross-section finite element model for torsion analysis of prismatic bars. Eur J Mech A/Solids 21:513–522
116. Kane C, Marsden JE, Ortiz M, West M (2000) Variational integrators and the Newmark algorithm for conservative and dissipative mechanical systems. Int J Numer Methods Eng 49:1295–1325
117. Kapania RK, Li J (2003) On a geometrically exact curved/twisted beam theory under rigid cross-section assumption. Comput Mech 30:428–443
118. Kapania RK, Li J (2003) A formulation and implementation of geometrically exact curved beam elements incorporating finite strains and finite rotations. Comput Mech 30:444–459

119. Kappos AJ (1997) Seismic damage indices for RC buildings: evaluation of concepts and procedures. Constr Res Commun Ltd 1(1):78–87
120. Kasai K, Fu Y, Watanabe A (1998) Passive control systems for seismic damage mitigation. J Struct Eng 124(5):501–512
121. Kelly J (1997) Earthquake-resistant design with rubber, 2nd edn. Springer, Telos
122. Kelly JM (1999) The role of damping in seismic isolation. Earthquake Eng Struct Dyn 28:3–20
123. Kikuchi M, Aiken I (1997) An analytical hysteresis model for elastomeric seismic isolation bearings. Earthquake Eng Struct Dyn 26(2):215–231
124. Kim JK, Lee TG (1993) Failure behavior of reinforced concrete frames by the combined layered and nonlayered method. Comput Struct 48(5):819–825
125. Kojima H, Yoshihide Y (1990) Performance, durability of high damping rubber bearings for earthquake protection. Rubber World 202(4)
126. Kwak H-G, Filippou FC (1990) Finite element analysis of reinforced concrete structures under monotonic loads. Technical Report n: UCB/SEMM–90/14. Department of Civil Engineering, University of California Berkeley, California, USA
127. Kwak H-G, Kim S-P (2001) Nonlinear analysis of RC beam subject to cyclic loading. J Struct Eng 127(12):1436–1444
128. Lafortune S, Goriely A, Tabor M (2006) The dynamics of stretchable rods in the inertial case. Nonlinear Dyn 43:173–195
129. Lee T, Leok M, McClamroch NH (2007) Lie group variational integrators for the full body problem. Comput Methods Appl Mech Eng 196:2907–2924
130. Lee D, Taylor DP (2001) Viscous damper development and future trends. Struct Des Tall Build 10:311–320
131. Lens EV, Cardona A, Géradin M (2004) Energy preserving time integration for constrained multibody systems. Multibody Syst Dyn 11:41–61
132. Lew A, Marsden JE, Ortiz M, West M (2004) An overview of variational integrators. In: Franca LP (ed) Finite element methods: 1970's and beyond. CIMNE, Barcelona
133. Lew A, Marsden JE, Ortiz M, West M (2004) Variational time integrators. Int J Numer Methods Eng 60:153–212
134. Li J (2000) A geometrically exact curved beam theory and its finite element formulation/implementation. MSc thesis, Virginia Polytechnic Institute and State University
135. Lim CW, Chung TY, Moon SJ (2003) Adaptive bang-bang control for the vibration control of structures under earthquakes. Earthquake Struct Dyn 32:1977–1994
136. Lin YY, Chang KC (2003) Study on damping reduction factors for buildings under earthquake ground motions. J Struct Eng 129:206–214
137. Lin WH, Chopra AK (2003) Asymmetric one-storey elastic system with non-linear viscous and viscoelastic dampers: earthquake response. Earthquake Eng Struct Dyn 32:555–577
138. Lin WH, Chopra AK (2003) Asymmetric one-storey elastic system with non-linear viscous and viscoelastic dampers: simplified analysis and supplemental damping system design. Earthquake Eng Struct Dyn 32:579–596
139. Liu JY, Hong JZ (2004) Dynamics of three-dimensional beams undergoing large overall motion. Eur J Mech A/Solids 23:1051–1068
140. López Almansa F, Barbat AH, Rodellar J (1988) SSP algorithm for linear and non-linear dynamic response simulation. Int J Numer Methods Eng 26(12):2687–2706
141. Love AEHA (1996) Treatise on the mathematical theory of elasticity. Dover, New York
142. Lu Y (2002) Comparative study of seismic behavior of multistory reinforced concrete framed structures. J Struct Eng 128(2):169–178
143. Lubliner J (1972) On the thermodynamic foundations of nonlinear solid mechanics. Int J Non-Linear Mech 7:237–254
144. Lubliner J (1985) Thermomechanics of deformable bodies, Technical Report, Department of Civil Engineering, University of California at Berkeley
145. Lubliner J (2008) Plasticity theory. Dover, New York
146. Lubliner J, Oliver J, Oller S, Oñate E (1989) A plastic-damage model for concrete. Int J Solids Struct 25:299–326
147. Luccioni BM, Rougier VC (2005) A plastic damage approach for confined concrete. Comput Struct 83:2238–2256
148. Magalhães de Souza R, Filippou FC, Maués Brabo Pereira A, Aranha GYR Jr (2003) Force formulation of a non-prismatic Timoshenko beam finite element for dynamic analysis of frames. In: CILAMNE, XXIV Iberian Latin–American congress on computational methods in engineering, Ouro Preto/MG Brasil
149. Mäkinen J (2001) Critical study of Newmark-scheme on manifold of finite rotations. Comput Methods Appl Mech Eng 191:817–828
150. Mäkinen J (2004) A formulation for flexible multibody mechanics. Lagrangian geometrically exact beam elements using constrain manifold parametrization. PhD thesis, Tampere University of Technology, Institute of Applied Mechanics and Optimization
151. Mäkinen J (2007) Total Lagrangian Reissner's geometrically exact beam element without singularities. Int J Numer Methods Eng 70:1009–1048
152. Mäkinen J, Marjamäki H (2005) Total Lagrangian parametrization of rotation manifold. In: ENOC, Hedinhoven, Netherlands, pp 522–530
153. Makris N, Burton SA, Hill D, Jordan M (1996) Analysis and design of ER damper for seismic protection of structures. J Mech Eng 122(10):1003–1011
154. Makris N, Changt SP (2000) Effect of viscous, viscoplastic and friction damping on the response of seismic isolated structures. Earthquake Eng Struct Dyn 29:85–107
155. Malvern LE (1969) Introduction to the mechanics of a continuous medium. Prentice-Hall, Englewood Cliffs
156. Marsden JE, Hughes TJR (1983) Mathematical foundations of elasticity. Prentice-Hall, Englewood Cliffs
157. Marsden JE, Wendlandt JM (1997) Mechanical systems with symmetry, variational principles, and integration algorithms. In: Alber M, Hu B, Rosenthal J (eds) Current and future directions in applied mathematics. Birkhäuser, Basel, pp 219–261
158. Marsden JE, West M (2001) Discrete mechanics and variational integrators. Acta Numer 10:357–514
159. Martínez Franklin CE (1997) A theoretical and numerical evaluation of nonlinear beam elements. Master of science thesis, Massachusetts Institute of Technology
160. Martinez X, Oller S, Rastellini F, Barbat AH (2008) Numerical procedure for the computation of RC structures reinforced with FRP using the serial/parallel mixing theory. Comput Struct 86(15–16):1604–1618
161. Mata P, Boroschek R, Barbat AH (2004) Analytical model for high damping elastomers applied to energy dissipating devices. Numerical study and experimental validation. In: 3CSC third European conference on structural control, Vienna, July 12–15, 2004
162. Mata P, Boroschek R, Barbat AH, Oller S (2007) High damping rubber model for energy dissipating devices. J Earthquake Eng 11(2):231–256
163. Mata P, Oller S, Barbat AH (2007) Static analysis of beam structures under nonlinear geometric and constitutive behavior. Comput Methods Appl Mech Eng 196:4458–4478
164. Mata P, Oller S, Barbat AH (2008) Dynamic analysis of beam structures considering geometric and constitutive nonlinearity. Comput Methods Appl Mech Eng 197:857–878

165. Mata P, Barbat AH, Oller S, Boroschek R (2008) Nonlinear seismic analysis of RC structures with energy dissipating devices. Int J Numer Methods Eng, 2008, submitted
166. Mazars J, Kotronis P, Ragueneau F, Casaux G (2006) Using multifiber beams to account for shear and torsion. Applications to concrete structural elements. Comput Methods Appl Mech Eng 195:7264–7281
167. Mazzolani FM (2001) Passive control technologies for seismic-resistant buildings in Europe. Progress Struct Eng Mater 3:277–287
168. Meek JL, Loganathan S (1989) Large displacement analysis of space-frame structures. Comput Methods Appl Mech Eng 72:57–75
169. Miyazakyi M, Mitsusaka Y (1992) Design of a building with 20% or greater damping. In: Tenth world conference on earthquake engineering, Madrid, Spain, pp 4143–4148
170. Monti G, Spacone E (2000) Reinforced concrete fiber beam element with bond-slip. J Struct Eng 126:654–661
171. Neuenhofer A, Filippou FC (1997) Evaluation of the nonlinear frame finite-element models. J Struct Eng 123(7):958–966
172. Neuenhofer A, Filippou FC (1998) Geometrically nonlinear flexibility–based frame finite element. J Struct Eng 124(6):704–711
173. Nukala PKVV, White DW (2004) A mixed finite element for three-dimensional nonlinear analysis of steel frames. Comput Methods Appl Mech Eng 193:2507–2545
174. Oliver J (1996) Modelling strong discontinuities in solid mechanics via strain softening constitutive equations. Part 1: fundamentals. Int J Numer Methods Eng 39:3575–3600
175. Oliver J, Cervera M, Oller S, Lubliner J (1990) Isotropic damage models and smeared crack analysis of concrete. In: Proceedings 2nd ICCAADCS, vol 2, Zell Am See, Austria. Pineridge Press, pp 945–958
176. Oliver J, Huespe AE (2004) Continuum approach to material failure in strong discontinuity settings. Comput Methods Appl Mech Eng 193:3195–3220
177. Oller S (2001) Fractura mecánica. Un enfoque global. International Center for Numerical Methods in Engineering, CIMNE
178. Oller S, Barbat AH (2006) Moment-curvature damage model for bridges subjected to seismic loads. Comput Methods Appl Mech Eng 195:4490–4511
179. Oller S, Luccioni B, Barbat AH (1996) Un método de evaluación del daño sísmico en pórticos de hormigón armado. Rev Int Métodos Numér Cálc Diseño Ing 12:215–238
180. Oller S, Oñate E, Miquel J (1996) Mixing anisotropic formulation for the analysis of composites. Commun Numer Methods Eng 12:471–482
181. Oller S, Oñate E, Miquel J, Botello S (1996) A plastic damage constitutive model for composites materials. Int J Solids Struct 33(17):2501–2518
182. O'Reilly OM (1998) On constitutive relations for elastic rods. Int J Solids Struct 35:1009–1024
183. Ovesy HR, Loughlan J, GhannadPour SAM (2006) Geometric non-linear analysis of channel sections under end shortening, using different versions of the finite strip method. Comput Struct 84:855–872
184. Papaioannou I, Fragiadakis M, Papadrakakis M (2005) Inelastic analysis of framed structures using the fiber approach. In: 5ht GRACM international congress on computational mechanics
185. Park MS, Lee BC (1996) Geometrically non-linear and elastoplastic three-dimensional shear flexible beam element of Von-Mises-type hardening material. Int J Numer Methods Eng 39:383–408
186. Parulekar YM, Reddy GR, Vaze KK, Kushwaha HS (2004) Lead extrusion dampers for reducing seismic response of coolant channel assembly. Nucl Eng Des 227:175–183
187. Petrolo AS, Casciaro R (2004) 3D beam element based on Saint Venànt's rod theory. Comput Struct 82:2471–2481
188. Pielorz A (2004) Nonlinear equations for a thin beam. Acta Mech 167:1–12
189. Popescu B, Hodges DH (2000) On asymptotically correct Timoshenko-like anisotropic beam theory. Int J Solids Struct 37:535–558
190. Rasouli SK, Yahyai M (2002) Control of response of structures with passive and active tuned mass dampers. Struct Des Tall Build 11:1–14
191. Reismann H (2001) Finite deformation of slender beams. ZAMM J Appl Math Mech 81:481–488
192. Reissner E (1972) On one-dimensional finite-strain beam theory: the plane problem. J Appl Math Phys 23:795–804
193. Reissner E (1973) On one-dimensional large-displacement finite-strain beam theory. Stud Appl Math LII:287–295
194. Reznikov BS (1991) Analysis of the nonlinear deformation of composites with allowance for finite rotations of structural elements. Translated from Zh Prikl Mekh Tekhn Fiz 4:161–165
195. Riley MA, Sadek F, Mohraz B (1999) Guidelines for testing passive energy dissipation devices. In: Proceedings, US/Japan Bridge engineering workshop, 15th, Tsukuba city, Japan
196. Ritto-Corrëa M, Camotin D (2002) On the differentiation of the Rodriguez formula and its significance for the vector-like parametrization of Reissner-Simo beam theory. Int J Numer Methods Eng 55:1005–1032
197. Robinson WH, Greenbank LR (2006) An extrusion energy absorber suitable for the protection of structures during an earthquake. Earthquake Eng Struct Dyn 4:251–259
198. Romero I (2004) The interpolation of rotations and its application to finite element models of geometrically exact rods. Comput Mech 34:121–133
199. Romero I, Armero F (2002) An objective finite element approximation of the kinematics and geometrically exact rod and its use in the formulation of an energy-momentum conserving scheme in dynamics. Int J Numer Methods Eng 54:1683–1716
200. Rosen A, Sabag M, Givoli G (1996) A general nonlinear structural model of a multirod (multibeam) system-I. Theoretical derivations. Comput Struct 61:617–632
201. Rubin MB (2007) A simplified implicit Newmark integration scheme for finite rotations. Comput Math Appl 53:219–231
202. Ryan KR, Chopra AK (2004) Estimating the seismic displacement of friction pendulum isolators based on non-linear response history analysis. Earthquake Struct Dyn 33:359–373
203. Salomón O, Oller S, Barbat AH (1999) Finite element analysis of base isolated buildings subjected to earthquake loads. Int J Numer Methods Eng 46(10):1741–1761
204. Salomón O, Oller S, Barbat AH (2000) Análisis sísmico de edificios con dispositivos de aislamiento de base elastoméricos. Rev Int Métodos Num Cálc Diseño Ing 16:281–304
205. Schimizze AM (2001) Comparison of P–$\Delta$ analyses of plane frames using commercial structural analysis programs and current AISC design specifications. Master of science thesis, Virginia Polytechnic Institute and State University, USA
206. Schulz M, Filippou F (2001) Non-linear spatial Timoshenko beam element with curvature interpolation. Int J Numer Methods Eng 50:761–785
207. Scott MH, Fenves GL (2006) Plastic hinge integration methods for the force-based beam-column elements. J Struct Eng 132(2):244–252
208. Shao Y, Aval S, Mirmiran A (2005) Fiber-element model for cyclic analysis of concrete-filled fiber reinforced polymer tubes. J Struct Eng 131(2):292–303
209. Shen KL, Soong TT (2005) Design of energy dissipation devices based on concept of damage control. J Struct Eng 122(1):76–82

210. Shi G, Atluri SN (1988) Elasto-plastic large deformation analysis of space–frames: a plastic hinge and stress–based explicit derivation of tangent stiffness. Int J Numer Methods Eng 26:589–615
211. Simmonds JG (2005) A simple nonlinear thermodynamic theory of arbitrary elastic beams. J Elast 81:51–62
212. Simo JC (1985) A finite strain beam formulation. The three-dimensional dynamic problem. Part I. Comput Methods Appl Mech Eng 49:55–70
213. Simo JC (1992) The (symmetric) Hessian for geometrically nonlinear models in solid mechanics: intrinsic definition and geometric interpretation. Comput Methods Appl Mech Eng 96:189–200
214. Simo JC, Hjelmstad KD, Taylor RL (1984) Numerical formulations of elasto-viscoplastic response of beams accounting for the effect of shear. Comput Methods Appl Mech Eng 42:301–330
215. Simo JC, Hughes TJR (1997) Computational inelasticity. Springer, New York
216. Simo JC, Ju J (1987) Strain and stress based continuum damage models–Part I: formulation. Int J Solids Struct 23:281–301
217. Simo JC, Tarnow N, Doblare M (1992) Non-linear dynamics of three–dimensional rods: exact energy and momentum conserving algorithms. Int J Numer Methods Eng 34:117–164
218. Simo JC, Tarnow N, Wong KK (1992) Exact energy-momentum conserving algorithms and symplectic schemes for nonlinear dynamics. Comput Methods Appl Mech Eng 100:63–116
219. Simo JC, Vu-Quoc L (1986) A three-dimensional finite-strain rod model. Part II: computational aspects. Comput Methods Appl Mech Eng 58:79–116
220. Simo JC, Vu-Quoc L (1988) On the dynamics in space of rods undergoing large motions—a geometrically exact approach. Comput Methods Appl Mech Eng 66:125–161
221. Simo JC, Vu-Quoc L (1991) A geometrically-exact rod model incorporating shear and torsion-warping deformation. Int J Solids Struct 27:371–393
222. Sivaselvan MV, Reinhorn AM (2002) Collapse analysis: large inelastic deformations analysis of planar frames. J Struct Eng ASCE 128(12):1575–1583
223. Soong TT, Dargush GF (1997) Passive energy dissipation systems in structural engineering. Wiley, New York
224. Soong TT, Spencer BF Jr (2002) Supplemental energy dissipation: state-of-the-art and state-of-the-practice. Eng Struct 24:243–259
225. Spacone E, El-Tawil S (2004) Nonlinear analysis of steel–concrete composite structures: state of the art. J Struct Eng ASCE 130(2):159–168
226. Spencer BF Jr, Nagarajajah S (2003) State of the art of structural control. J Struct Eng 129(7):845–856
227. Spiliopoulos KV, Lykidis GC (2005) An efficient three–dimensional solid finite element dynamic analysis of reinforced concrete structures. Earthquake Eng Struct Dyn 35(2):137–157
228. Stammers CW, Sireteanu T (2000) Control of building seismic response by means of three semi-active friction dampers. J Sound Vib 237(5):745–759
229. Stuelpnagel J (1964) On the parametrization of the three–dimensional rotation group. SIAM Rev 6:422–430
230. Taucer FF, Spacone E, Filipou FC (1991) A fiber beam-column element for seismic response analysis of reinforced concrete structures. Technical Report No UCB/EERC-91/17. Earthquake Engineering Research Center, College of Engineering, University of California, Berkeley
231. Thanoon WA, Hamed AMM, Noorzaei J, Jaafar MS, Al-Silayvani BJ (2004) Inelastic analysis of composite sections. Comput Struct 82:1649–1656
232. Towashiraporn P, Park J, Goodno BJ, Craig JI (2002) Passive control methods for seismic response modification. Progress Struct Eng Mater 4:47–86
233. Trainelli L (2002) The vectorial parametrization of rotation and motion. Technical Report, Politecnico di Milano, Dipartimento de Ingegneria Aerospaziale
234. Uriz P, Whittaker AS (2001) Retrofit of the pre-Northridge steel moment-resisting frames using fluid viscous dampers. Struct Des Tall Build 10:371–390
235. Valles RE, Reinhorn AM, Kunnath SK, Li C, Madan A (1996) IDARC 2D version 4.0: a program for the inelastic damage analysis of buildings. Technical Report NCEER-96-0010. National Center for Earthquake Engineering Research, State University of New York at Buffalo, January 8
236. Vignjevic R (1997) A hybrid approach to the transient collapse analysis of thin walled frameworks I. Comput Methods Appl Mech Eng 148:407–421
237. Vignjevic R (1997) A hybrid approach to the transient collapse analysis of thin walled frameworks II. Comput Methods Appl Mech Eng 148:423–437
238. Vu-Quoc L, Li S (1995) Dynamics of sliding geometrically-exact beams: large angle maneuver and parametric resonance. Comput Methods Appl Mech Eng 120:65–118
239. Wada A, Huang Y-H, Iwata M (2000) Passive damping technology for buildings in Japan. Progress Struct Eng Mater 2:335–350
240. Wagner W, Gruttmann F (2001) Finite element analysis of Saint-Venant torsion problem with exact integration of the elastic-plastic constitutive equations. Comput Methods Appl Mech Eng 190:3831–3848
241. Wen YK (1976) Method for random vibration of hysteretic systems. J Eng Mech Div 102:249–263
242. Williamson EB (2003) Evaluation of damage and $P-\Delta$ effects for systems under earthquake excitation. J Struct Eng 129(8):1036–1046
243. Wolfe RW, Masri SF, Caffrey J (2002) Some structural health monitoring approaches for nonlinear hydraulic dampers. J Struct Control 9:5–18
244. Yang JN, Kim Y-H, Agrawal AK (2000) Reseting semiactive stiffness damper for seismic response control. J Struct Eng 126(12):1427–1433
245. Yeung N, Pan ADE (1998) The effectiveness of viscous-damping walls for controlling wind vibrations in multi-story buildings. J Wind Eng Ind Aerodyn 77&78:337–348
246. Youssef N (2001) Viscous dampers at multiple levels for the historic preservation of the Los Angeles City Hall. Struct Des Tall Build 10:339–350
247. Yu W, Hodges DH (2004) Elasticity solutions versus asymptotic sectional analysis of homogeneous, isotropic, prismatic beams. J Appl Mech 71:15–23
248. Yu W, Volovoi VV, Hodges DH, Hong X (2002) Validation of the variational asymptotic beam sectional analysis. J Am Inst Aeronaut Astronaut 40(10):2105–2112
249. Yu AM, Yang XG, Nie GH (2006) Generalized coordinate for warping of naturally curved and twisted beams with general cross–sectional shapes. Int J Solids Struct 43:2853–2867
250. Zupan D, Saje M (2003) Finite-element formulation of geometrically exact three-dimensional beam theories based on interpolation of strain measures. Comput Methods Appl Mech Eng 192:5209–5248
251. Zupan D, Saje M (2003) The three-dimensional beam theory: finite element formulation based on curvature. Comput Struct 81:1875–1888
252. Zupan D, Saje M (2005) Analytical integration of stress field and tangent material moduli over concrete cross-sections. Comput Struct 83:2368–2380
253. Zupan D, Saje M (2006) The linearized three-dimensional beam theory of naturally curved and twisted beams: the strain vectors formulation. Comput Methods Appl Mech Eng 195:4557–4578